



UNIVERSITAT DE  
BARCELONA

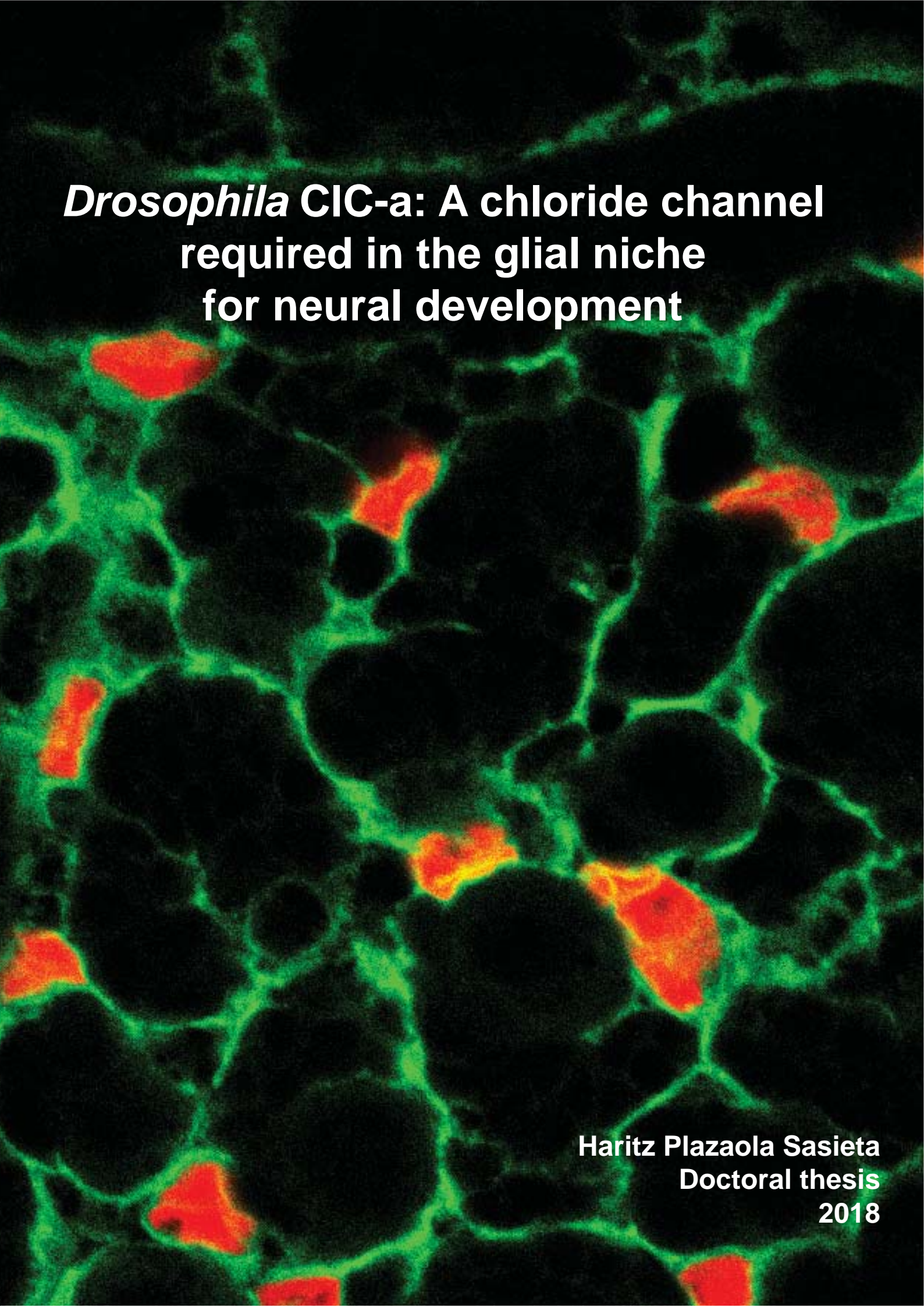
## **Drosophila CIC-a: A chloride channel required in the glial niche for neural development**

Haritz Plazaola Sasieta

**ADVERTIMENT.** La consulta d'aquesta tesi queda condicionada a l'acceptació de les següents condicions d'ús: La difusió d'aquesta tesi per mitjà del servei TDX ([www.tdx.cat](http://www.tdx.cat)) i a través del Dipòsit Digital de la UB ([diposit.ub.edu](http://diposit.ub.edu)) ha estat autoritzada pels titulars dels drets de propietat intel·lectual únicament per a usos privats emmarcats en activitats d'investigació i docència. No s'autoritza la seva reproducció amb finalitats de lucre ni la seva difusió i posada a disposició des d'un lloc aliè al servei TDX ni al Dipòsit Digital de la UB. No s'autoritza la presentació del seu contingut en una finestra o marc aliè a TDX o al Dipòsit Digital de la UB (framing). Aquesta reserva de drets afecta tant al resum de presentació de la tesi com als seus continguts. En la utilització o cita de parts de la tesi és obligat indicar el nom de la persona autora.

**ADVERTENCIA.** La consulta de esta tesis queda condicionada a la aceptación de las siguientes condiciones de uso: La difusión de esta tesis por medio del servicio TDR ([www.tdx.cat](http://www.tdx.cat)) y a través del Repositorio Digital de la UB ([diposit.ub.edu](http://diposit.ub.edu)) ha sido autorizada por los titulares de los derechos de propiedad intelectual únicamente para usos privados enmarcados en actividades de investigación y docencia. No se autoriza su reproducción con finalidades de lucro ni su difusión y puesta a disposición desde un sitio ajeno al servicio TDR o al Repositorio Digital de la UB. No se autoriza la presentación de su contenido en una ventana o marco ajeno a TDR o al Repositorio Digital de la UB (framing). Esta reserva de derechos afecta tanto al resumen de presentación de la tesis como a sus contenidos. En la utilización o cita de partes de la tesis es obligado indicar el nombre de la persona autora.

**WARNING.** On having consulted this thesis you're accepting the following use conditions: Spreading this thesis by the TDX ([www.tdx.cat](http://www.tdx.cat)) service and by the UB Digital Repository ([diposit.ub.edu](http://diposit.ub.edu)) has been authorized by the titular of the intellectual property rights only for private uses placed in investigation and teaching activities. Reproduction with lucrative aims is not authorized nor its spreading and availability from a site foreign to the TDX service or to the UB Digital Repository. Introducing its content in a window or frame foreign to the TDX service or to the UB Digital Repository is not authorized (framing). Those rights affect to the presentation summary of the thesis as well as to its contents. In the using or citation of parts of the thesis it's obliged to indicate the name of the author.

A fluorescence microscopy image of Drosophila tissue. The image shows a network of green-stained cells, likely representing the glial niche, with several red-stained cells interspersed among them. The background is dark, highlighting the cellular structures.

***Drosophila* CIC-a: A chloride channel  
required in the glial niche  
for neural development**

**Haritz Plazaola Sasieta  
Doctoral thesis  
2018**

Departament de Genètica, Microbiologia i Estadística  
Programa de Doctorat en Genètica  
Facultat de Biologia  
Universitat de Barcelona

# ***Drosophila* CIC-a: A chloride channel required in the glial niche for neural development**

Memòria presentada per l'

**Haritz Plazaola Sasieta**

Per a optar al grau de

**Doctor**

per la Universitat de Barcelona



Tesi doctoral realitzada sota la direcció de la Dra. Marta Morey Ramonell.  
Realitzada en el Departament de Genètica, Microbiologia i Estadística  
de la Facultat de Biologia de la Universitat de Barcelona.

La directora i tutora,

L'autor,

Dra. Marta Morey Ramonell

Haritz Plazaola Sasieta

Barcelona, Setembre 2018



## FRONT AND BACK COVERS

On the cover, *05423<sup>CIC-aGal4</sup>* mediated membrane (*UAS-mCD8GFP*) and nuclear (*UAS-H2BRFP*) labeling in a late L3 *05423<sup>CIC-aGal4/+</sup>* larva. The title is ensheathed in the s-IPC neuroepithelium cortex glial niche. Below the title the central brain starts, where neuroblasts glial chambers could be observed.



*Gizonen lana jakintza dugu,  
ezagutuz aldatzea*

*The duty of men is to know,  
know to change*

*Xabier Lete*





## ACKNOWLEDGMENTS

Gracias Marta (Morey) por haberme dado la oportunidad de hacer la tesis en este laboratorio y haber luchado para que pudiera acabarla. Gracias también Florenci y Montse por vuestros consejos durante estos años.

También gracias a toda la gente que ha pasado por el laboratorio y me ha hecho sentir rodeado de tantos amigos. Empezando por las umpa-lumpas, Sandra, Elena, Paula y Qi, por haberme hecho pasar tantos buenos momentos juntos!! Sandra, no voy a resumir todos los momentos en los que hemos desesperado durante estos años, pero ya los dos somos doctores!!! Me ha encantado conocerte y estos cuatro años no hubieran sido los mismos sin ti!! Elena, empezamos el máster juntos, y juntos lo acabamos. Empezamos el doctorado juntos, y juntos lo estamos acabando!! Has sido un gran apoyo durante estos años, un placer haber compartido toda esta experiencia contigo!! Paula, gracias por todos los buenos momentos que me has hecho pasar! Tu punto de locura mezclado con tu punto de cordura ha hecho mella en nosotros!! Y por último Qi, mi pequeña padawan. MUCHISISISISISISISISISISISISISISISISIMAS GRACIAS por toda la ayuda que me has dado durante estos años y por todo el esfuerzo que has hecho para sacar las cosas adelante. Este proyecto no hubiera salido adelante sin ti. Pero no todo es trabajo... Como amiga también me has apoyado mucho durante estos años, gracias por bajar al pozo conmigo para sacarme! Ah! Pero no puedo acabar sin mencionar las FIESTAKAS que nos hemos pegado!! ¿Cuándo la siguiente? ¿Vestidos de cordobés?

También no me puedo olvidar de las fly girls Paula y Mireia, fuisteis las primeras personas que conocí aquí, y nos apoyamos mutuamente muchísimo. ¡Otras dos amigas para siempre que me llevo!

Y por supuesto toda la gente que ha ido pasando por el laboratorio y fue tan cercana como la gente que he mencionado. Marc, Irene P, Irene M, Marina gracias por todo!

Y por último la nueva oleada de gente que ha pasado por el lab, Martí, Giacomo, Jose, Inma, Camille, Carlos... hemos pasado grandes momentos!!

No em puc oblidar tampoc del gran suport que he tingut durant aquests anys, Marta (Mairal). Gràcies per donar-me suport quan mes ho necessitava i fer-me feliç!

Azkenik, eskerrak eman nahi nizkioke nere familiari. Beti gomendio onak eman dizkidazue, aurrera egiten lagundu didatenak.

No parecía que acabaría el doctorado... Pero se acabo!!!

Ez zuen doktoradutza amaituko nuenaren itxura... Baina bukatu da!!! Aupa PATXI!



# TABLE OF CONTENTS

<b>Figure index</b> .....	1
<b>Table index</b> .....	5
<b>Abbreviations and acronyms</b> .....	7
<b>Introduction</b> .....	11
<i>Drosophila</i> central nervous system.....	14
Neurogenesis in <i>Drosophila</i> .....	15
<i>Drosophila</i> glia: functional similarities with vertebrate glia .....	19
The niche: a close relationship between neurogenesis and glia.....	22
Roles of ion channels in glia .....	26
The CIC family.....	31
<b>Objectives</b> .....	35
<b>Materials and methods</b> .....	39
<b>Results</b> .....	53
Chapter I.....	55
Chapter II.....	67
Chapter III.....	75
Chapter IV.....	83
<b>Discussion</b> .....	103
<b>Conclusions</b> .....	115
<b>Bibliography</b> .....	119
<b>Annexes</b> .....	139



# FIGURE INDEX

## Introduction

<b>Figure 1.</b> Structure of a larval and adult brain.....	14
<b>Figure 2.</b> Neurogenesis in the optic lobe.....	17
<b>Figure 3.</b> Neurogenesis in the central brain.....	19
<b>Figure 4.</b> <i>Drosophila</i> glial types .....	20
<b>Figure 5.</b> Comparison between vertebrate and invertebrate glia and their roles.....	22
<b>Figure 6.</b> Illustration of known extrinsic signals in the neuroepithelial glial niche.....	24
<b>Figure 7.</b> Illustration of known extrinsic signals in the neuroblast glial niche.....	25
<b>Figure 8.</b> Extracellular and intracellular ion concentrations of astrocytes.....	27
<b>Figure 9.</b> Na <sup>+</sup> dependent organic molecule transporters.....	28
<b>Figure 10.</b> Ca <sup>2+</sup> regulated secretion of neurotransmitters.....	29
<b>Figure 11.</b> Molecular/structural features of CIC-2 channels.....	32

## Materials and Methods

<b>Figure 12.</b> Genetic structure of <i>MiMIC05423</i> , <i>CIC-aGFP</i> and <i>05423<sup>CIC-aGal4</sup></i> insertions.....	43
<b>Figure 13.</b> Brain measurements.....	44
<b>Figure 14.</b> Schematic of the molecular mechanisms of the G-TRACE system.....	46
<b>Figure 15.</b> Schematic of the EGUF-hid method.....	48
<b>Figure 16.</b> Schematics for MARCM clones in a heterozygous mutant background.....	49
<b>Figure 17.</b> Schematics for MARCM in homozygous mutant background.....	49
<b>Figure 18.</b> Schematics for the design of induced MARCM clones.....	50

## Results

<b>Figure 19.</b> CIC-a expression in the developing brain. ....	57
<b>Figure 20.</b> CIC-a channel expression in glia during development.....	59
<b>Figure 21.</b> CIC-a channel expression in cortex glia.....	61

<b>Figure 22.</b> <i>CIC-a</i> expression in some types of ensheathing glia.....	62
<b>Figure 23.</b> <i>CIC-a</i> MiMIC mutants are strong loss of function alleles.....	64
<b>Figure 24.</b> <i>CIC-a</i> mutants have smaller brains.....	69
<b>Figure 25.</b> <i>CIC-a</i> mutants show photoreceptor guidance phenotypes.....	70
<b>Figure 26.</b> R8s targeting defects.....	72
<b>Figure 27.</b> <i>CIC-a</i> is required in glia for a correct guidance of photoreceptor and a proper optic lobe size.....	73
<b>Figure 28.</b> Photoreceptor phenotypes are non-autonomous.....	74
<b>Figure 29.</b> Cortex glial morphology remain unaltered in <i>CIC-a</i> mutants.....	77
<b>Figure 30.</b> Neuroepithelial proliferation decrease in <i>CIC-a</i> mutants.....	78
<b>Figure 31.</b> The anterior OPC is absent in late L3 <i>CIC-a</i> mutants.....	80
<b>Figure 32.</b> <i>CIC-a</i> is required for neuroblast proliferation and neuronal survival.....	81
<b>Figure 33.</b> Size and growth rate of the larval hemispheres is reduced in mutants.....	81
<b>Figure 34.</b> A subset of <i>CIC-a</i> <sup>+</sup> glial cells, showing strong reduction in mutant animals, act as guidepost cells for photoreceptors.....	86
<b>Figure 35.</b> Developmental details of the glial barrier.....	87
<b>Figure 36.</b> Boundary glia migration and cell death in the barrier.....	89
<b>Figure 37.</b> <i>slit</i> mutants show similar photoreceptor guidance phenotypes compared to <i>CIC-a</i> mutants.....	90
<b>Figure 38.</b> <i>slit</i> -GFP confirms described <i>slit</i> expression.....	91
<b>Figure 39.</b> <i>slit</i> is expressed in the glial barrier during photoreceptor innervation.....	92
<b>Figure 40.</b> Slit is necessary in boundary glia for correct photoreceptor guidance.....	93
<b>Figure 41.</b> <i>mir8Gal4</i> expression is restricted to cortex glia based on an intersectional strategy.....	94
<b>Figure 42.</b> <i>CIC-a</i> expression in cortex glia rescues boundary glia reduction and photoreceptor phenotypes.....	95
<b>Figure 43.</b> Boundary glia reduction could be a consequence of DL1 mispositioning.....	96
<b>Figure 44.</b> Boundary glia reduction could be a consequence of decreased proliferation in DL1 lineage.....	97

**Figure 45.** Neurons of the mushroom body show guidance defects.....99  
**Figure 46.** Cortex glia, showing DM type II neuroblast encasing defects.....101

**Discussion**

**Figure 47.** Hypothetic physiological mechanism of CIC-a.....111  
**Figure 48.** Model of CIC-a function in the glial niche.....114

**Annexes**

**Figure 49.** *CIC-a* mutant photoreceptor clones .....149





# TABLE INDEX

## Introduction

<b>Table 1.</b> A summary of human and <i>Drosophila</i> CICs.....	31
--	----

## Materials and Methods

<b>Table 2.</b> List of <i>Drosophila</i> strains utilized in this work.....	41
--	----

<b>Table 3.</b> Composition of standard fly food.....	42
---	----

<b>Table 4.</b> List of used primary antibodies and dyes.....	42
---	----

<b>Table 5.</b> List of components of a classical PCR reaction.....	51
---	----



## ABBREVIATIONS AND ACRONYMS

**AEL:** after egg lay  
**Alk:** anaplastic lymphoma kinase  
**ana:** Anachronism  
**APF:** after puparium formation  
**ATP:** adenosine triphosphate  
**BBB:** blood brain barrier  
**bg:** boundary glia  
**Bn:** Bolwig's nerve  
**CB:** central brain  
**CC2L:** CLCN2-related  
**CIC-2:** chloride channel 2  
**CIC-a:** chloride channel a  
**Cno:** Canoe  
**CNS:** central nervous system  
**Cx:** calyx  
**cxg:** cortex glia  
**D:** Dichaete  
**DAG:** diacylglycerol  
**dc:** distal cell  
**deGradFP:** degrade Green Fluorescent Protein  
**d-IPC:** distal inner proliferation center  
**dILP:** insulin-like peptide  
**DL:** Dorsolateral  
**Dlp:** Dally-like  
**DM:** Dorsomedial  
**Dpn:** Deadpan  
**dsg:** distal satellite glia  
**E-cad:** E-cadherin  
**EAAT:** excitatory amino acid transporter  
**ed:** eye disc  
**EGFR:** epidermal growth factor receptor  
**EGUF/hid:** Eyeless-GAL4, UAS-FLP/hid  
**EMT:** epithelial-mesenchymal transition  
**eng:** ensheathing glia  
**ep:** epithelial glia  
**ES:** embryonic stem  
**Ey:** Eyeless

**FRT:** flippase recognition target  
**GABA:** gamma-Aminobutyric acid  
**GAT:** GABA transporter  
**GFP:** green fluorescent protein  
**GlyT1:** Glycine transporter 1  
**GlyT2:** Glycine transporter 2  
**GMC:** ganglion mother cell  
**GMR:** glass multiple reporter  
**Hth:** Homothorax  
**iGluR:** Ca<sup>2+</sup> permeable ionotropic glutamate channel  
**INP:** intermediate neural progenitor  
**IP<sub>3</sub>:** inositol 1,4,5-trisphosphate  
**IP3R:** Inositol trisphosphate receptor  
**iPS:** induced pluripotent stem  
**JAK/STAT:** Janus kinase/signal transducer and activator of transcription  
**JEB:** jelly belly  
**Kcc:** kazachoc  
**Kir4.1:** inwardly rectifying K<sup>+</sup> channel 4.1  
**lc:** lobula complex  
**L1:** first instar  
**L2:** second instar  
**L3:** third instar  
**LF:** lamina furrow  
**LKPAT:** leukoencephalopathy with ataxia  
**Ln:** lamina neuron  
**lopn:** lobula plate neuron  
**lopneg:** lobula plate neuropil ensheathing glia  
**Lp:** lamina plexus  
**LPC:** lamina precursor cell  
**I'sc:** Lethal of scute  
**IPC:** inner proliferation center  
**MARCM:** Mosaic analysis with a repressible cell marker  
**Mb Nb:** Mushroom body neuroblasts  
**me:** medulla  
**mg:** marginal glia  
**midg:** midline glia  
**mir-8:** microRNA-8  
**mL:** medial lobe  
**MLC:** Megalencephalic leukoencephalopathy with subcortical cysts

**mn:** medulla neuron  
**mneg:** medulla neuropil ensheathing glia  
**mng:** medulla neuropil glia  
**Nb:** neuroblast  
**Ncc69:** Na<sup>+</sup>-K<sup>+</sup>-Cl<sup>-</sup> cotransporter  
**NE:** neuroepithelia  
**NSC:** neural stem cell  
**OL:** optic lobe  
**OPC:** outer proliferation center  
**os:** optic stalk;  
**pag:** palisade glia  
**PCR:** polymerase chain reaction  
**Pe:** peduncle  
**pg-spg:** perineural-subperineural glia  
**PI3K/Akt:** Phosphoinositol-3 kinase/protein kinase B  
**PIP<sub>2</sub>:** phosphatidylinositol biphosphate  
**p-IPC:** proximal inner proliferation center  
**pn:** peripheral nerve  
**PNS:** peripheral nervous system  
**psg:** proximal satellite glia  
**PUFA:** polyunsaturated fatty acid  
**RFP:** red fluorescent protein  
**RMP:** resting membrane potential  
**ROS:** reactive oxygen species  
**RPE:** retinal pigment epithelia  
**RT-PCR:** reverse transcription polymerase chain reaction  
**RTT:** Rett syndrome  
**Ser:** Serrate  
**SeSAME/EAST:** Seizures, Sensorineural deafness, Ataxia, intellectual (Mental) disability, and Electrolyte imbalance/ Epilepsy, Ataxia, Sensorineural deafness, and Tubulopathy  
**sg:** satellite glia  
**s-IPC:** surface inner proliferation center  
**Slp:** Sloppy paired 1 and 2  
**TF:** transcription factor  
**TGF-β:** transforming growth factor beta  
**Tll:** Tailless  
**Trpa1:** transient receptor potential ankyrin 1  
**TZ:** transition zone  
**VGCC:** voltage-gated calcium channels

**VRAC:** volume-regulated anion channels

**vL:** vertical lobe

**VNC:** ventral nerve cord

**wg:** wrapping glia

**Xg<sub>i</sub>:** inner chiasm glia

**Xg<sub>o</sub>:** outer chiasm glia

**YFP:** yellow fluorescent protein

**Yki:** Yorkie

**Zydeco:** Na<sup>+</sup>/Ca<sup>2+</sup>, K<sup>+</sup> exchanger

# **INTRODUCTION**





The nervous system is a complex network that carries messages to the brain and to various parts of the body. It is the center of all mental activity, including thought, learning, and memory and it keeps us in touch with our environment. The basic unit of the nervous system is the neuron, an electrically excitable cell, that receives, processes, and transmits information through electrical and chemical signals (Reviewed in: Sidiropoulou et al. 2006; Galic et al. 2012; Camp 2012). For many years, neurons were considered the unique functional unit of the nervous system.

Rudolf Virchow was the first to term neuroglial cells, also referred to as glia (named from the Greek for “glue”), and described these, as a connective tissue. Historically, glial cells have only been associated with a physically supportive role, whereas neurons have been considered essential for brain function and behavior. Therefore glial cells were never studied as much as neurons. However, very recently, new glial roles have been recognized and glia are now being considered as active players in the nervous system. Nowadays, we know that glia are the most abundant cell type in the mammalian nervous system and have vital roles in neural development, function, and health (Reviewed in: Barres 2008; Reemst et al. 2016). However, our understanding of the biology of glia is only starting to grow..

Both, neurons and glia, are continually generated by neural stem cells (NSCs) in the developing central nervous system (CNS) and in some other select regions of the adult brain (Reviewed in: Temple 2001; Bond et al. 2015). The process of formation of new neurons and glia is called neurogenesis and includes cell division, production of migratory precursors and progeny, differentiation, and integration into circuits. Many features of neurogenesis are controlled by intrinsic signals of NSCs. Nevertheless, it is essential to consider the whole developmental context of an organism and not just the NSC as an isolated entity to understand its physiology. During development, neurogenesis has to adapt to each developmental stage and has to react to systemic changes. There is emerging evidence, that extrinsic signals from the NSC microenvironment, referred to as neurogenic niche, regulate multiple neurogenesis steps, adapting it to the developmental context. In mammals, such a microenvironment is composed by different cell types, such as, glial cells, meningeal cells, pericytes, endothelial cells and choroid plexus. Niche cells are responsible for modulating NSC behavior through mechanical and diffusible signals that pass between cell populations. Indeed, specific factors released by niche cells regulate NSC proliferation, self-renewal, differentiation, or migration (Reviewed in Bjornsson et al. 2015).

It is well known, that different ion channels and transporters are expressed in glial cells of the mature CNS to regulate their homeostasis (Reviewed in Olsen and Sontheimer 2009). Such ion channels also regulate neuronal behavior. They do so by controlling the extracellular ionic concentration, secretion, and/or uptake of different organic compounds (Djukic et al. 2007; Reviewed in Kirischuk et al. 2015). Glial cells also act as niche cells in the neurogenic niche, but the possible implication of ion channels for a correct regulation of the niche microenvironment remains to be elucidated. Ion channels are expressed in stem cells and

it has been shown that they can intrinsically regulate their proliferation and differentiation (Reviewed in Li and Deng 2011). Thus, ionic balance in the niche microenvironment should be tightly regulated by niche cells.

To investigate the possible function ion channels have during CNS development, we used a simple model, the developing brain of *Drosophila melanogaster*. We chose the chloride channel CIC-a as a candidate to investigate, since it might be associated to possible developmental CNS defects in humans.

## DROSOPHILA CENTRAL NERVOUS SYSTEM

The first developmental steps of *Drosophila* start as an embryo and after going through different larval stages (L1-L2-L3), it pupariates and after some days, emerges as an adult fly (Figure 1). This also implies progressive development of the CNS, such as its growth and substantial structural changes.

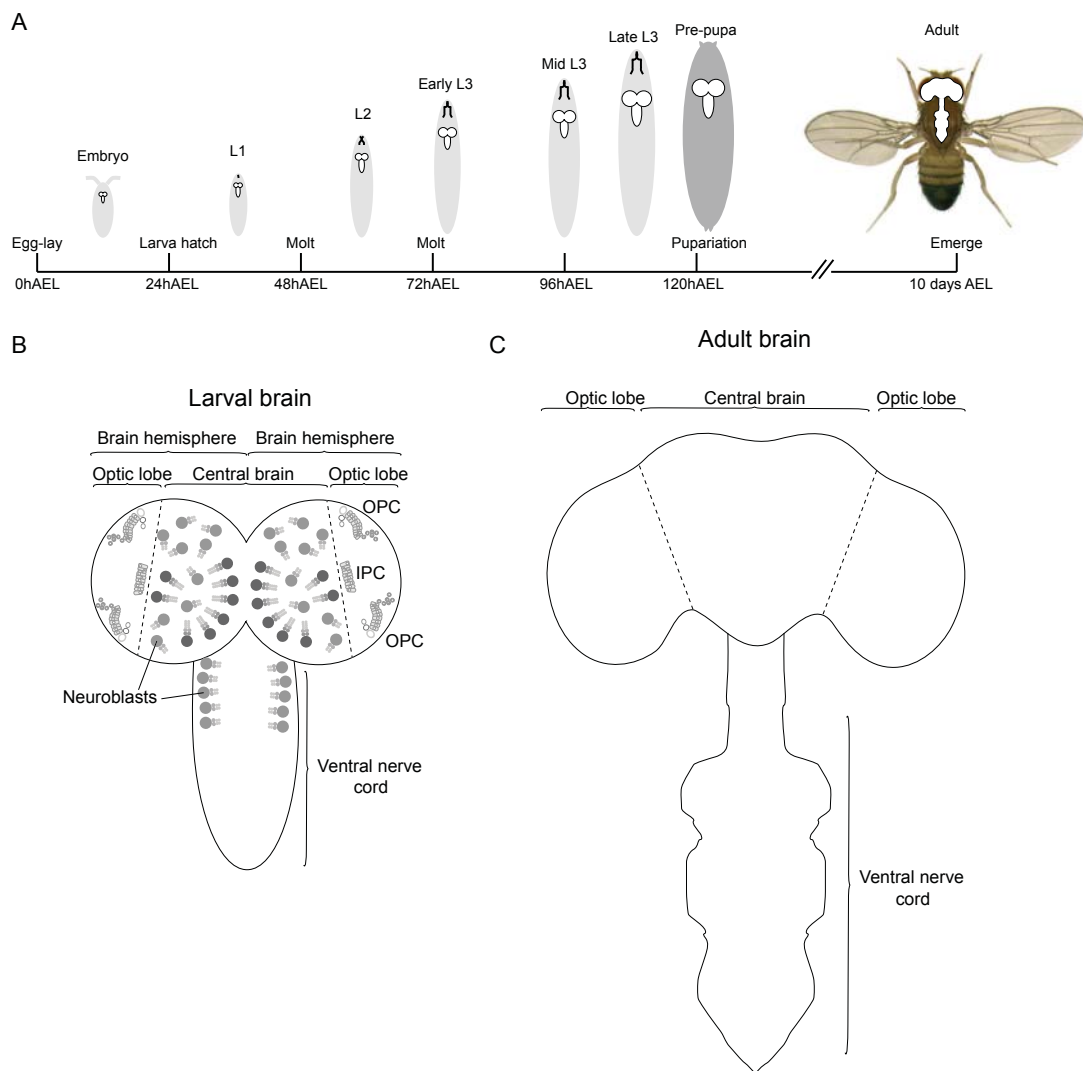


**Figure 1. Structure of a larval and adult brain.** (A) The developmental stages of *Drosophila* and the CNS are shown. (B) Illustration of a larval brain, where two hemispheres are composed by the optic lobe and the central brain. Connected to these structures, the ventral nerve cord is illustrated. (C) Adult *Drosophila* brain hemispheres cannot be identified as spheres any more, since the optic lobe has been separated from the central brain. Optic lobe and central brain are now located in the fly's head, while the ventral nerve cord moved to the thorax. AEL, after egg lay.

During larval development the CNS comprises the optic lobe (OL), central brain (CB), and the ventral nerve cord (VNC). All of these will give rise to the equivalent structures in the mature CNS (Figure 1). The adult optic lobe is composed by four major synaptic ganglia or neuropils (lamina, medulla, lobula and lobula plate), and receives visual input from the eye, processing it for higher order visual functions, like motion detection and color vision. Photoreceptors, light-sensitive neurons that collect visual information, are responsible for sending visual information to the optic lobe. During larval stages, they innervate the optic lobe and project to lamina and medulla neuropils at adult stage.

The central brain is far more complex, composed by more neuropils than the optic lobe. These accomplish a higher variety of functions. For example, the mushroom body (MB) is a structure in the central brain involved in learning and memory (Davis 1993; Heisenberg 1998; Pascual and Pr at 2001). Additionally, the central complex is, for example, involved in the control of walking (Strauss and Heisenberg 1993).

## NEUROGENESIS IN *DROSOPHILA*

During the dynamic development of the organism, environmental stimuli and behavior completely change requiring the CNS development to adapt to these variations. For example, the larvae have a basal visual system, but an adult fly has a very complex compound eye. Therefore the nervous system has to adapt, to process all visual information, received through this complex structure. Neurogenesis plays an important role in this adaptation, since new neurons are necessary to fulfill new functions.

The CNS, together with an embryonic brain, starts developing at the embryonic stage, and will accomplish basic larval functions. Neurons with embryonic origin are called primary neurons and, while development goes on at larval stages, secondary neurons are generated. After metamorphosis, these secondary neurons are responsible for the adult brain to accomplish more complex tasks. Determination of the number of neuroblasts and the number of cell divisions suggest that there are ~10,000–15,000 neurons in the larval brain, a number 10- to 20-fold lower than in the adult (Hartenstein and Campos-Ortega 1984; Hartenstein et al. 1987; Truman et al., 1993). The second wave of neurogenesis at larval stages makes the *Drosophila* CNS a good system to study the potential role ionic homeostasis has in the neurogenic niche.

Two different strategies have been evolved to create the complexity of the central nervous system in *Drosophila* (Figure 1). On the one hand, two neuroepithelia are present in the optic lobe, which at late larval stages differentiate to neuroblasts (the stem cells of the developing fly brain) and give rise to all the neurons and glia of the adult optic lobe (Reviewed in Suzuki and Sato 2014; Apitz and Salecker 2015). On the other hand, neuroblasts differentiated at embryonic stages, give rise to the central brain and ventral nerve cord (Reviewed in Homem and Knoblich 2012). Hence, since two different mechanisms of neurogenesis are used, the extrinsic signals necessary in the neurogenic niche must also be different. For this reason, we will consider neurogenesis of both the optic lobe and the central brain separately.

### Optic lobe neurogenesis

The optic lobe comes from two different neuroepithelia, the outer proliferation center (OPC) and the inner proliferation center (IPC), which are originated from an optic placode of about 30–40 epithelial cells (Hofbauer and Campos-Ortega 1990). After larval hatching, the neuroepithelial stem cells start to divide symmetrically and quickly separate into the two neuroepithelia. In a first phase, the pseudostratified neuroepithelia grow by symmetric cell division to a size of several thousand epithelial progenitor cells (Hofbauer and Campos-Ortega 1990; Egger et al. 2007; Ngo et al. 2010). During the second phase, which begins at late L2 stage, the progenitors undergo an epithelial-mesenchymal transition (EMT), becoming neuroblasts, that enter a phase of asymmetric cell division, with each neuroblast producing a neuronal lineage. The asymmetric cell division generates a self-renewing neuroblast and a ganglion mother cell (GMC), which divides once to produce two neurons.

Neuroepithelial cells at the medial edge of the OPC sequentially transform into medulla neuroblasts (Figure 2), while cells at the opposite lateral edge of the OPC become lamina precursor cells (LPCs) (Figure 2) (Selleck and Steller 1991; Egger et al. 2007). When photoreceptor innervation begins, LPCs will differentiate to lamina neurons.

The neuroepithelial cell to medulla neuroblast transition at the medial edge is controlled by a proneural wave of *lethal of scute* (*l'sc*) expression, that sweeps across the neuroepithelium (Yasugi et al. 2008). Medulla neuroblasts express five transcription factors (TFs) in a sequential order: *Homothorax* (*Hth*), *Eyeless* (*Ey*), *Sloppy paired 1 and 2* (*Slp*), *Dichaete* (*D*) and *Tailless* (*Tll*) and this temporal cascade regulates the specification of different neuronal identities (Li et al. 2013). Ahead of the wave that produces neuroblasts, uncommitted neuroepithelial cells continue to divide symmetrically, expanding the pool of prospective neuroblasts.

The IPC gives rise to the lobula plate and lobula neurons and is subdivided into three different domains, proximal (p-IPC), surface (s-IPC) and distal (d-IPC) domains. In the p-IPC, neuroepithelial cells differentiate into progenitors and migrate to a secondary proliferation

zone, the d-IPC, where they mature into neuroblasts and give rise to lobula plate neurons and distal cells (Figure 2). The s-IPC extends toward the optic lobe surface and produces lobula neurons (Apitz and Salecker 2015).

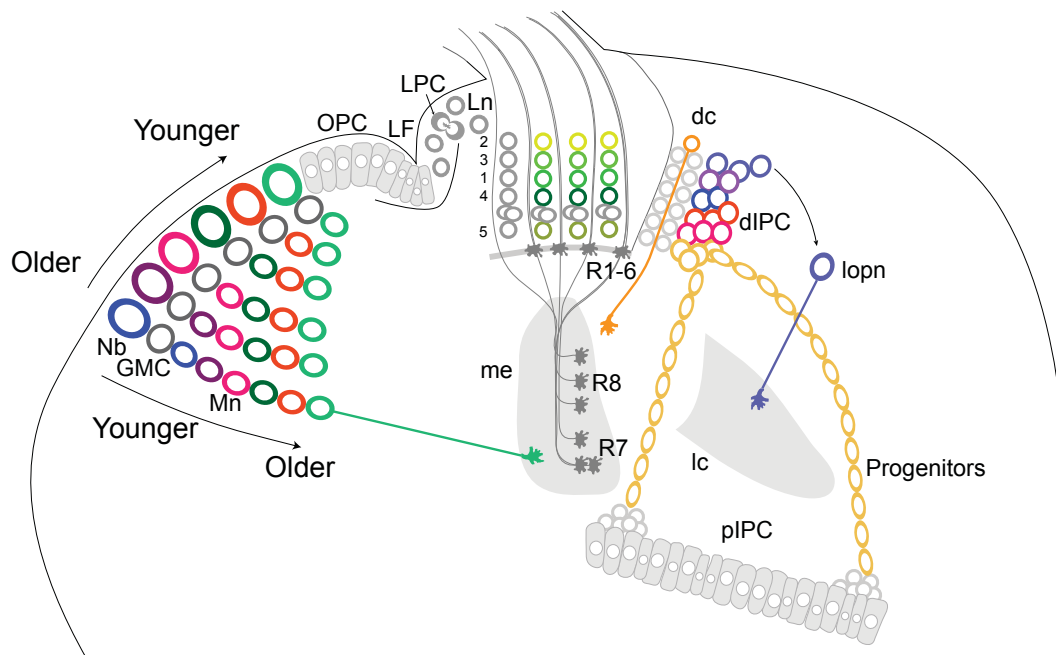


**Figure 2. Neurogenesis in the optic lobe.** Illustration of a late third instar larval optic lobe. Medulla and lamina neurons are generated from the OPC neuroepithelium. On its lateral side, after the lamina furrow (LF), lamina precursor cells (LPC) are generated. On its medial side, medulla neurons (Mn) originate from a proneural wave that transforms the NE into neuroblasts (Nb). As Nb age, their progeny expresses distinct transcription factors (different colors refer to different TF expression), giving rise to different types of medulla neurons. These integrate into developing columns. Another neuroepithelium, the proximal inner proliferation center (pIPC) generates migratory progenitors, that will migrate to the distal inner proliferation center (dIPC), where they convert into neuroblasts and generate distal cells (dc) and lobula plate neurons (lopn). dc, distal cell; dIPC, distal inner proliferation center; GMC, ganglion mother cell; lc, lobula complex; LF, lamina furrow; Ln, lamina neuron; lopn, lobula plate neuron; LPC, lamina precursor cell; me, medulla; Mn, medulla neuron; Nb, neuroblast; OPC, outer proliferation center; pIPC, proximal inner proliferation center.

Several pathways are responsible for neuroepithelial maintenance and neuroepithelia to neuroblast transition regulation in the OPC. Similar mechanism might be used in the IPC, although not much work has focused on this aspect. The progression of l'sc expression is positively regulated through epidermal growth factor receptor (EGFR) signaling and negatively, through Notch signaling (Egger et al. 2010; Ngo et al. 2010; Reddy et al. 2010; Yasugi et al. 2010; Wang et al. 2011b). Increased signaling from the JAK/STAT and EGFR pathways (Yasugi et al. 2008; Ngo et al. 2010; Wang et al. 2011a), or loss of Hippo pathway activity (Reddy et al. 2010; Kawamori et al. 2011) cause delay in the emergence

of neuroblasts. In contrast, loss of the Notch pathway, advances neuroblast progression and causes a premature termination of neuroepithelial growth (Egger et al. 2010; Ngo et al. 2010; Reddy et al. 2010; Yasugi et al. 2010; Wang et al. 2011a).

### **Central brain and ventral nerve cord neurogenesis**

The central brain and the ventral nerve cord emerge from neuroblasts that are specified during embryonic stages (9 to 11). Once these are specified from a proneural field, they undergo EMT, meaning delamination from the embryonic neuroepithelium (Hartenstein et al. 1994).

Delaminated neuroblasts divide asymmetrically several times, generating a self-renewing neuroblast and a differentiating GMC. GMCs will divide once more, giving rise to glia, neurons, or both. Each embryonic neuroblast will form 10 to 20 primary neurons, giving rise to all the neurons of the *Drosophila* larva but only 10% of the adult fly (Reviewed in Homem and Knoblich 2012; Kang and Reichert 2015). Towards the end of embryonic neurogenesis, most neuroblasts in the central brain and VNC exit the cell cycle and enter a mitotic dormancy stage. This is known as quiescence, separating the embryonic and postembryonic phase (Hartenstein et al. 1987; Truman and Bate 1988; Prokop and Technau 1991; Ito and Hotta 1992). Only four neuroblasts, which do not enter quiescence, will keep dividing and generate the mushroom body lineage (Ito and Hotta 1992; Ito et al. 1997).

Further, neuroblasts emerge from quiescence and reenter mitosis during late L1 stage, approximately 8 to 10 h after larval hatching. This second wave of neurogenesis gives rise to secondary neurons. Neurogenesis continues throughout all larval stages up until at pupal stage, neuroblasts exit the cell cycle and disappear (Reviewed in: Knoblich 2010; Homem and Knoblich 2012).

There are two distinct types of neuroblasts, which differ in their asymmetric division mode. Type I neuroblasts make up the majority in the central brain (about 90 per brain lobe) and VNC, and divide asymmetrically generating a GMC and a self-renewing neuroblast (Figure 3) (Reviewed in Homem and Knoblich 2012). The central brain also contains eight mushroom body neuroblasts (4 per brain lobe), which belong to type I neuroblasts. They exclusively generate neurons and glial cells of the mushroom body (Ito and Hotta 1992; Ito et al. 1997). Furthermore, eight type II neuroblasts are located in the dorso-posterior side of the brain hemisphere. They also divide asymmetrically, but generate an intermediate neural progenitor (INP), which generates a GMC as well as another INP, after asymmetric division (Figure 3) (Bello et al. 2008; Boone and Doe 2008; Bowman et al. 2008; Bayraktar et al. 2010; Weng and Lee 2011). INPs divide several times, generating between 6 and 12 neurons or glia. Due to the presence of INPs, type II neuroblast lineages contain many more cells than type I lineages (Bowman et al. 2008; Bello et al. 2008; Boone and Doe 2008).

Similarly to neuroblasts of the optic lobe, each central brain neuroblast sequentially expresses a series of temporal TFs, which dictate the fate of the neurons and glia in the lineage (Kambadur et al. 1998; Brody and Odenwald 2000; Isshiki et al. 2001; Pearson and Doe 2003; Grosskortenhaus et al. 2005).

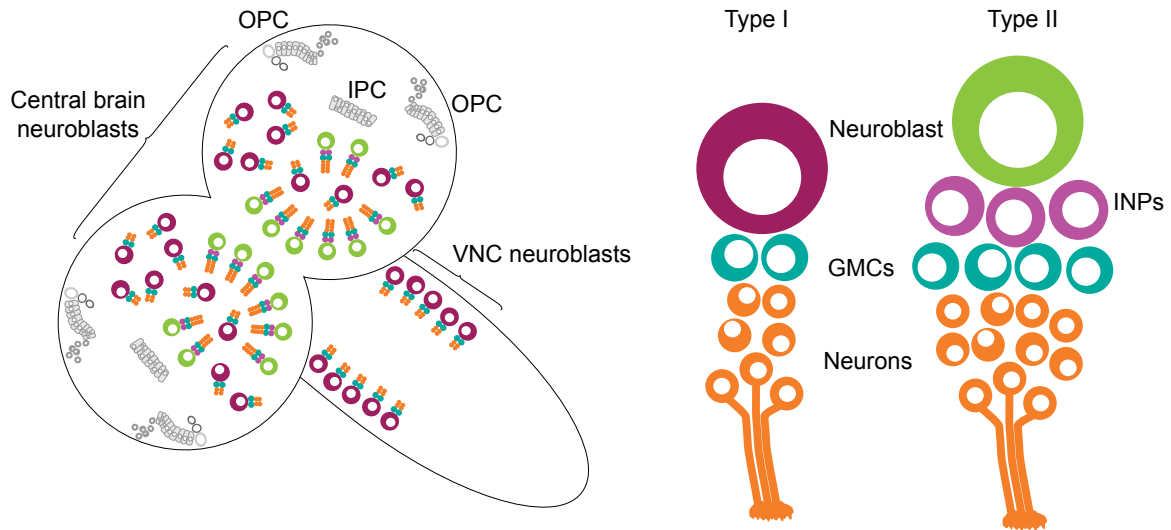


**Figure 3. Neurogenesis in the central brain.** Illustration of late third instar larval brain. Two different types of neuroblasts exist. All neuroblasts in the VNC and the majority in the central brain, are type I neuroblasts. These divide asymmetrically generating a GMC and self-renewing neuroblast. 8 neuroblasts in each central brain hemisphere are type II neuroblasts. These generate INPs, dividing asymmetrically and generating a GMC and self-renewing INP. GMCs divide into two neurons or glia. GMCs, ganglion mother cells; INPs, intermediate neural progenitors; OPC, outer proliferation center; IPC, proliferation center.

Despite the differences in lineage output size, the division patterns of type I and type II neuroblasts are both similar to those seen in the mammalian cerebral cortex. Apical stem cells in the cortex divide to generate another apical stem cell and either a neuron or a basal progenitor cell, with the latter typically dividing once to generate two postmitotic neurons (Haubensak et al. 2004; Miyata et al. 2004; Noctor et al. 2004).

### **DROSOPHILA GLIA: FUNCTIONAL SIMILARITIES WITH VERTEBRATE GLIA**

As aforementioned, NSCs (both neuroepithelial cells and neuroblasts) cannot be considered as isolated entities, as they have to adapt to systemic changes during nervous system development. Extrinsic signals from the neurogenic niche, together with stem cell intrinsic signals are also necessary for the correct regulation of both, optic lobe and central brain neurogenesis. In *Drosophila*, the neurogenic niche is composed exclusively by glial cells, hence, it is important to know the glial types present in the fly CNS and its respective

role. Although initial events in glial specification could be triggered by distinct molecular mechanisms in vertebrates and invertebrates, later molecular aspects of glial morphogenesis and function in the mature CNS are very similar.

*Drosophila* glia are classified according to their association with different brain structures. Three groups exist, being surface glia, associated with the surface of the nervous system, cortex glia, linked to neuronal cell bodies and neuropil glia, associated with neuropil structures (Figure 4) (Reviewed in Hartenstein 2011).

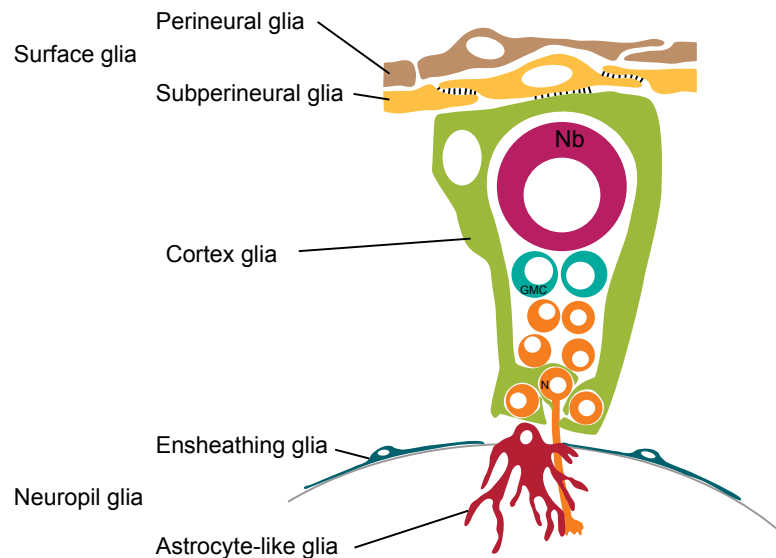


**Figure 4. *Drosophila* glial types.** *Drosophila* glia are classified in three types, surface glia, cortex glia and neuropil glia. Surface glia create the blood-brain-barrier, being composed of two glial layers, the perineural and subperineural glia. Cortex glia wrap neuroblasts and neuronal cell bodies in chambers. Neuropil glia are associated with neuropils, and can be subdivided into two groups, ensheathing glia, wrapping different neuropils and axon tracts, and astrocyte-like glia, being in close contact to synapses. GMC, ganglion mother cell; Nb, neuroblast; N, neuron.

### Surface glia

Surface glia isolate neural elements from surrounding tissues and hemolymph in both, CNS and peripheral nervous system (PNS), forming the blood-brain-barrier (BBB). Two different glial types are responsible for creating the barrier, each one forming one layer: the perineural glial layer lies on top of the subperineural glial layer. The BBB plays a dual role by offering chemoprotection, as well as selective transcellular transport of nutrients (Featherstone 2011; Hindle and Bainton 2014). At early larval stages subperineural glia also trophically support neuroblasts during their reactivation through extrinsic signals (Chell and Brand 2010; Spéder and Brand 2014). In vertebrates, astrocytes, together with endothelial cells, create the BBB, which provides a link between the blood vessels and neurons transporting glucose and other substances out of the bloodstream (Tsacopoulos and Magistretti 1996; Magistretti and Pellerin 1999).



### *Cortex glia*

Cortex glia have extended membranes, wrapped around neuronal cell bodies. The glial processes form a honey-combed like structure, called trophospongium, which invades spaces between neuronal cell bodies, (Hoyle 1986; Hoyle et al. 1986; Dumstrei et al. 2003). They are responsible to trophically support neurons, a role accomplished by astrocytes in vertebrates. Cortex glia also propagate cellular processes to the brain surface and establish close contacts to the BBB and trachea (Ito et al. 1995; Poreanu et al. 2007). Thus, cortex glia might contribute to nutrient/oxygen supply and metabolism. Interestingly, it exhibits activity-dependent calcium oscillations and regulates seizure susceptibility (Melom and Littleton 2013). Many of those functions are accomplished by astrocytes in vertebrates. During development, cortex glia also ensheath the optic lobe neuroepithelia and central brain neuroblasts, creating a glial niche for those stem cells.

### *Neuropil glia*

Neuropil glia are present in neuropil regions and subdivided into two types, ensheathing glia and astrocyte-like glia. Ensheathing glia wrap the neuropils and axon bundles. By contrast, astrocyte-like glia project to the neuropil, forming a dense net, having finest processes close to synapses (Stork et al. 2012; Muthukumar et al. 2014). Similar to axon ensheathing glia, in vertebrates, oligodendrocytes wrap axons and generate sheaths for saltatory conduction of action potentials (Ransom and Sontheimer 1992; Edgar and Garbern 2004), electrically insulating axons and regulating conduction velocity. An important role of neuropil glia has been described in ionic and neurotransmitter homeostasis (Edwards et al. 2012; Stork et al. 2012, 2014) as well as synapse regulation (Tasdemir-Yilmaz and Freeman 2014). This function is accomplished by astrocytes and microglia in vertebrates (Reviewed Chung et al. 2015). Additionally, neuropil glia are responsible for correct axon guidance (Spindler et al. 2009) during development. In the PNS, a type of ensheathing glia, called wrapping glia, ensheath and support peripheral nerves containing motor and sensory axons, much like mammalian Schwann cells (Reviewed in Rodrigues et al. 2011).

Thus, although different glial types are present in vertebrates and invertebrates, the functions they accomplish are conserved (Figure 5).

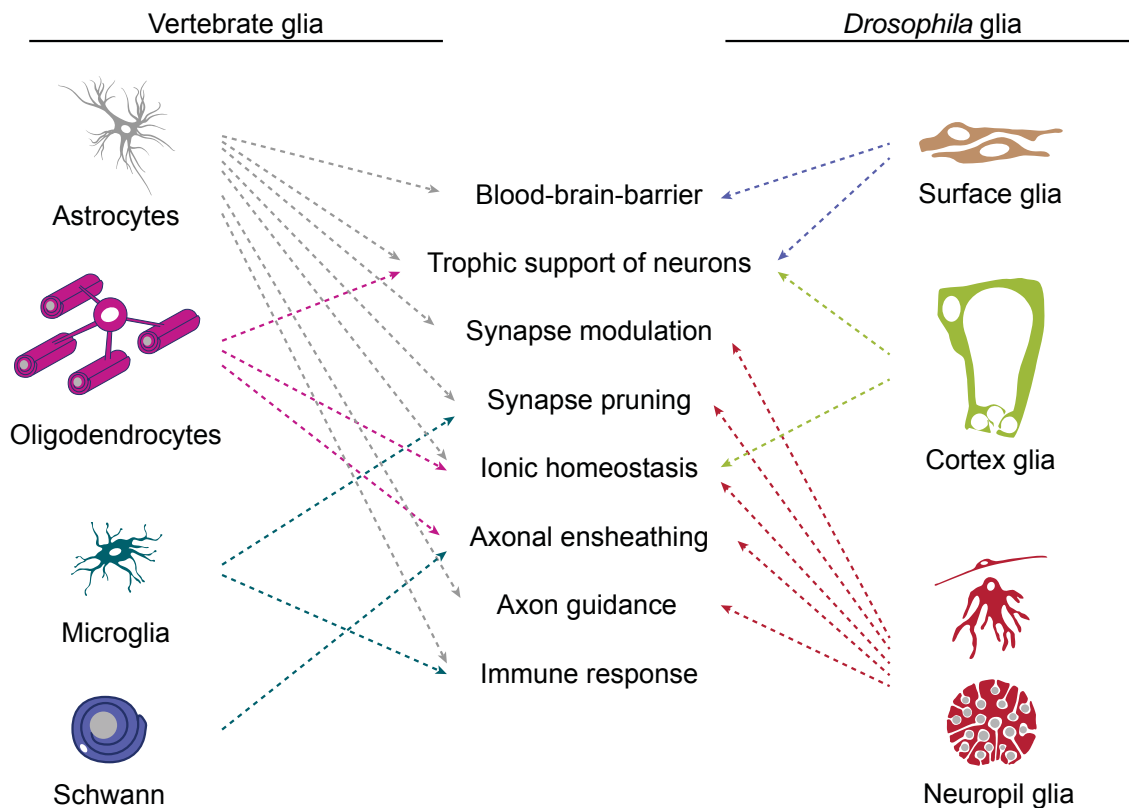


**Figure 5. Comparison of vertebrate and invertebrate glia and their roles.** Although glial types vary from vertebrates to invertebrates, their roles are very similar. For example, different astrocyte roles in vertebrates are covered by different glial types in invertebrates. Hence the specific glial types change, but the functions are conserved.

## THE NICHE: A CLOSE RELATIONSHIP BETWEEN NEUROGENESIS AND GLIA

### The stem cell niche

The concept of the niche in the maintenance of stem cells was first proposed by Schofield, using haematopoietic stem cell as a model (Schofield 1978). He hypothesized that the continuous proliferation of a stem cell population depends on the surrounding cells, which constitute a specialized microenvironment. It is referred to as a niche, and is involved in sustaining long-term cell proliferative capacity.

Today, we know that stem cell niches support the normal function of neural stem cells. In the mammalian CNS, both mechanical and diffusible signals pass between cell populations to influence NSCs. Extrinsic signals from different niche cells (choroid plexus, meninges, blood vessels, pericytes, microglia, etc) provide a permissive environment for appropriate neurogenesis (Reviewed in: Silva-Vargas et al. 2013; Bjornsson et al. 2015). Until today, most of the described extrinsic signals are signaling molecules. For example, microglia secrete several growth factors and cytokines, such as TGF- $\beta$ , that influence neurogenesis (Battista et al. 2006). Moreover, other factors, such as oxygen tension, define the niche

environment (Reviewed in Mohyeldin et al. 2010). These are also important regulators of stem cell characteristics.

In *Drosophila*, several types of stem cells and their associated niches have been identified. Some examples are the niches of male and female germline stem cells and intestinal stem cells (Reviewed in Morrison and Spradling 2008). In these tissues, stem cells reside in close proximity to their surrounding cells, which provide external signals leading to the long-term maintenance of the stem cell identity (Fuller and Spradling 2007).

In the brain, neuroepithelia and neuroblasts also establish a complex cellular microenvironment, which influences their behavior. In contrast to the mammalian neurogenic niche, the niche in *Drosophila* is exclusively composed by glial cells, and is often referred to as the “glial niche”. It is yet to be determined how the niche controls different aspects of neurogenesis. However, some studies have already started to decipher the interactions between glia and neurogenesis.

### **The glial niche and neuroepithelia**

The neuroepithelia grow by symmetric divisions and they convert into asymmetrically dividing neuroblasts. These processes are tightly regulated. Notch, EGFR and JAK/STAT signaling pathways were described to control the transition intrinsically (Yasugi et al. 2008; Egger et al. 2010; Ngo et al. 2010; Reddy et al. 2010; Yasugi et al. 2010; Wang et al. 2011b, 2011a). Nevertheless, recently, some extrinsic signals regulating these pathways have been described as well.

For the first time, Morante and colleagues (Morante et al. 2013) described the “optic-lobe-associated cortex glia” or “surface-associated cortex glia”, a glial cell layer ensheathing the OPC neuroepithelium. This third glial layer lies under the two previously characterized surface glial layers, described as the perineural and subperineural glia. It was shown, that these glia are the source of the EGFR ligand Spitz. Spitz production is regulated by the *mir-8* microRNA, the fly homolog of the human mir-200 gene family of tumor suppressors (Brabletz et al. 2011; Vallejo et al. 2011). *mir-8* negatively regulates Spitz levels, preventing premature and excess signaling in the underlying neuroepithelium (Figure 6). The surface-associated cortex glia play a role in regulating EGFR signaling, controlling the balance between neuroepithelial proliferation and neuroblast emergence. Thus, these glial cells represents a niche that sends signals for neuroepithelial growth and morphogenesis.

Furthermore, it has been shown that the Notch ligand Serrate (Ser), which is expressed in glia, is crucial for determining the correct spatial activation of Notch in the OPC neuroepithelium. The interaction between Ser and Notch restricts EGFR–Ras–PntP1 signaling and hence, *l’sc* expression in the transition zone. Therefore, Ser (present in glia) creates a complex with Cno and Notch (present in neuroepithelial cells), controlling the progression of the proneural

wave in the OPC (Figure 6) (Perez-Gomez et al. 2013). Although the publication suggests that *Ser* is expressed in subperineural glia, published images support the hypothesis that *Ser* expression can be associated to surface-associated cortex glia.

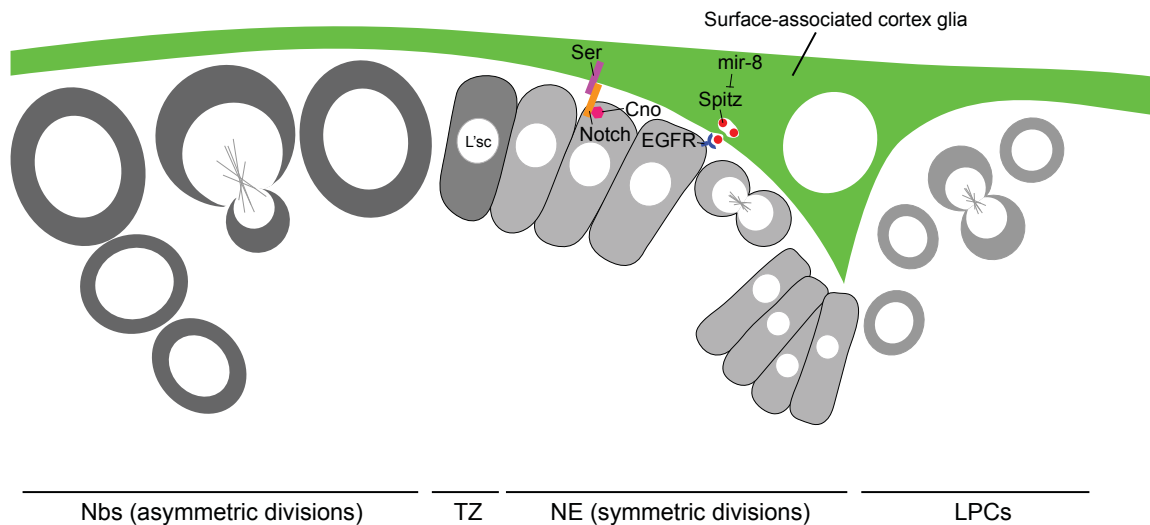


**Figure 6. Illustration of known extrinsic signals in the neuroepithelial glial niche.** Surface-associated cortex glia secretes Spitz, which controls EGFR signaling in neuroepithelial. This extrinsic signal controls the balance between neuroepithelial proliferation and neuroblast emergence. Spitz levels are regulated by *mir-8*. Surface-associated cortex glia also expresses the Notch ligand Serrate, which creates a complex with Notch and Cno, expressed in neuroepithelial cells. This complex is important for the progression of the proneural wave. LPCs, lamina precursor cells; Nbs, Neuroblasts; NE, neuroepithelia; TZ, transition zone.

Overall, the glial niche plays a role in regulating neuroepithelial proliferation and their transition to neuroblasts. However, to unravel aspects associated to the interactions between those cell types more studies are needed.

### The glial niche and neuroblasts

The most studied process, in which glia control neuroblast behavior, is related to quiescence exit at late L1 stage. The first studies proposed, that Anachronism (Ana), a glia secreted glycoprotein, played a critical role in maintaining neuroblasts in quiescence (Figure 7) (Ebens et al. 1993; Datta 1995). Which glial type is responsible for Ana secretion is still unknown.

Moreover, the BBB regulates neuroblast reactivation. Essential amino acids in the larval diet trigger the local production and secretion of insulin-like peptides (dILPs) released by the subperineural glia of the BBB (Figure 7) (Chell and Brand 2010; Spéder and Brand 2014). dILPs bind to Insulin receptors on neuroblasts and activate the PI3K/Akt pathway, leading to neuroblasts exit from quiescence (Chell and Brand 2010; Sousa-Nunes et al. 2011). Early

in larval development, during reactivation, cortex glia architecture allows subperineural glia derived dILPs to reach neuroblasts. After that, cortex glial chamber formation is fully achieved (Figure 7) (Spéder and Brand 2018).

Another pathway regulating the reactivation of neuroblasts is the Hippo signaling pathway (Ding et al. 2016; Poon et al. 2016). Cell–cell contact proteins, Crumbs and Echinoid, are expressed in glial cells and neuroblasts, and by homophilic interactions in *trans* (Figure 7) regulate Hippo and Warts. During reactivation, Crumbs and Echinoid are downregulated in glia. This is a response to nutrition, which inactivates the Hippo pathway and activates Yorkie in the neuroblast (Ding et al. 2016). Echinoid and Crumbs are expressed in glial cells, however, it is not specifically known in which glial types.

It has been described, that overexpression of a dominant negative of the cell adhesion molecule DE-cadherin in cortex glial cells results in reduced proliferation of neuroblasts. Hence, once neuroblasts emerge from quiescence and are mitotically active, the niche keeps controlling their mitotic activity (Dumstrei et al. 2003).

Later during development, the growth of neuroblast lineages becomes largely independent of all dietary nutrients. At this stage, niche glia express a secreted growth factor, *jelly belly* (*Jeb*), which activates its receptor, anaplastic lymphoma kinase (Alk) in neuroblasts (Figure 7), thus promoting constitutive, rather than nutrient-dependent PI3K signaling and growth (Cheng et al. 2011). Based on published images, it looks like *Jeb* is expressed in cortex glial cells, nevertheless the authors do not specify if this is the case.

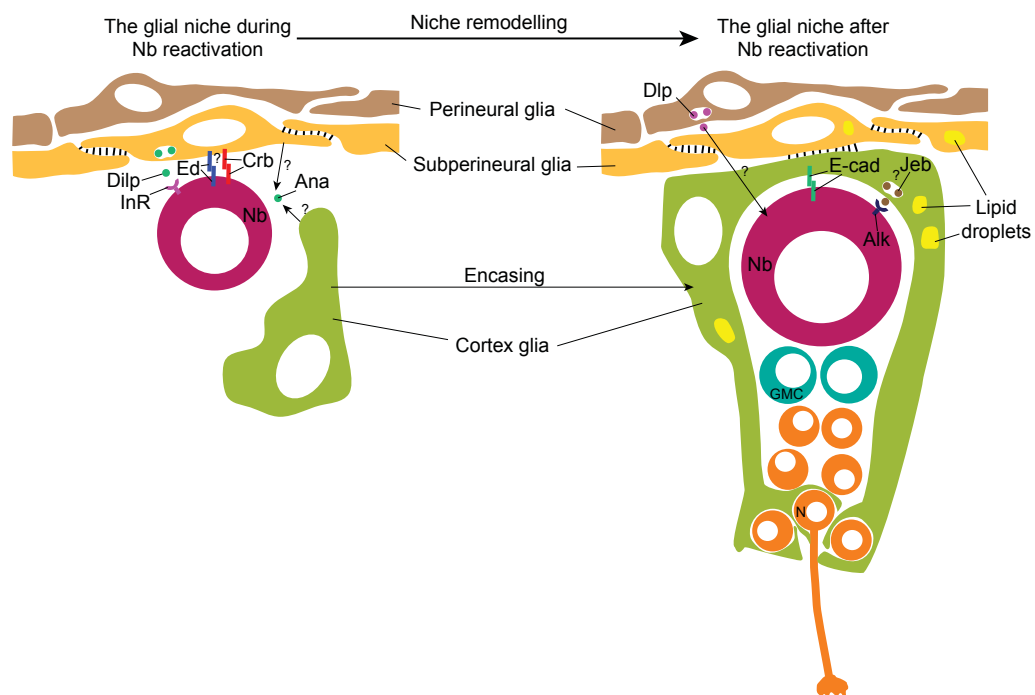


**Figure 7. Illustration of known extrinsic signals in the neuroblast glial niche.** During neuroblast quiescence and reactivation, cortex glial encasing of neuroblasts is not completed. This allows subperineural glial signals to directly reach neuroblasts. After neuroblast reactivation and niche cell remodeling, neuroblasts encasing is fully achieved. The glial type requirement of some signals is unknown, so they are highlighted with a question mark. Also, it is still unknown how Dlp is transported from the perineural glia to Nb.

Furthermore, the glial cell niche also preserves neuroblast proliferation under hypoxia and oxidative stress conditions. Subperineural glia and cortex glia accumulate lipid droplets (Figure 7), which work as antioxidant organelles, defending membrane polyunsaturated fatty acids (PUFAs) from damage by reactive oxygen species (ROS)-induced peroxidation. This helps to safeguard, not only glial cells of the niche, but also neighboring neuroblasts and their neuronal progeny (Bailey et al. 2015).

Perineural glia has also been associated to the glial niche, confirming, that cellular communication between NBs and surface glia is critical for the development of both cell types. Also, Dally-like (Dlp), a heparan sulfate proteoglycan is required in surface glia for proper NB proliferation (Figure 7) (Kanai et al. 2018).

In summary, the glial niche controls neuroblast maintenance at quiescence and neuroblast reactivation. Also, once a neuroblast is reactivated, the glial niche keeps controlling their proliferation and well-being.

## ROLES OF ION CHANNELS IN GLIA

In the CNS, both neurons and glia express ion channels and transporters. However, neurons are excitable cells and glia are not. This means, that channels can accomplish different functions in distinct cell types. While in neurons ion channels and transporters are responsible for the transmission of action potentials (Reviewed in Kress and Mennerick 2009), in glia they accomplish different functions. For example, they regulate the neuronal synaptic activity (Reviewed in Kirischuk et al. 2015). Glia is the cell type that creates the neurogenic niche of *Drosophila*, so the many ion channels in glia could be responsible for niche microenvironment regulation and stem cell well-being.

Further, recent studies have demonstrated that multiple ion channels are present in different mammalian stem cells. They include different  $K^+$ ,  $Na^+$ ,  $Ca^{2+}$ , and  $Cl^-$  channels and have been found heterogeneously expressed in embryonic stem (ES) cells, mesenchymal stem cells from bone marrow, fat tissue and human umbilical cord vein, neural progenitor cells, cardiac progenitor cells, or induced pluripotent stem (iPS) cells derived from different species (Reviewed in Li and Deng 2011). Interestingly, it has been shown, that those ionic channels can regulate proliferation and differentiation of stem cells (Reviewed in Li and Deng 2011). This intrinsic role of ion channels in stem cell regulation is very interesting and supports the hypothesis, that niche ionic concentrations ( $Ca^{2+}$ ,  $Na^+$ ,  $K^+$ ,  $Cl^-$  or  $H^+$ ) are important for stem cells. Because of the lack of information regarding ion channel function in niche cells, this part of the introduction will focus on the functions ion channels carry out in glia. It is possible, that similar functionalities are responsible for the regulation of stem cell behavior in the niche

## Glial ionic regulation

In the 1960s, Kuffler and colleagues did the first physiological studies examining glial cells (Kuffler and Potter 1964; Kuffler et al. 1966; Orkand et al. 1966). These studies showed, that glial cells rest at a more hyperpolarized resting membrane potential, relative to neurons (Figure 8). 50 years later, we know that glial cells express a high variety of ion channels ( $K^+$ ,  $Na^+$ ,  $Ca^{2+}$ , and  $Cl^-$  channels). Although expression and currents of different ion channels have been described in glia, most of their roles remain unknown. Due to the close link between different ion channels and some brain pathologies, studying these in the mature CNS became of great interest (Reviewed in Kim 2014). However, there are almost no examples of ion channels required during CNS development.

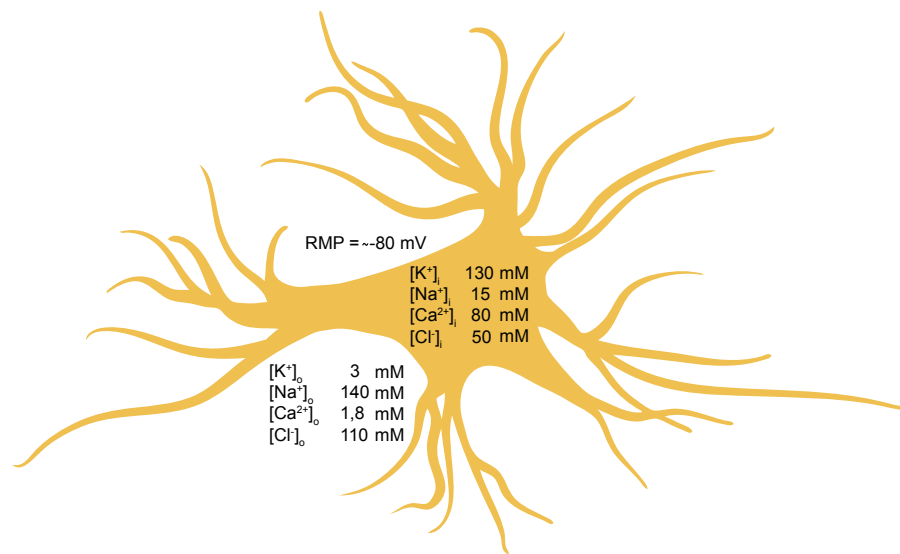


**Figure 8. Extracellular and intracellular ion concentrations of astrocytes.** The resting membrane potential (RMP) is more hyperpolarized than the neuronal one. Potassium ( $K^+$ ) and calcium ( $Ca^{2+}$ ) have higher intracellular concentrations, while sodium ( $Na^+$ ) and chloride ( $Cl^-$ ) concentrations are higher in the extracellular compartment.

Some examples of ion channel functions in glia are described below, when possible, focusing on functions in the developing CNS. As ion channels in *Drosophila* glia are almost unstudied, examples are predominantly taken from mammalian glia.

### Potassium ( $K^+$ ):

In glia, the membrane potential is largely determined by the transmembrane  $K^+$  gradient, because of the predominating  $K^+$  conductance of the glial membrane (Kuffler and Nicholls 1966). The most important and abundant potassium channel in glia is the inwardly rectifying  $K^+$  (Kir) channel Kir4.1, which is responsible for setting and maintaining the resting potential. It is expressed exclusively in glial cells in the nervous system and apart from setting the resting potential, its putative functions include buffering excess extracellular  $K^+$ , the facilitation of glutamate uptake from synapses, and glial cell volume regulation (Olsen et al. 2006; Dibaj et al. 2007; Djukic et al. 2007; Kucheryavykh et al. 2007; Seifert et al.

2009).  $K^+$  has been related to several pathologies, such as, epilepsy, Alzheimer's disease, amyotrophic lateral sclerosis, spinal cerebellar ataxia, among others. Interestingly, the neurodevelopmental syndromes SeSAME/EAST (Bockenbauer et al. 2009; Scholl et al. 2009) and RTT (Kahanovitch et al. 2018) have been related to Kir4.1. In both syndromes, mutations or alteration on Kir4.1 expression lead to neurodevelopmental defects. Underlying mechanisms responsible for these defects are yet to be elucidated.

Furthermore, TWIK1 and TREK1 ( $K_2P$  channels) play a role in the glutamate release from astrocytes (Woo et al. 2012; Mi Hwang et al. 2014). This could facilitate the glutamine-glutamate cycle for replenishment of neurotransmitters in neurons.

Also, some studies have shown, that  $Ca^{2+}$ -activated  $K^+$  channels (BK channels), in astrocytes, are crucial regulators of blood vessel dilation and constriction (Filosa et al. 2006; Girouard et al. 2010).

### Sodium ( $Na^+$ ):

The extracellular concentration of neurotransmitters in the CNS is mainly regulated by glial specific transporters, which use the transmembrane  $Na^+$  gradient as a driving force. Between them, we can find glutamate (EAATs), GABA (GATs), and glycine (GlyT1 and GlyT2) transporters, which take up sodium together with the neurotransmitter (Figure 9) (Reviewed in Kirischuk et al. 2015). This  $Na^+$  dependent neurotransmitter clearance, after a synaptic transmission, is essential for correct signaling between neurons. Moreover, glutamine, released from astrocytes through sodium dependent SNAT3, can be transported directly into presynaptic terminals, to support glutamatergic neurotransmission (Billups et al. 2013).

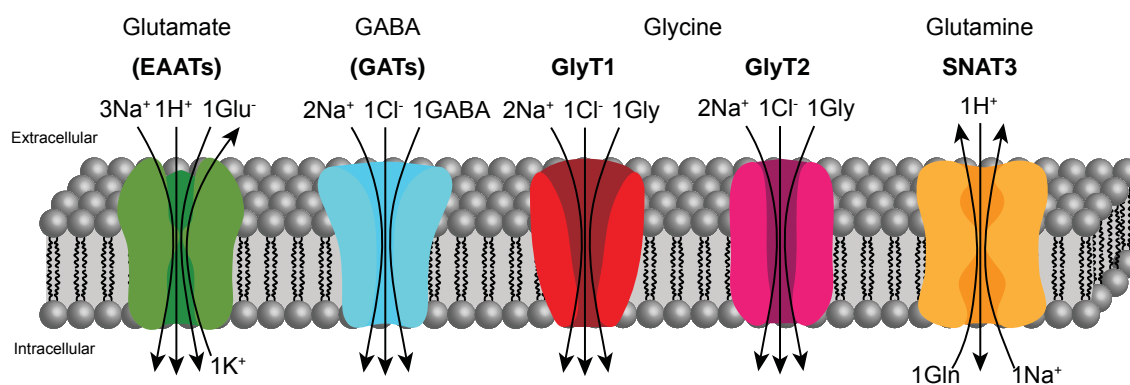


**Figure 9.  $Na^+$  dependent organic molecule transporters.** These channels use the sodium gradient between intracellular and extracellular compartments to transport different organic compounds through the membrane (Modified from Kirischuk et al. 2015).

$Na^+$  fluxes also play a role in the regulation of the astrocytic energy metabolism. This complex mechanism, involving different  $Na^+$  channels and transporters, is used in astrocytes to modulate glucose transport, glycolysis, glycogen degradation, glucose oxidation, and the production of lactate (Reviewed in Chatton et al. 2016).



Upon CNS injury, sodium channels influence the response of reactive glia. In astrocytes, Nav1.5 plays an important role in astrogliosis, where the channel is necessary for correct proliferation and motility (Pappalardo et al. 2014). During microglial response, Nav1.6 is involved in phagocytosis (Craner et al. 2005; Black et al. 2009), chemokine/cytokine release (Black et al. 2009; Morsali et al. 2013), and migration (Black et al. 2009; Persson et al. 2014).

*Calcium ( $Ca^{2+}$ ):*

$Ca^{2+}$  ions act as signaling molecules in all living cells. Activation of metabotropic receptors in the plasma membrane trigger production of inositol 1,4,5-trisphosphate ( $IP_3$ ).  $IP_3$  triggers  $Ca^{2+}$  release from the endoplasmic reticulum via  $IP_3R$  channel.  $Ca^{2+}$  also enters the cell through  $Ca^{2+}$  permeable ionotropic glutamate channels (iGluRs) or voltage-gated calcium channels (VGCCs) in the plasma membrane (Reviewed in Achour et al. 2010). The increase in intracellular calcium concentration leads to exocytosis of neurotransmitters, such as, glutamate, ATP, D-serine, GABA, and prostaglandins, from astrocytes (Figure 10) (Parpura et al. 1994; Bezzi et al. 1998; Newman 2001; Mothet et al. 2005). This mechanism is very important for synapse modulation, where astrocytes are directly activated by neurotransmitters and signal back to neurons to modulate their output. Alterations in glial calcium signaling could also lead to epilepsy (Reviewed in Carmignoto and Haydon 2012).

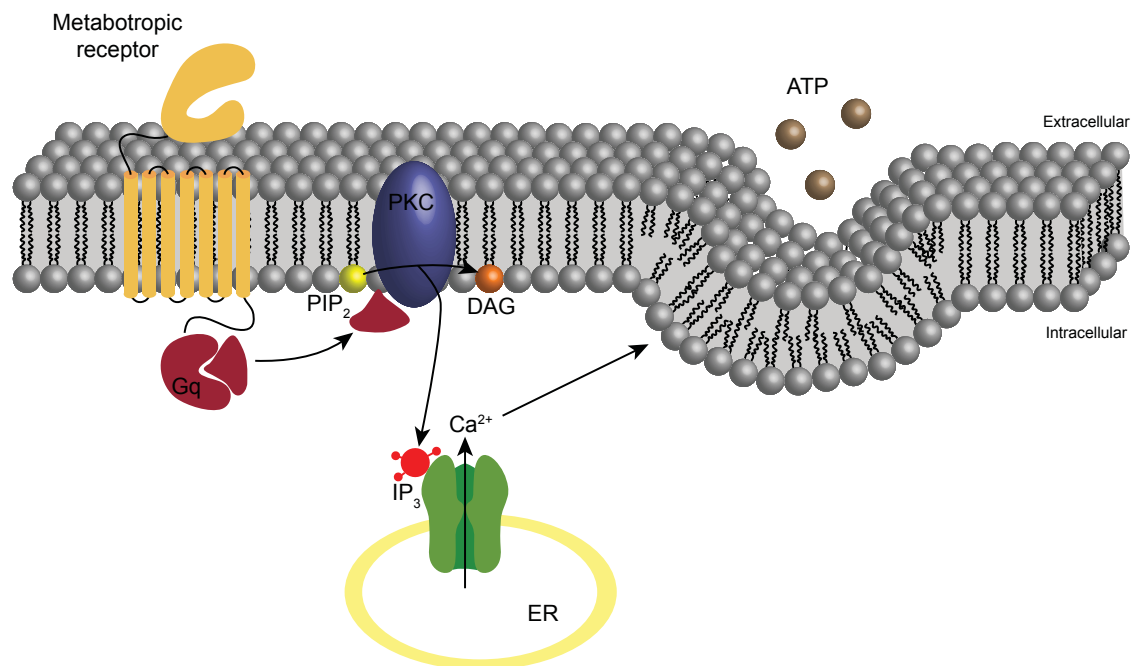


**Figure 10.  $Ca^{2+}$  regulated secretion of neurotransmitters.** Activation of metabotropic receptors in the plasma membrane trigger the production of inositol 1,4,5-trisphosphate ( $IP_3$ ). G-protein activated phospholipase PKC transforms  $PIP_2$  into DAG and  $IP_3$ .  $IP_3$  induces  $Ca^{2+}$  release from the endoplasmic reticulum, via  $IP_3R$  channel. The increase in intracellular  $Ca^{2+}$  concentration triggers exocytosis of neurotransmitters, such as, ATP.

In *Drosophila*, Tdc2<sup>+</sup> neurons release tyramine or octopamine, the invertebrate analogues of norepinephrine, and activate Ca<sup>2+</sup> signaling in astrocyte-like glia, through a metabotropic receptor. This intracellular calcium increase triggers ATP exocytosis, which inhibits dopaminergic neurons. Hence, neuromodulatory signaling, in at least some cases, passes through astrocytes-like glia (Ma et al. 2016).

Moreover, a glial-specific Na<sup>+</sup>/Ca<sup>2+</sup>, K<sup>+</sup> exchanger (zydeco) is required for microdomain Ca<sup>2+</sup> oscillatory activity in cortex glia during development and adult stages. When removed, animals exhibit increased susceptibility to seizures, in response to a variety of environmental stimuli (Melom and Littleton 2013).

#### *Chloride (Cl<sup>-</sup>):*

Chloride is the only anion between the most important ions. However, it is important to highlight that most Cl<sup>-</sup> channels are also permeable for other anions, including amino acids and other organic and inorganic anions. Only very limited information is available regarding chloride channels in glia, since amongst channels, these are the least studied ones.

It is known that volume-regulated anion channels (VRACs) open upon cell swelling and play a role in regulating glial cell volume. In astrocytes, the activity of the VRAC is crucial for restoring astrocyte cell volume, after a hypotonic shock (Hoffmann et al. 2009). Apart from chloride, this channel can also release other organic anions, such as taurine, glutamate, and even ATP (Qiu et al. 2014; Voss et al. 2014; Gaitán-Peñas et al. 2016; Lutter et al. 2017).

In *Drosophila*, the K<sup>+</sup>/Cl<sup>-</sup> cotransporter Kcc and Na<sup>+</sup>/K<sup>+</sup>/2Cl<sup>-</sup> cotransporter Ncc69 are expressed in glia, and exclusive removal of either of them from glia, lead to an increase in seizure-sensitivity and fluid accumulation between glia and axons (Leiserson et al. 2010; Rusan et al. 2014).

Apart from these channels, some members of the Chloride Channel (ClC) family have been described to be expressed in glia as well. During last years, extensive work focused on elucidating possible ClC-2 roles in the mature CNS. ClC-2's *Drosophila* homologue, ClC-a, is the chloride channel that has been studied in this thesis.

## THE CLC FAMILY

CLCs form a large family of proteins that mediate voltage-dependent transport of  $\text{Cl}^-$  ions across cell membranes. They are present in all *phyla*, with nine members present in mammals. Four of them are expressed in the plasma membrane, whereas the other five appear in intracellular membranes functioning as  $\text{Cl}^-/\text{H}^+$  exchangers (Table 1). Interestingly, some of CLCs are expressed in glia, such as CIC-2, CIC-3 and CIC-7.

CLCs are involved in a wide range of physiological processes, including the regulation of resting membrane potential in skeletal muscle, the facilitation of transepithelial  $\text{Cl}^-$  reabsorption in kidneys, and the regulation of pH and the  $\text{Cl}^-$  concentration in intracellular compartments through coupled  $\text{Cl}^-/\text{H}^+$  exchange mechanisms (Poroca et al. 2017).

A $\text{Cl}^-$ channels (cell surface)				
	Gene	Tissue	Function	Disease
Human CLCs	CIC-1	Skeletal muscle	Recover resting membrane potential	Myotonia congenita
	CIC-2	Glia, neurons, kidney, liver, heart, pancreas, skeletal muscle, lungs	Transepithelia transport	Leukodystrophy, azoospermia, retinal degeneration
	CIC-Ka	Inner ear, kidney	Transepithelia transport	Loss of both: Bartter IV
	CIC-Kb			Loss of CIC-Kb: Bartter III
<i>Drosophila</i> CLCs	CIC-a	Malpighian tubules ?	Transepithelia transport ?	

B $\text{Cl}^-/\text{H}^+$ exchangers (Endo/lysosomes)				
	Gene	Tissue	Function	Disease
Human CLCs	CIC-3	Glia, Broad	Ion homeostasis of intracellular vesicles	
	CIC-4	Skeletal muscle, brain, heart	Ion homeostasis of endosomes	Intellectual disabilities?
	CIC-5	Kidney, intestine	Ion homeostasis of early endosomes	Dent's disease
	CIC-6	Neurons	Ion homeostasis of late endosomes	
	CIC-7	Glia, neurons, kidney, liver, bone	Acidification of resorption lacuna in osteoclasts; ion homeostasis of lysosomes	Osteopetrosis, retinal degeneration, lysosomal storage disease
<i>Drosophila</i> CLCs	CIC-b	?	?	
	CIC-c	Malpighian tubules ?	?	

**Table 1. A summary of human and *Drosophila* CLCs.** CLC  $\text{Cl}^-$  channels (A) and intracellular  $\text{Cl}^-/\text{H}^+$  exchangers (B) of humans and *Drosophila* are shown. Their function, and the tissue they are expressed in, is also included. In the case of human CLCs, links to human diseases are shown.

*Drosophila* have three different CICs, one is expressed in the plasma membrane (Cabrero et al. 2014), while the other two are expressed intracellularly (Table 1) (Saha et al. 2015). Their tissue expression, as well as their functions are still unknown, since only very few studies have addressed these topics.

## Mammalian CIC-2

Mammalian CIC-2 is a two-pore homodimeric voltage gated plasma membrane chloride channel (Middleton et al. 1996) (Figure 11) and possesses unique biophysical characteristics and pharmacological properties. These confer its unique cellular functions and distinguish it from other ion channels, mainly through its activation during hyperpolarization conditions and its creation of inwardly rectifying currents. Its voltage dependent gating is modulated by the concentration of  $\text{Cl}^-$  and  $\text{H}^+$ . An increase in the intracellular concentration of  $\text{Cl}^-$  shifts the voltage-dependence to a more positive voltage, activating the channel. CIC-2 is also activated by mild decreases in extracellular pH, although a stronger decrease in pH reduces the current (Niemeyer and Yusef 2004). It is expressed in many tissues and published studies point towards a high degree of conservation and regulation across various species from nematodes to humans (Cid et al. 1995). However, its function *in vivo* is not well understood.

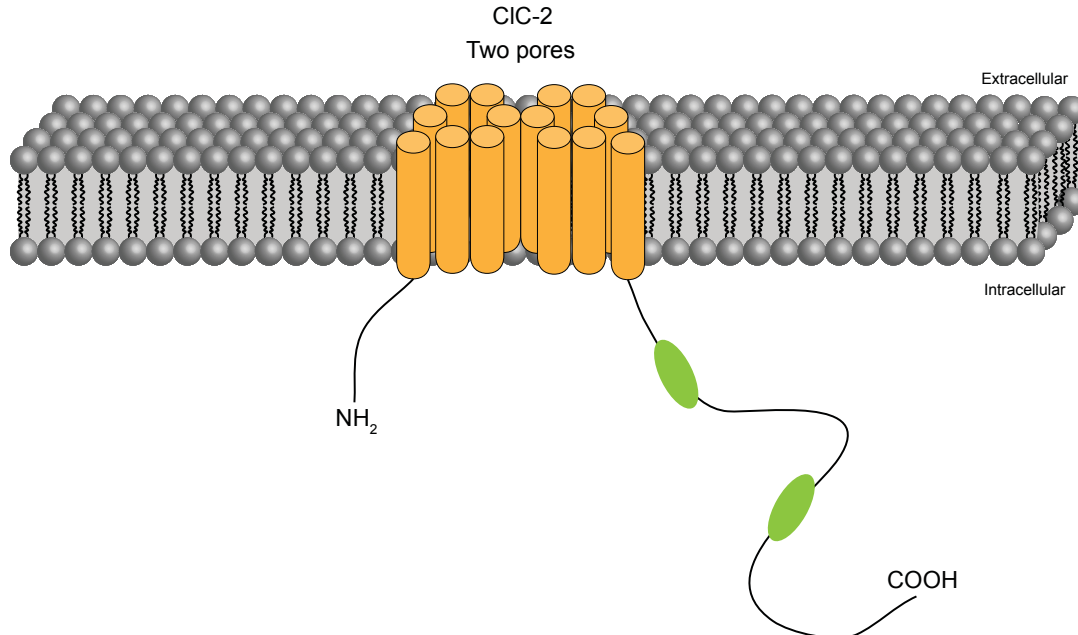


**Figure 11. Molecular/structural features of CIC-2 channels.** The predicted membrane topology of a CIC-2 monomer is shown (Modified from Bi et al. 2014).

A lot of cellular functions have been suggested for CIC-2. One example is its essential role in lung development (Murray et al. 1995), where it acts as an alternative pathway for

Cl<sup>-</sup> secretion in cystic fibrosis (Thiemann et al. 1992), or its link to nephrogenesis, where it plays a key role during early stages (Huber et al. 1998). Moreover, some functions related to neurons, such as the participation in modulation of post-synaptic responses to GABA, have been suggested (Smith et al. 1995).

CIC-2 also shows functions in glia. Knock-out mice develop leukodystrophy (the general term for diseases affecting the growth or maintenance of the brain white matter), which culminates in gradual development of vacuoles in the glial myelin sheath of the central nervous system, worsening with age (Blanz et al. 2007a). Human patients, carrying mutations that disrupt CIC-2 function develop similar leukodystrophy symptoms (Depienne et al. 2013). Hence, human *CLCN2* mutations have been related to different leukodystrophies.

*CLCN2*-related leukoencephalopathy (CC2L), also referred to as leukoencephalopathy with ataxia (LKPAT), is one of those leukodystrophies. Most affected individuals have coordination and balance difficulties (ataxia). Individuals diagnosed during childhood usually also suffer from learning disabilities and mild to moderate mental retardation. Patients with symptoms starting in adulthood typically show additional vision problems. As a result of the reduction in CIC-2 channel activity, certain brain cells and the myelin that surrounds neurons, become filled with too much water and cannot function properly. This has also been confirmed in mice. Since fluid-filled myelin cannot transmit nerve impulses effectively, this results in neurological problems (Depienne et al. 2013; Zeydan et al. 2017).

Another related leukoencephalopathy is the Megalencephalic Leukoencephalopathy with subcortical Cysts (MLC), a rare type of leukodystrophy characterized by dysfunction of the glial cell role in regulating brain fluid and ion homeostasis. Patients affected by MLC present macrocephaly, cysts, and white matter vacuolation, which lead to motor and cognitive impairments. In MLC, CIC-2 works as a subunit of GLIALCAM and mutations on the subunit eliminate the targeting of the channel to cell junctions, causing fluid accumulation, leading to myelin vacuolization (Jeworutzki et al. 2012). CIC-2 is necessary in glia to compensate the considerable increase in intracellular K<sup>+</sup> due to potassium buffering mechanisms (Reviewed in Estévez et al. 2018).

Interestingly, some ionic homeostatic roles in supporting cells have been described for CIC-2. CIC-2 knock-out mice are blind and sterile. In the retina and male gonads, CIC-2 is required in the supporting cells to avoid photoreceptor or male germ cell degeneration. In the testes, Sertoli cells are responsible to nurture germ cells during maturation and differentiation of spermatogonia, creating a niche. Disruption of CIC-2 function results in transepithelial transport defects in Sertoli cells and subsequent degeneration of male germ cells (azoospermia) (Bösl et al. 2001; Edwards et al. 2010). In the retina, the retinal pigment epithelia (RPE) is responsible for forming the blood–organ barrier in the eye, creating the optimal microenvironment for photoreceptor function. CIC-2 is involved in the ionic homeostasis of the narrow subretinal space, that is formed between the RPE and

photoreceptors. The lack of the channel leads to photoreceptor degeneration (Bösl et al. 2001; Edwards et al. 2010). In this case, the channel is necessary for microenvironment regulation for cell survival. Hence, even though not being a niche, the same functional principles are applied.

Keeping this scenario in mind, CIC-2 could have an unidentified role in the neurogenic niche during CNS development, which might explain some of the learning disabilities and mild to moderate mental retardation symptoms observed in human patients.

## **CIC-a**

In *Drosophila melanogaster* three potential *CIC* genes are present, *CIC-a*, *CIC-b* and *CIC-c*, but only *CIC-a* shows homology with mammalian plasma membrane *CIC* genes. *CIC-b* and *CIC-c* are close to mammalian homologs coding for intracellular proteins. *CIC-a* shows high homology (41% residue identity) to the mammalian CIC-2 Cl<sup>-</sup> channel (Flores et al. 2006). Also, *CIC-a* generates inwardly rectifying Cl<sup>-</sup> currents, similar to CIC-2's activation and deactivation characteristics (Flores et al. 2006).

*CIC-a* has been poorly studied in *Drosophila melanogaster*, with very few studies and only one about its functions. CIC-2-like currents have been recorded via patch-clamp technology in photoreceptors (Ugarte et al. 2005) and muscle (Rose et al. 2007). However, *CIC-a* was not identified as being expressed in those tissues. Moreover, similar to CIC-2, *CIC-a* is necessary for transepithelial transport in the Malpighian tubules. It is exclusively expressed in the stellate cells and is required for *Drosophila* kinin-mediated induction of diuresis and chloride shunt conductance (Denholm et al. 2013; Cabrero et al. 2014).

Interestingly, some studies point towards the expression of *CIC-a* in the nervous system, where, by in situ hybridization in the embryo, it could be concluded, that the channel may be involved in glial function (Kearney et al. 2004). Also, some RT-PCR experiments, done with larval central nervous system RNA extracts (Rose et al., 2007), suggest *CIC-a* expression in this tissue.

In summary, *CIC-a* makes a good candidate to investigate the role of ion channels during *Drosophila* CNS development and it could help to describe chloride channel functions in glia during this process.

# OBJECTIVES





Glia act as niche cells in the neurogenic niche of both vertebrates and *Drosophila* during development. The chloride channel *CICN2* is expressed in glia in the mature nervous system of vertebrates and some physiological functions have been proposed. In addition, human patients with mutations in the gene or dysfunction of the protein, have, among other defects, learning disabilities and mental retardation. Since these later symptoms usually arise from errors in the assembly of neural circuits during development, it is possible that CIC-2 has a role in glia during development. Our main goal has been to study the role of its fly homologue *CIC-a* during CNS development.

We propose three specific goals:

- Describe *CIC-a* expression pattern during CNS development, from early larva to adulthood.
- Characterize the first *CIC-a* mutants.
- Study in detail any observed developmental phenotype in *CIC-a* mutants.



# **MATERIALS AND METHODS**



# MATERIALS

## *Drosophila* strains

The *Drosophila* strains used in this work and their origin are indicated in Table 2:

Stock	Origin
<i>MiMIC 14007</i>	Bloomington Stock Center (BL 59247)
<i>MiMIC 05423</i>	Bloomington Stock Center (BL 43680)
<i>CIC-aGFP</i>	Bloomington Stock Center (BL 59296)
<i>05423<sup>CIC-aGal4</sup></i>	Bloomington Stock Center (BL 66801)
<i>Df(3R)PS2</i>	Bloomington Stock Center (BL 37742)
<i>repoGal4 II</i>	A gift from B. W. Jones
<i>repoGal4 III</i>	Bloomington Stock Center (BL 7415)
<i>repoFLP6:2</i>	A gift from C. Klämbt
<i>GMRGal4</i>	Bloomington Stock Center (BL 1104)
<i>mir8Gal4</i>	A gift from J. Morante
<i>UASH2BRFP</i>	A gift from J. Morante
<i>UASH2BYFP</i>	A gift from J. Morante
<i>UASmCD8GFP</i>	A gift from L. Zipursky
<i>UASmCD8RFP.LG</i>	Bloomington Stock Center (BL27398)
<i>25A01Gal4</i>	Bloomington Stock Center (BL49102)
<i>43H01LexA</i>	Bloomington Stock Center (BL47931)
<i>38H02Gal4</i>	Bloomington Stock Center (BL47352)
<i>G-trace</i>	Bloomington Stock Center (BL 28280)
<i>54H02Gal4 (wrapperGal4)</i>	Bloomington Stock Center (BL 45784)
<i>wrapper932i-Gal80</i>	A gift from M. R. Freeman
<i>wrapper932i-LexA</i>	A gift from M. R. Freeman
<i>UAS RNAi CIC-a</i>	Vienna <i>Drosophila</i> RNAi Center (110394)
<i>UAS RNAi Slit</i>	Vienna <i>Drosophila</i> RNAi Center (108853)
<i>Slit<sup>dui</sup></i>	Bloomington Stock Center (BL 9284)
<i>slit<sup>05428</sup> (Slit lacZ)</i>	Bloomington Stock Center (BL 12189)
<i>SlitGFP</i>	Bloomington Stock Center (BL 64472)
<i>UAS-mCD8GFP, lexO-CD2RFP</i>	Bloomington Stock Center (BL 67093)
<i>UAS-Nslmb-vhhGFP4(deGradFP)</i>	Bloomington Stock Center (BL 38422)
<i>UAS-Slit</i>	A gift from I. Salecker
<i>tubGAL4,UASmCD8GFP</i>	A gift from C. Gonzalez
<i>UASsytGFP</i>	A gift from L. Zipursky
<i>hsFLP,FRT19A,tubGal80</i>	A gift from C. Gonzalez
<i>UASGal80</i>	Bloomington Stock Center
<i>Rh1Gal4</i>	A gift from M. Wernet
<i>Rh4EGFP</i>	Bloomington Stock Center (BL 7462)
<i>Rh6lacZ</i>	Bloomington Stock Center (BL 8117)
<i>UASCIC-a</i>	This study
<i>UASRatCIC-2</i>	This study
<i>Tub&gt;Gal80&gt;</i>	Bloomington Stock Center (BL 38879)
<i>FRT82B</i>	Bloomington Stock Center (BL 2051)
<i>EGUF-hid</i>	Bloomington Stock Center (BL 5253)
<i>UAS-Dcr2</i>	Vienna <i>Drosophila</i> RNAi Center
<i>Ey3,5Flpg5d</i>	A gift from L. Zipursky

**Table 2. List of *Drosophila* strains utilized in this work.** The genotype is indicated in the left column and origin in the right one.

Fly strains utilized in this work were maintained in temperature-controlled chambers at 25°C. They were fed with standard fly food (Table 3).

Ingredient	Quantity per litre
Distilled water	1 L
Yeast	64 g
Dextrose	67,2 g
Agar	8,8 g
Flour	40 g
Nipagin (methyl p-hydroxibenzoate)	1,6 g
Propionic Acid	5 ml

**Table 3. Composition of standard fly food.** In the left column ingredients are detailed and in the right the quantity of each one for 1L.

### Antibodies and dyes:

Primary antibodies and dyes used in this work are depicted in Table 4:

Antigen	Host	Concentration	Origin
Chaoptin	Mouse	1:50	DSHB (24B10)
Repo	Mouse	1:50	DSHB (8D12)
DE-cadherin	Rat	1:50	DSHB (DCAD2)
CIC-a	Rabbit	1:100	(Cabrero et al., 2014)
CIC-a	Rabbit	1:100	Gift from R. Estévez
Dpn	Guinea pig	1:2000	Gift from A. Carmena
Lethal of scute	Rat	1:5000	Gift from A. Brand
P-Histone-H3	Rat	1:1000	Abcam (HTA28)
Mira	Rabbit	1:500	Gift from C. Gonzalez
GFP	Chicken	1:800	Abcam (ab13970)
RFP	Rabbit	1:200	Clonetech (632496)
β-Galactosidase	Mouse	1:1000	Promega (Z3783)
Slit	Mouse	1:20	DSHB (C555.6D)
Fas II	Mouse	1:20	DSHB (1D4)
Neurotactin	Mouse	1:10	DSHB (BP106)
Dcp-1	Rabbit	1:200	Cell Signaling (Asp 216)
β-Galactosidase	Rabbit	1:1000	Cappl (0855976, Out of market)
TOPRO-3	-	1:1000	Life technologies (T3605)

**Table 4. List of used primary antibodies and dyes.** Characteristics of each antigen as host, concentration and origin are detailed.

### MiMIC mutants and MiMIC derived strains

MiMIC transposon contains a gene trap cassette flanked by two inverted bacteriophage ΦC31 integrase *attP* sites. The gene trap cassette consists of a splice acceptor followed by stop codons in all reading frames and the EGFP coding sequence with a polyadenylation

signal (Figure 12). When the transposon is inserted in an intron between coding exons and in the orientation of gene transcription, the splice acceptor in the transposon is used instead of the endogenous acceptor in the next exon. The incorrect splicing results in the formation of truncated transcripts (Venken et al. 2011). In some few cases, the splicing machinery can skip the splice acceptor of the insertion and give some wild type protein.

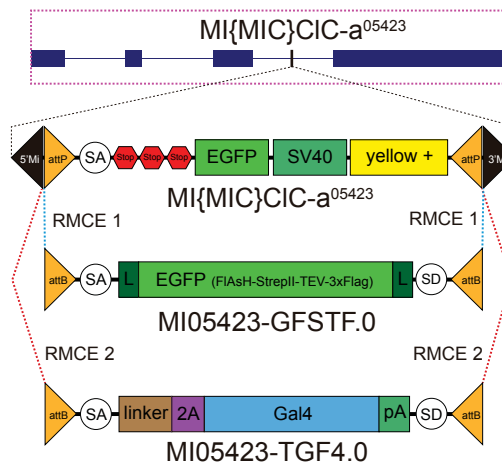


**Figure 12. Genetic structure of *MiMIC05423*, *CIC-aGFP* and *05423<sup>CIC-aGal4</sup>* insertions.** *MiMIC* insertions in coding introns truncate the protein by addition of a splice acceptor, followed by STOP codons. By recombinase-mediated cassette exchange (RMCE), it can be exchanged for other transgenes. In this case the *MiMIC05423* is turned into *CIC-aGFP* (RMCE 1), which adds a GFP tag to the protein, or *05423<sup>CIC-aGal4</sup>* which truncates the protein generating a Gal4 (RMCE 2).

*CIC-a-GFP* and the *05423<sup>CIC-aGal4</sup>* line we have used are derived from *Mi(MiC)CIC-a<sup>05423</sup>*. The *attP* sites flanking the transposon's gene trap cassette allow the replacement of the intervening sequence with any other sequence through recombinase-mediated cassette exchange (RMCE) (Figure 12). The protein trap cassette used to generate *CIC-a-GFP* contains the GFSTF tag (EGFP-FIAsh-StrepII-TEV-3xFlag) flanked by flexible linkers on both sides in the appropriate phase (Nagarkar-Jaiswal et al. 2015a, 2015b). The *CIC-a* tagged protein generated includes the GFP sequence in frame in an extracellular loop that corresponds to the beginning of helix M of the (vertebrate) protein. Homozygous animals are viable and show no phenotypes, indicating that the *CIC-a-GFP* protein is functional.

To generate the *05423<sup>CIC-aGal4</sup>* line a Trojan-Gal4 cassette in the appropriate phase was used. This cassette contains a splice acceptor that ensures that the T2A-Gal4 open reading frame is included in the mRNA of the *CIC-a* gene (Figure 12). The T2A sequence truncates the native gene product translation and promotes the separate translation of Gal4. Hence, a mutant allele is generated that expresses Gal4 under the control of *CIC-a* regulatory sequences.

# METHODS

## Immunohistochemistry

Fly brains were dissected in Schneider medium and fixed in 4% PFA in PBL (75mM lysine, 37mM sodium phosphate buffer pH 7,4) for 25 min. After fixation, the tissue was washed in PBS with 0.5% Triton-X-100 (PBST) and blocked with PBST with 10% normal goat serum. Primary and secondary antibody incubations were in PBST and 10% normal goat serum, typically overnight at 4 °C. Brains were mounted for confocal microscopy in Vectashield (Vector Laboratories).

The Alexa Fluor 488, 568 and 647 secondary antibodies raised in rabbit, mouse, rat, guinea pig or chicken (Life technologies) were used at 1:250 concentration.

## Imaging

Images were acquired with a Leica TCS SPE and a Zeiss LSM 880 confocal microscopes and processed using imageJ (W. S. Rasband, National Institutes of Health, Bethesda, Maryland, <http://rsb.info.nih.gov/ij/>, 1997–2009), Adobe Photoshop and Adobe Illustrator. For 3D reconstruction images Imaris 8.0 software (Bitplane, South Windsor, CT, USA) was used.

### Brain measurements

To assess brain size at different larval stages in controls and CIC-a mutants, larval brain hemisphere diameter were measured in the antero-posterior axis using imageJ.

To assess adult optic lobe and central brain size, we measured the antero-posterior and dorso-ventral axis using imageJ and multiplied them, obtaining an arbitrary unit (a.u.) parameter (Figure 13).

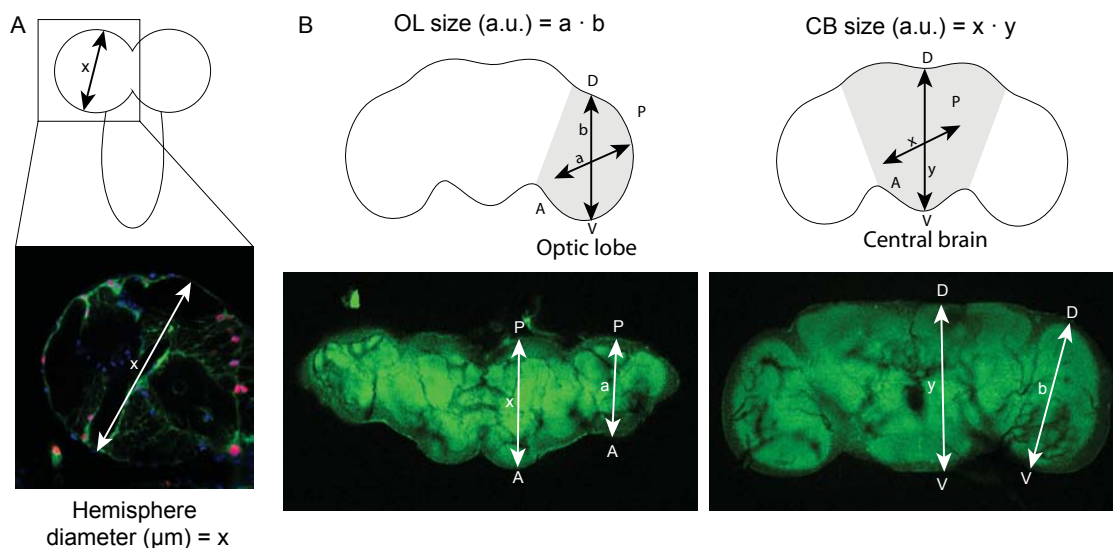




**Figure 13. Brain measurements.** (A) Larval brain hemisphere diameters were measured in the antero-posterior axis, x. (B) Adult optic lobe and central brain were measured in the antero-posterior (a for the optic lobe, x for the central brain) and the dorso-ventral axis (b for the optic lobe, y for the central brain). After multiplying them, we obtained the volume of those parts of the brain in arbitrary units (a.u.).

### *Photoreceptor phenotypes*

We classified adult brains depending on photoreceptor phenotype strength in four categories: No phenotype, Weak, Medium and Strong. We observed that phenotypes in both optic lobes of the same brain were not independent, as a strong phenotype in one optic lobe will be accompanied with a strong or medium phenotype in the other optic lobe, but never with no phenotype. Because of that, instead of doing the classification by optic lobes, we classified the phenotypes by brains, taking into account the strongest phenotype between the two optic lobes to determine the strength of the brain.

### *Neuroepithelia volume measurement in 3D*

To measure neuroepithelia volume in controls and *CIC-a* mutants, neuroepithelia were labelled by anti-E-cadherin antibody and manually segmented using the “SURFACE” tool of Imaris 8.0 (*Bitplane*, South Windsor, CT, USA). The surface tool provides the volume in  $\mu\text{m}^3$  of the generated surfaces.

### *Counting of nuclei*

To assess cell number for different experiments, we manually counted the nuclei in confocal stacks using the Cell Counter plugin of imageJ, which keeps track of the counted dots and helped us to be more accurate.

For glial cells in the glial barrier, Repo<sup>+</sup>, CIC-a<sup>+</sup> nuclei were counted.

For cells in MARCM clones, we used TOPRO-3 staining and membrane labelling to identify individual cells.

For INPs in the DL1-2, we used Dpn staining and type II neuroblast lineage labelling R9D11tdtomato membrane labelling to identify them. When the two lineages were close, we took advantage of labelling cortex glial membranes and identify cells belonging to one lineage chamber or the other.

### *Measuring cell death*

To assess cell death levels in controls and *CIC-a* mutants, we manually counted Dcp-1<sup>+</sup> puncta per brain hemisphere. To avoid background dots and be sure Dcp-1<sup>+</sup> puncta belonged to cells, we helped by labelling nuclei by TOPRO-3. Then, we obtained the volume of the hemispheres manually segmenting them using the “SURFACE” tool of Imaris 8.0 (*Bitplane*, South Windsor, CT, USA). Dividing the two parameters, we obtained the Dcp1<sup>+</sup> puncta per  $\mu\text{m}^3$ .

## DL1-2 axonal tracts

To assess DL1-2 axonal tract path in reference to the mushroom body we used the *R9D11tdtomato* driver, which labels the type II lineages, together with their axons, combined with FasII staining. We manually segmented the axonal tracts and the mushroom body using the “SURFACE” tool of Imaris 8.0 (*Bitplane*, South Windsor, CT, USA).

## DeGradFP

The deGradFP technique (degrade Green Fluorescent Protein), is a genetically encoded method for direct and fast depletion of GFP tagged proteins (Caussin et al. 2012). A target protein fused to a GFP would be specifically degraded through the proteasome by a GFP recognizing nanobody (NSImb-vhhGFP4) expression.

## G-trace

This system reveals real-time Gal4 expression, but also marks cell lineages derived from Gal4-expressing cells. The key feature is that the initiation of lineage reporter expression is Gal4-dependent whereas maintenance of lineage reporter expression is not. G-TRACE makes use of fluorescent protein reporters for both real-time analysis (RFP) and lineage-based analysis (enhanced GFP (EGFP)), thereby increasing screening throughput as there is no requirement for antibody staining (Evans et al. 2009).

To initiate lineage tracing, Gal4 mediates the expression of FLP recombinase, which in turn removes an FRT-flanked transcriptional termination cassette inserted between a Ubiquitin-p63E (Ubi-p63E) promoter fragment and the EGFP open reading frame. Thereafter, the Ubi-p63E promoter maintains EGFP expression perpetually in all subsequent daughter cells, independent of Gal4 activity (Figure 14) (Evans et al. 2009).

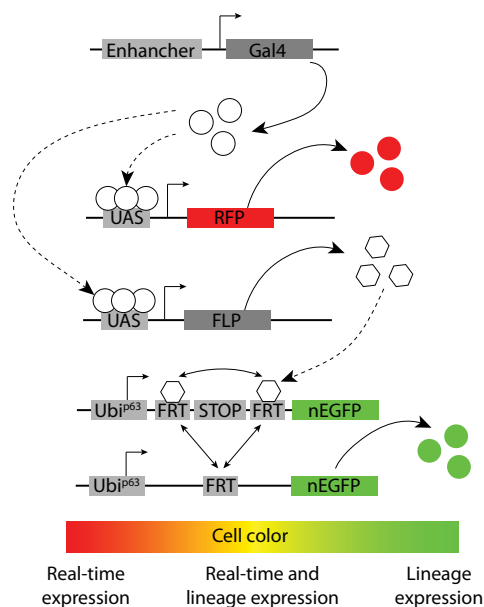


**Figure 14. Schematic of the molecular mechanisms of the G-TRACE system.** The Gal4 activates the expression of nuclear RFP and FLP recombinase. Cells expressing FLP recombinase then excise the FRT-flanked stop cassette separating the Ubi-p63E promoter and nuclear EGFP (nEGFP) open reading frame. This initiates expression of EGFP, which is heritably maintained in all daughter cells. The 'cell color' gradient represents the apparent color of cells after initiation of Gal4 expression. (Modified from Evans et al. 2009).

### FRT82B-MiMIC recombination

The MiMIC-*CIC-a* alleles were recombined in the same chromosome as FRT82B, a target for FLP recombinase (Xu and Rubin 1993), which is located near the base of 3R chromosome arm. The FRT82B has a neomycin resistance. Females laying recombined eggs were kept in vials with G418 neomycin (0,5 mg/ml) (Steller and Pirrotta 1985). The egg containing vials were heat-shocked for 30 minutes to enhance the expression of the neomycin resistance gene. Only the larvae containing the FRT will grow up in the neomycin food, allowing the selection of possible recombinants.

### Clones

#### *EGUF/hid*

The EGUF/hid is a genetic method for generating *Drosophila* eyes composed exclusively of mitotic clones of a single genotype (Stowers and Schwarz 1999). This method combines the GAL4/UAS system (Brand and Perrimon 1993), and the FLP/FRT system (Xu and Rubin 1993). A GAL4 is expressed under the enhancer of *eyeless*, a gene expressed in eye precursor cells (eyGAL4) and UAS construct is combined with the flipase (UAS-FLP) (Duffy et al. 1998). When the matched homologous chromosomes containing FRTs are present in the cell, FLP mediated mitotic recombination occurs (Figure 15). To eliminate all photoreceptor cells that are not homozygous for the mutation of interest, a chromosome containing an FRT and a dominant photoreceptor cell lethal transgene GMR-hid is used. This transgene kills photoreceptors because of eye-specific expression of cell death gene *hid* under the GMR enhancer. This enhancer drives expression of gene *hid* much after mitotic clones are induced under *eyeless* enhancer. To improve this method, a recessive cell lethal mutation was added to the chromosome arm containing the GMR-hid. Because GMR-hid induce cell death after cell division in the developing eye is ceased, there is relatively little developmental time left before adulthood for the eye to compensate for the injury. Adding a recessive cell lethal mutation the eye disc has more time to make compensations, because homozygous cells for this chromosome arm would die immediately after recombination, producing a recombinant adult eye that more closely resembles wild type (Stowers and Schwarz 1999). Flies were developed at 25°C and dissected immediately after emerging.

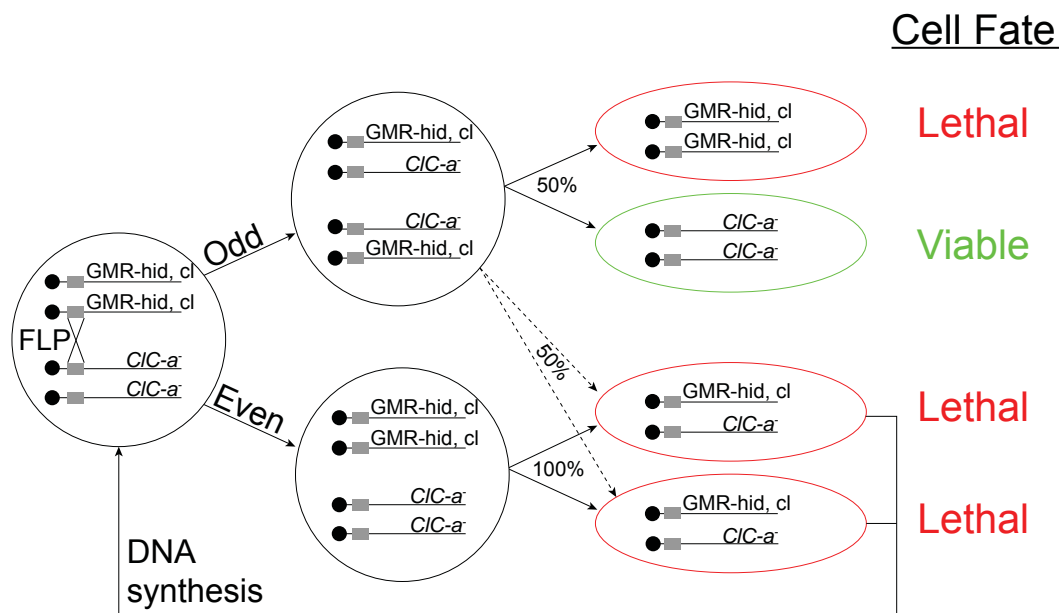


**Figure 15. Schematic of the EGUF-hid method.** Divisions after FLP-mediated mitotic recombination between homologous chromosome arms are shown. Photoreceptors containing *GMR-hid* will die, so as the cells containing recessive *cl* mutation in homozygosis, allowing homozygosis for the mutant allele in the whole eye. (Modified from Stowers & Schwarz, 1999).

## MARCM

The Mosaic Analysis with a Repressible Cell Marker or MARCM is a genetic mosaic system in which a dominant repressor of a cell marker is placed in *trans* to a mutant of interest. Mitotic recombination events between homologous chromosomes by a flipase, generate homozygous mutant cells, which are exclusively labeled due to loss of the Gal80 repressor (Lee and Luo 1999). This method combines the FRT/FLP system and the GAL4/UAS system with the GAL80, a protein that antagonizes GAL4 activity by binding to the activation domain of GAL4. We did two different types of MARCM clones:

-Mutant MARCM clones in a heterozygous background

The technique allowed us to determine the behavior of *CIC-a* mutant clones in a heterozygous background, where *CIC-a* will be only removed from clones. All the other cells in the organism will have one wild type copy of the gene.

For generation of *CIC-a* mutant photoreceptor MARCM clones, we used the flipase *ey3.5FLPg5d*, a FLP that is expressed in the precursor cells of photoreceptors. Clones were labelled by an actGAL4 and *UASsytGFP*. The actin enhancer drives the expression of GAL4 and in the absence of GAL80. The GAL4 will activate the expression of GFP, obtaining labeled homozygous mutant photoreceptors after FLP mediated recombination

(Figure 16). Flies were developed at 25°C and dissected immediately after eclosion.

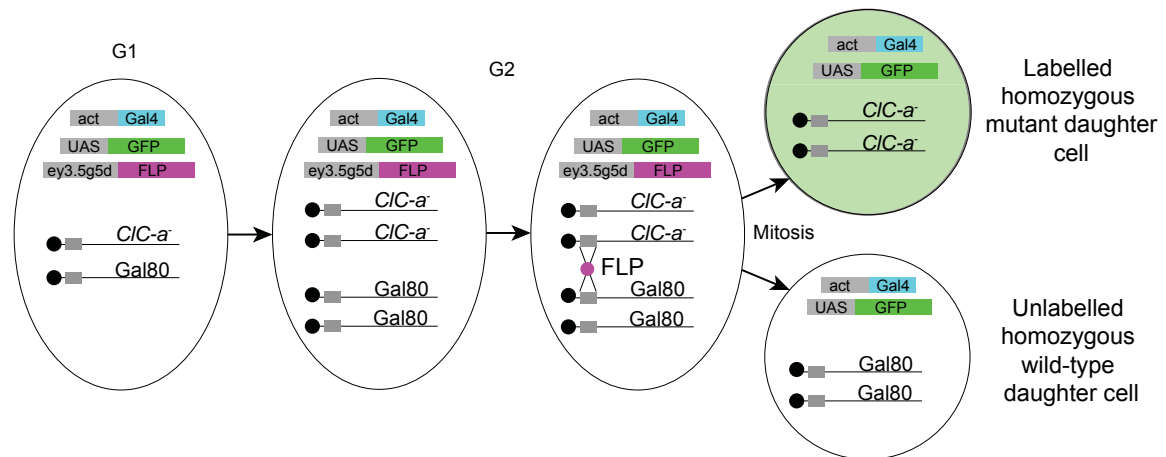


**Figure 16. Schematics for MARCM clones in a heterozygous mutant background.** Mitotic division after FLP mediated mitotic recombination. Homozygous mutant clones will not contain the GAL80 repressor and will express the GFP marker. The clones will be the only homozygous mutant cells in the animal. (Modified from Lee and Luo, 1999).

#### MARCM clones in homozygous mutant background

This technique allowed us to determine the proliferation of neuroepithelial and neuroblast clones in a homozygous mutant background, where all cells of the organism will be mutant for *CIC-a*. The glia that is in close contact with the clones and normally expresses the channel, will not express it. This is achieved due to the localization of the mutation in a different chromosome from the one that will mitotically recombine. For generation of MARCM clones, we used the *hsFLP*, a FLP that is expressed after heat-shock induction. The flipase will mitotically recombine the homologous chromosomes of the cells that are in mitosis during the heat-shock. Clones were labelled by an *actGAL4* and *UASmCD8GFP* (Figure 17).

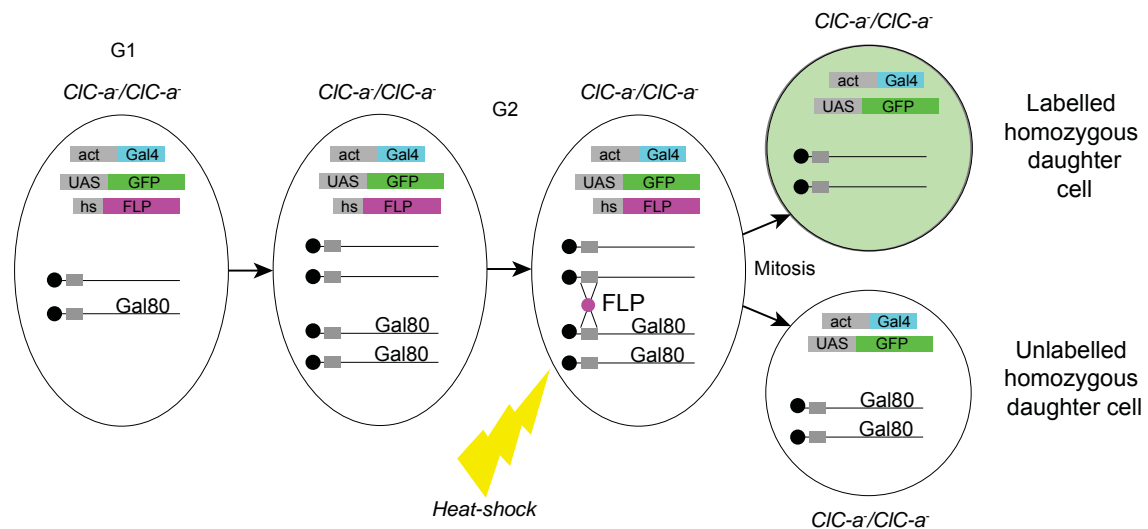


**Figure 17. Schematics for MARCM in homozygous mutant background.** Mitotic division after FLP mediated mitotic recombination. Clones will not contain the GAL80 repressor and will express the GFP marker. All the cells in the animal are homozygous mutant. (Modified from Lee and Luo, 1999).

To stage the larvae, flies were left for egg-laying for 3 hours. After 48 hours after egg lay (AEL) the vials were heat-shocked (Figure 18) in the water-bath during 30 minutes at 37°C. After 48 hours, at 96h AEL, larvae were collected and brains dissected. Apart from the heat-shock, larvae were kept at 25°C.

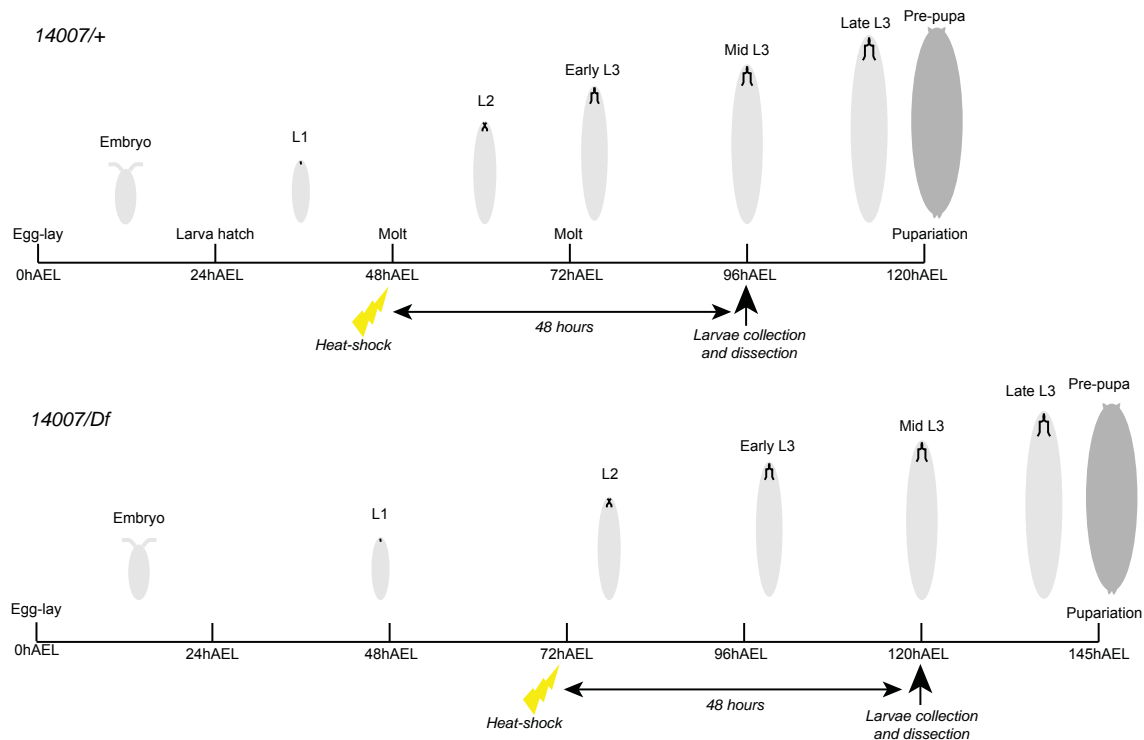


**Figure 18. Schematics for the design of induced MARCM clones.** For *14007/+* controls, larvae were heat shocked at early L2 (48h AEL) and collected for brain dissection 48 hours later at mid L3 (96h AEL). For *14007/Df* mutants, larvae were heat shocked at 72h AEL, 24 hours later due to the developmental delay and collected for brain dissection 48 hours later at mid L3 (120h AEL).

For the mutant, due to the developmental delay of 24 hours, we heat-shocked the larvae at 72h AEL and dissected at 120h AEL, shifting both time-point for 24 hours. The same as for the control, we left the clones grow for 48 hours (Figure 18).

### Construction of transgenics

For generation of UAS-CIC-a and UAS-Rat-CIC-2 transgenes, we cloned the cDNA of *CIC-a*'s isoform C within the plasmid pBID-UASC-G (Addgene plasmid #35202) in collaboration with Raul Estevez's group. The isoform C was chosen because it was previously tested for electrophysiological properties in *Xenopus oocytes* (Jeworutzki et al. 2012) and HEK-293 cells and described to be expressed in *Drosophila*'s head and body (Flores et al. 2006). Plasmids were injected in embryos and by germ-line specific  $\Phi$ C31 integrase-mediated transgenesis (Thorpe and Smith 1998), transgenic flies were obtained.  $\Phi$ C31 integrase-mediated transgenesis systems are based on the site-specific bacteriophage PhiC31

integrase which mediates sequence-directed, irreversible and highly efficient integration between a bacterial attachment site (*attB*) and a phage attachment site (*attP*). Injecting plasmid containing *attB* site and white marker into *attP*-containing docking site strain(s) with PhiC31 activity makes the resultant stable *w<sup>+</sup>* transformants containing the plasmid of interest between *attL* and *attR* sites. Both UAS-CIC-a and UAS-Rat-CIC-2 were inserted at *attP40* site (band 25C6) in the 2<sup>nd</sup> chromosome and *attP3B* (band 62E1) in the 3<sup>rd</sup> chromosome.

## PCR

Standard PCRs were used for recombinant validation of *MiMIC14007* with different *w<sup>+</sup>* transgenes. MiMICs have a *y<sup>+</sup>* marker that could be followed if working in a *y* mutant background. As we were not working in that background, we identified the *MiMIC14007* flies were identified by PCR, using primers for the EGFP inserted in the MiMIC. All reaction components were assembled on ice and quickly transferred to a preheated thermocycler. Primers:

EGFP FWD ACGTAAACGGCCACAAGTTC

EGFP RV TGCTCAGGTAGTGGTTGTCC

A list of components for a classical PCR reaction are depicted in Table 5.

Ingredient	Volume
Template DNA	2µl
10mM dNTPs	0,5µl
25Mm MgCl <sub>2</sub>	1,5µl
20mM Primer FW	1µl
20mM Primer RV	1µl
5x Taq reaction Buffer	4µl
Taq polymerase	0,2µl
H2O	9,8µl
Total volume	20µl

**Table 5. List of components of a classical PCR reaction.** Left column shows all necessary components for standard PCRs and right column indicates the quantity of each one for a final volume of 20 µl.

## Statistics

When the data followed a normal distribution, the parametric one-way ANOVA and t-student test was used to obtain p-values. The graphics are depicted showing the mean value with error bars indicating the Standard Deviation.

In cases where the data did not follow a normal distribution or we multiplied different parameter to obtain the data, the non-parametric Kruskal-Wallis and Mann-Whitney test was used to obtain p-values. The data is shown using box-plots, where the box shows the first and the second quartiles. The band inside the box is the second quartile (the median) and the ends of the whiskers the minimum and maximum of all of the data.



# RESULTS



## **CHAPTER I:**

# **The CIC-a expression pattern and characterization of CIC-a mutants**



## CIC-a channel expression in glia of the developing brain

*CIC-a* has been poorly studied in the *Drosophila*'s brain, so we started characterizing its expression pattern. We first used a published antibody against *CIC-a* (Cabrero et al. 2014) to determine its expression by immunostaining in late third instar larval brains (120h After Egg Lay (AEL)). This antibody has been previously used to describe expression in stellate cells of the Malpighian tubules, which we also observed when doing the same experiment as Cabrero and colleagues (Figure 19A).

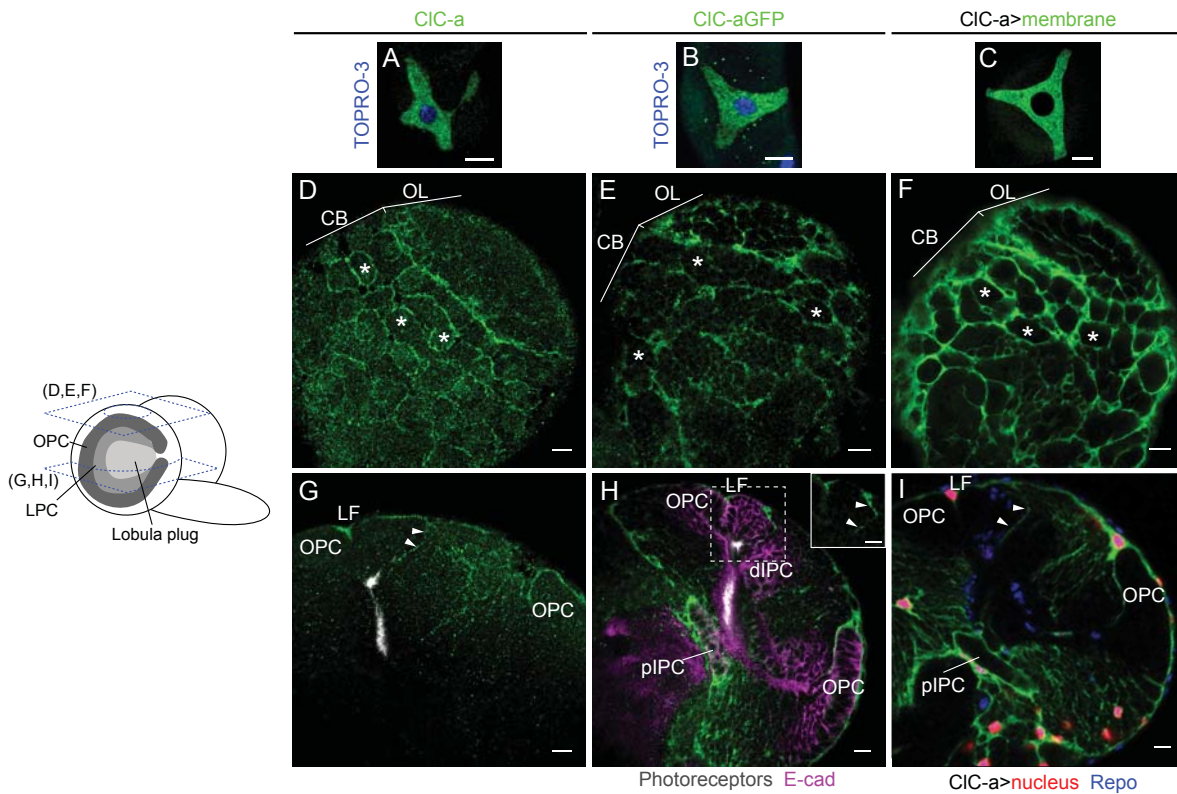


**Figure 19. *CIC-a* expression in the developing brain.** (A-C) *CIC-a* expression (green) in stellate cells of adult Malpighian tubules. Staining was carried out with the *CIC-a* antibody (A), a *CIC-aGFP* reporter (B) and via *05423<sup>CIC-aGal4</sup>* mediated membrane (*UAS-mCD8GFP*) labeling (C). (D-F) A horizontal view of the surface of the larval brain hemisphere (see illustration). In the illustration, the OPC is depicted in dark grey, the lamina precursor cells (LPC) in medium-grey and the lobula plug in light grey. *CIC-a* is expressed in the surface of the central brain, where *CIC-a*<sup>+</sup> cells compartmentalize it, creating what resembles central brain neuroblast glial chambers (asterisks). (G-I) A horizontal view of a deeper brain area focusing on the optic lobe (see illustration). *CIC-a* is expressed on top of the OPC neuroepithelium, with the highest concentration in the lamina furrow. A cellular process between the developing lamina and lobula plug is observed (see arrowheads). In (H), *CIC-aGFP* labels inner tissues allowing to see the expression of *CIC-a* around the IPC neuroepithelium, labeled by E-cad (magenta). Photoreceptors are labeled by 24B10 (grey). In (I), *05423<sup>CIC-aGal4</sup>* mediated membrane labeling leads to very similar result, as observed with *CIC-a* antibody and *CIC-aGFP* staining. The *CIC-a*<sup>+</sup> nuclei (labeled using an *UAS-H2BRFP*) could be observed on top of the OPC and in cortical areas where it colocalizes with the Repo (blue) nuclei. CB, central brain; dIPC, distal inner proliferation center; LF, lamina furrow; OL, optic lobe; OPC, outer proliferation center; pIPC, proximal inner proliferation center. Scale bars represent 10 μm.

In the *Drosophila* brain, we detected signal in the optic lobe's surface, more specifically on top of the OPC neuroepithelium, and with the strongest signal in the lamina furrow (Figure 19G). Additionally, a thin line between the developing lamina and lobula plug was labeled (Figure 19G). In the central brain, we observed *CIC-a* expression in the surface. The pattern of such expression seemed to create chambers, similar to the glial chambers that encase the central brain neuroblasts (Figure 19D). The antibody seemed to not penetrate well into deeper tissues and although we created our own antibody, to obtain better performance (in collaboration with Raúl Estévez's group), we did not achieve improvement of the signal or see it penetrate into deeper tissue zones. We tried different concentrations and even used a Pierce Immunostain Enhancer (ThermoFisher), none of which led to improvements. This could be due to the low expression the protein has in brain tissues.

To better assess protein localization, we used a MiMIC derived *CIC-a-GFP* protein trap line. The reporter labeled stellate cells of the Malpighian tubules (Figure 19B), therefore being useful to assess *CIC-a* expression. The signal obtained in homozygous animals was very low, so we used an anti-GFP antibody to increase the signal. Unlike *CIC-a* antibody, the reporter was labeling deeper tissues in the brain. On the surface, we could observe the same cells expressing *CIC-a*, as when using the antibody (Figure 19H). *CIC-a* was not only expressed surrounding the OPC neuroepithelium (Figure 19H), but also around the IPC neuroepithelium (p-IPC and s-IPC) (Figure 19H). Signal was also observed in the medulla cortex (Figure 19H), medulla neuron cell bodies are located there. In the central brain surface, *CIC-a* showed a pattern, that resembled neuroblast glial chambers (Figure 19E). Interestingly, we could also see the mentioned thin line separating the developing lamina and lobula plug (Figure 19H).

Although the above used tools allowed us to describe a general expression pattern of the protein, we used a MiMIC derived  $05423^{CIC-aGal4}$ , reporting *CIC-a* expression from the endogenous gene locus, to further describe the expression pattern in detail during development. We want to note that  $05423^{CIC-aGal4}$  is a Trojan Gal4, so it creates a truncated *CIC-a* protein in order to generate Gal4. We used the Gal4/UAS system, combining the  $05423^{CIC-aGal4}$  line with UAS transgenes, that outlined the cytoplasmic membrane (*UAS-mCD8-GFP*) and labeled the nucleus (*UAS-H2B-RFP*) of *CIC-a* expressing cells. As for *CIC-a-GFP*, we first confirmed, that  $05423^{CIC-aGal4}$  was labeling stellate cells of the Malpighian tubules (Figure 19C).

*CIC-a* expression was already detected in L1 brains (30hAEL), where we could observe *CIC-a*<sup>+</sup> cells in the optic lobe and central brain (Figure 20A,B). The nuclear marker RFP and the pan glial nuclear marker Repo colocalized, leading to the conclusion, that *CIC-a* was expressed in a subset of glial cells. At this stage, some *CIC-a*<sup>+</sup> glial cells were already surrounding the small neuroepithelia (Figure 20B), thus indicating, that those cells would be the same glial cells, which at later stages wrap the OPC and IPC. In slightly more developed brains, at early L2 stage (50h AEL), *CIC-a*<sup>+</sup> glial cells were already wrapping both neuroepithelia in

the optic lobe (Figure 20D). Also, glial membranes started to compartmentalize the central brain in chambers, encasing neuroblasts (Figure 20C).

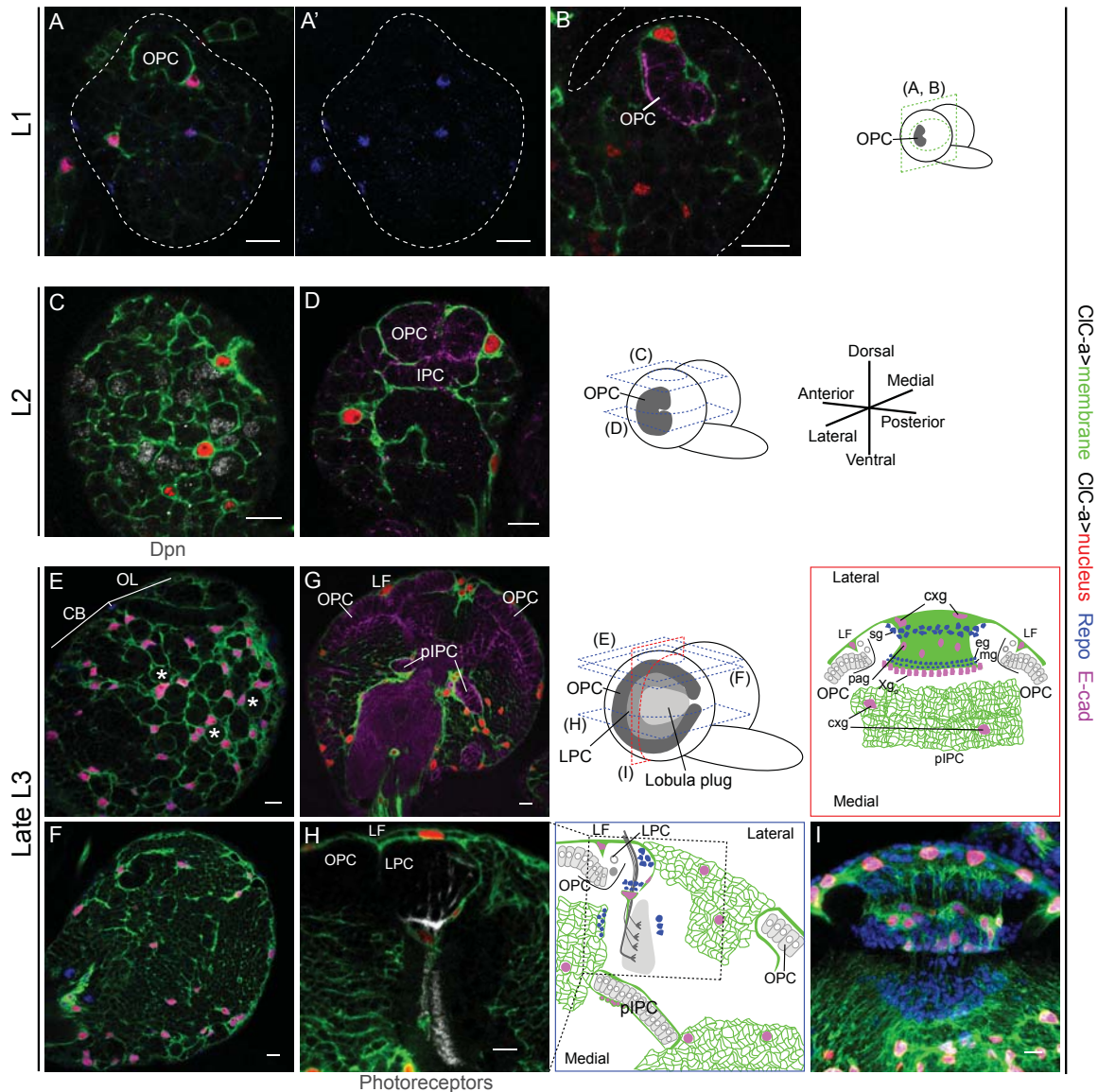


**Figure 20. *CIC-a* channel expression in glia during development.** In (A-I), *05423<sup>CIC-aGal4</sup>* mediated membrane (*UAS-mCD8GFP*, green) and nuclei (*UAS-H2BRFP*, red) are labeled. Illustrations show focal planes of the images at different time-points. (A-B) *CIC-a* is expressed in a subset of glial cells, which are already in close contact with the neuroepithelia (L1 brain), labeled by E-cad (magenta). Glial nuclei are labeled with Repo (blue). (C, D) Surface and deeper horizontal views of L2 brain hemispheres. *CIC-a*<sup>+</sup> glial membranes started encasing *Dpn*<sup>+</sup> (grey) neuroblasts and wrapped the OPC and IPC completely. (E, F) At late L3, the number of *CIC-a*<sup>+</sup> glial cells around the central brain neuroblasts increased, and their glial membranes confine the neuroblasts and their lineages in chambers (asterisks) and ensheath mature neurons, creating the trophospongium. (G) Neuroepithelia are surrounded by *CIC-a*<sup>+</sup> glial membranes in late L3 brains. (H) Photoreceptors, labeled by 24B10 (grey) are in close contact with the *CIC-a*<sup>+</sup> glial boundary between the developing lamina and lobula plug. (I) A frontal view of a 3D image of the optic lobe. Different *CIC-a*<sup>+</sup> glial cells could be observed creating a barrier between the developing lamina and lobula plug. CB, central brain; LF, lamina furrow; LPC, lamina precursor cells; OL, optic lobe; OPC, outer proliferation center; pIPC, proximal inner proliferation center. Scale bars represent 10  $\mu$ m.

The expression pattern of *05423<sup>CIC-aGal4</sup>* observed at late L3 brains was very similar to that of the CIC-a antibody and *CIC-a-GFP* (Figures 19F,I and 20E,G). Neuroblasts in the central brain (Figure 20E) and both neuroepithelia in the optic lobe (Figure 20G) were wrapped by CIC-a<sup>+</sup> glial cells. Also, all throughout the brain CIC-a<sup>+</sup> cellular processes intermingle between differentiated neurons, ensheathing them and creating the so-called trophospongium (Figure 20F). In close contact with photoreceptors, we could observe the mentioned CIC-a<sup>+</sup> glial process between the developing lamina and the lobula plug compartments, establishing a boundary (Figure 20H,I). These two compartments are formed by neurons of different origin, which never mix.

### **The CIC-a channel expression in cortex glia and some types of ensheathing glia**

We next aimed to identify which types of glial cells expressed *CIC-a*. The described *CIC-a* expression pattern resembled the cortex glia. Their glial processes encapsulate neuronal cell bodies, together with neuroblasts and neuroepithelia, forming a honey-combed structure, the “trophospongium” (Hoyle 1986; Hoyle et al. 1986; Dumstrei et al. 2003). The cortex glia on top of the OPC has a different morphology compared to the rest of the cortex glia and has been called “surface-associated cortex glia” (Morante et al. 2013). Unlike the rest of cortex glia, the surface-associated cortex glia does not create trophospongium, and remain morphologically flat. This glia creates a third layer below the two surface glial layers: perineural and subperineural glia. To confirm that the CIC-a<sup>+</sup> nuclei observed on top of the OPC neuroepithelium (Figure 21A) belonged to surface-associated cortex glia, we took advantage of the *mir8Gal4* driver, a Gal4 *P* element insertion at the *miR-8* gene (Karres et al. 2007), which is expressed in the mentioned glia (Morante et al. 2013). CIC-a protein colocalized with *mir8Gal4* expressing surface-associated cortex glia over the OPC and the glial process between developing lamina and lobula plug (Figure 21B). Colocalization was also observed in the central brain cortex glia (Figure 21C).

Supporting this, the *CIC-a* general expression pattern was very similar to previously characterized cortex glial drivers, such as, *R54H02Gal4*, which uses the 932-base-pair (bp) sequence of the first intron of *wrapper* gene to drive Gal4 expression and specifically labels cortex glia in the brain (Coutinho-Budd et al. 2017) (Figure 21D). Extensive membrane colocalization was also observed between *05423<sup>CIC-aGal4</sup>* and *wrapper932iLexA* (the *lexA* equivalent for *R54H02Gal4*) in the central brain (Figure 21E) and the optic lobe, including the surface-associated cortex glia (Figure 21F).



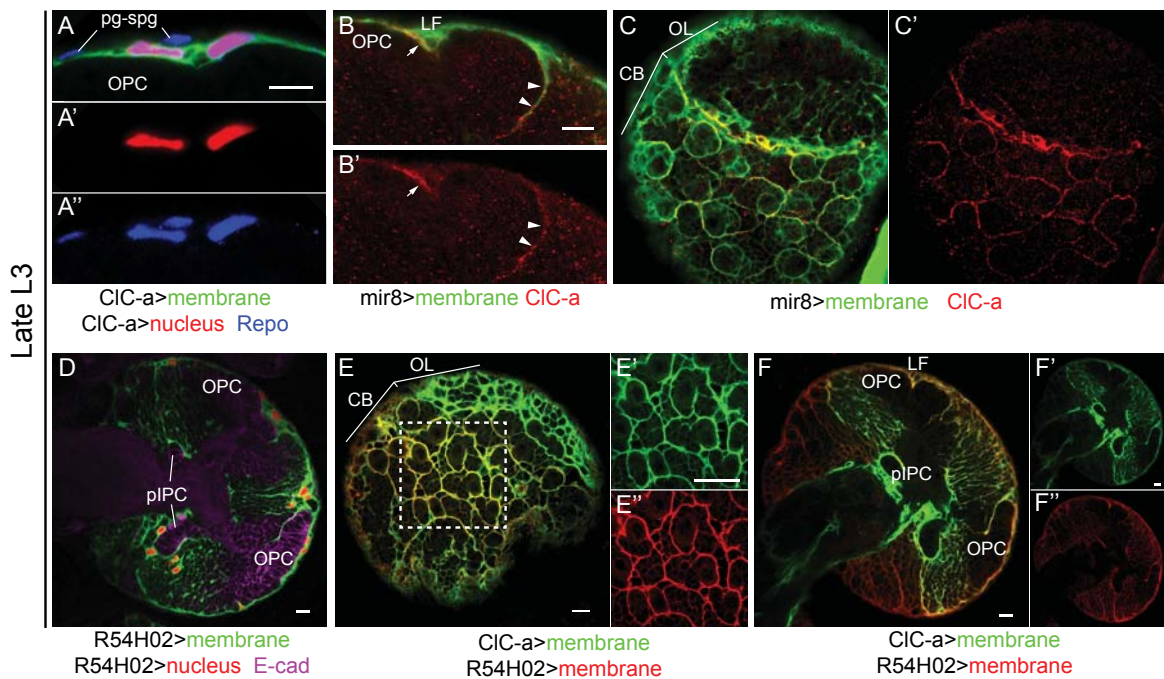


**Figure 21. *CIC-a* channel expression in cortex glia.** (A) Some *CIC-a* glial nuclei (labeled by Repo, blue) are present on top of the *CIC-a* glial layer (*05423<sup>CIC-aGal4</sup>* mediated membrane (*UAS-mCD8GFP*, green) and nuclei (*UAS-H2BRFP*, red) labeling). (B-C) *CIC-a* protein (red) colocalizes with *mir8Gal4* membranes (*UASmCD8GFP*, green) in surface-associated cortex glia (B, B'), including the lamina furrow (arrow) and the line between the developing lamina and lobula plate (arrowheads). These also colocalize in central brain cortex glia creating central brain neuroblast chambers (C, C'). (D) The cortex glia specific driver R54H02 membranes (*UAS-mCD8GFP*, green) and nuclei (*UAS-H2BRFP*, red) resembles *05423<sup>CIC-aGal4</sup>*. (E-F) *CIC-a* is expressed in cortex glia. *05423<sup>CIC-aGal4</sup>* membranes (green) colocalize with cortex glial membranes (red), labeled by *wrapper932iLexA*, in the central brain and optic lobe, including the surface-associated cortex glia. CB, central brain; LF, lamina furrow; OL, optic lobe; OPC, outer proliferation center; pg-spg, perineural-subperineural glia; pIPC, proximal inner proliferation center. Neuroepithelia are labeled by E-cad (magenta). Scale bars represent 10  $\mu$ m.

In order to assess whether *CIC-a* was also expressed in non-cortex glial cells, we used a strategy which combined the *05423<sup>CIC-aGal4</sup>* with the *wrapper932iGal80*. We observed that *CIC-a* was also expressed in different types of ensheathing glia (Figure 22B-E). We could identify neuropil ensheathing glia in the central brain and VNC (Figure 22E,I), including a type of neuropil ensheathing glia, which ensheathed the calyx and peduncle of the mushroom body (Figure 22B,C,J). In the optic lobe, we identified the outer chiasm glia ( $Xg_0$ ) and another glial cell type, which to our knowledge had not been described before (Figure 22D). We named it palisade glia (pag). Further below in the text we will describe these glial cell types in detail. Also, we observed *CIC-a* expression in wrapping glia of the optic stalk (Figure 22F) and peripheral nerves (Figure G-L).

At pupal stages and in the adult, we could still observe *CIC-a* expression in cortex glia, and when other ensheathing glial types start to differentiate some of them will still express the channel (Figure 22K-M). At 50h after pupae formation (APF) we could already see in

the optic lobe what will be the expression pattern of *CIC-a* in the adult optic lobe: Cortex glia, both chiasm glia ( $Xg_o$ ,  $Xg_i$ ), medulla and lobula plate neuropil ensheathing glia (meng, lpeng) and wrapping glia derived distal satellite glia (dsg) in the lamina (Figure 22L,M).

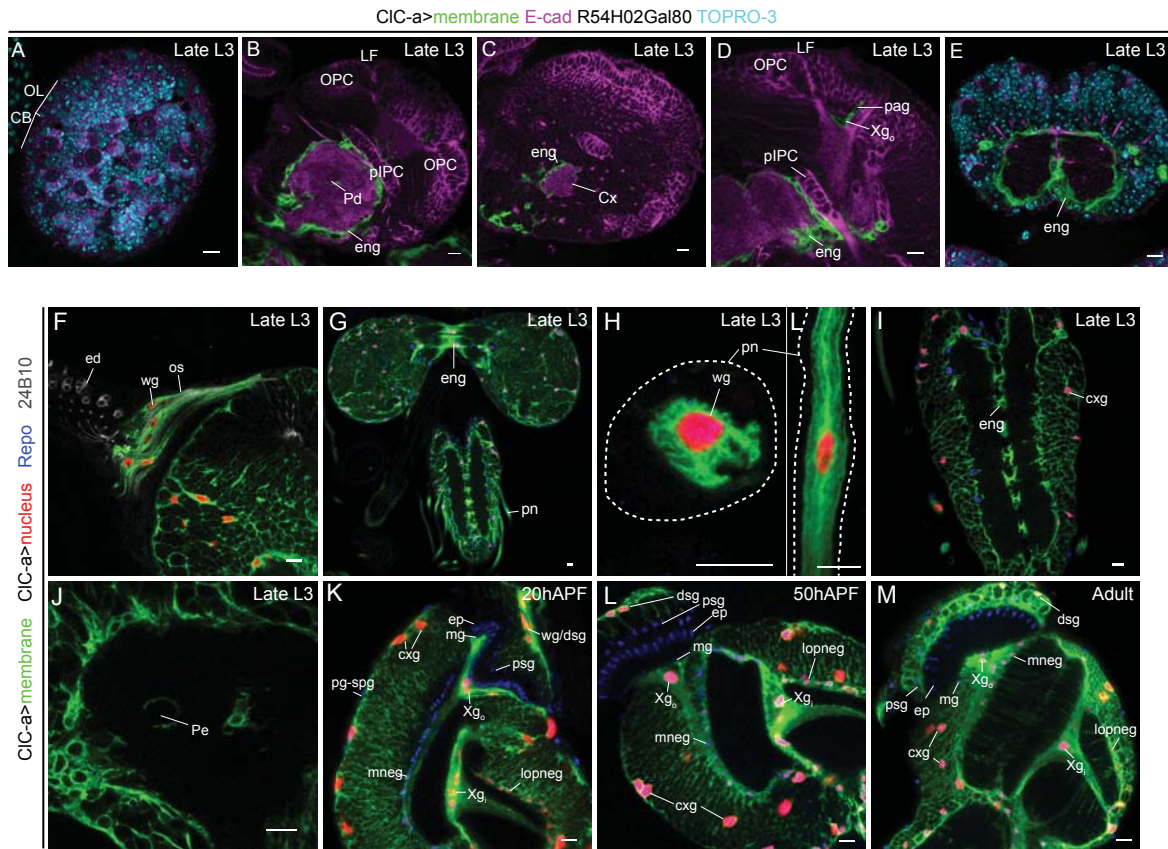


**Figure 22. *CIC-a* expression in some types of ensheathing glia.** (A-E) Inhibition of *05423<sup>CIC-aGal4</sup>* function, specifically in cortex glial cells by *wrapper932/Gal80*, showed *CIC-a* expression in some types of ensheathing glia. In the surface of the central brain, surrounding the neuroblasts, no expression is observed (A). Neuropil ensheathing glia can be observed surrounding the central brain neuropils including the peduncle (B) and the calyx (C), and ventral nerve cord neuropils (E). The ensheathing glia, outer chiasm glia, and palisade glia express *CIC-a* in the optic lobe (D). (F-H) Wrapping glia of the optic stalk (F) and peripheral nerves (G,H) express *CIC-a*. (I) Together with neuropil ensheathing glia, cortex glia of the ventral nerve cord also expresses *CIC-a*. (J) A detailed image of the neuropil ensheathing glia that ensheathes the peduncle of the mushroom body. (K-M) At pupal and adult stages cortex glia and different types of ensheathing glia expresses *CIC-a*. At pupal stages the medulla and lobulla neuropil ensheathing glia starts to express *CIC-a* (K, L), which at adult stages sends some cellular processes inside the neuropils (M). CB, central brain; Cx, calyx; cxg, cortex glia; dsg, distal satellite glia; ed, eye disc; eng, ensheathing glia; ep, epithelial glia; LF, lamina furrow; lpeng, lobula plate neuropil ensheathing glia; mg, marginal glia; mneg, medulla neuropil ensheathing glia; OL, optic lobe; OPC, outer proliferation center; os, optic stalk; pag, palisade glia; Pe, peduncle; pg-spg, perineural-subperineural glia; pIPC, proximal inner proliferation center; pn, peripheral nerve; psg, proximal satellite glia; wg, wrapping glia;  $Xg_i$ , inner chiasm glia;  $Xg_o$ , outer chiasm glia. Glial nuclei are labeled with the pan-glial nuclear marker Repo (blue), neuroepithelia by E-cad (magenta), photoreceptors by 24B10 (grey), and all nuclei by TOPRO-3 (cyan). Scale bars represent 10  $\mu$ m.

Thus, *CIC-a* is expressed in cortex glia and surface-associated cortex glia from early development (wrapping the OPC, IPC and central brain neuroblasts) to adulthood. Moreover, it is also expressed in some types of neuropil and axon ensheathing glia.

### Characterization of *CIC-a* mutants

To explore the role of *CIC-a* in glia we sought to characterize a set of *Minos*-mediated integration cassette Mi(MiC) insertions into the *CIC-a* locus. Although three different MiMiCs were available in coding introns of the *CIC-a* locus, we focused on *Mi(MiC)CIC-a<sup>05423</sup>* and *Mi(MiC)CIC-a<sup>14007</sup>* alleles (from now on referred to as *05423* and *14007*), since their insertion sites were predicted to interrupt all isoforms of *CIC-a* gene (Figure 23A).

Initial viability characterization of these insertions over the *Df(3R)PS2* deficiency (from now on referred to us as *Df*), which covers the *CIC-a* region, revealed the presence of escapers. The *05423/Df* allelic combination displayed a developmental delay at pupariation of almost 48 hours compared to the wild type. In addition, most *05423/Df* escapers did not emerge from the pupal case (Figure 23F), and the ones that did, remained immobile on the food before dying, shortly after emerging. We detected that *05423* chromosome had a second site mutation, as it did not survive in homozygosis, although it did over the deficiency. The *05423* derived *05423<sup>CIC-aGal4</sup>* showed a similar behavior. Escapers for the *14007/Df* allelic combination were also developmentally delayed at pupariation (around 24hrs), but compared to *05423/Df* were more abundant and healthier, and all emerged from the pupal case. The behavior of the *05423/14007* allelic combination was similar to *14007/Df*. The *14007* allele lived in homozygosis and did not have the mentioned second site mutation. It also seemed, that *14007/14007* homozygotes are healthier than other allelic combinations.

The predicted loss of function of the MiMiC insertions was confirmed by immunostaining and western blot. We could not detect *CIC-a* in the brain (Figure 23B,C) or stellate cells (Figure 23D,E) by antibody staining in *05423/Df*, *14007/Df*, *05423/14007*, and *14007/14007* allelic combinations. Additionally, western blot, done in collaboration with Raúl Estévez's group and his PhD student Hector Gaitán Peñas, revealed a substantial reduction in *CIC-a* protein levels in mutant animal brains (Figure 23G). We could observe a strong *CIC-a* reduction in heterozygotes and a loss of protein in different allelic combinations. It is described that with very low frequency the splice machinery can use the endogenous splice acceptor instead of the MiMiC one, generating wild type transcripts. Combined with the different strength of mutant phenotypes described in the next section, we classified the characterized alleles as strong loss of function mutations, rather than nulls.

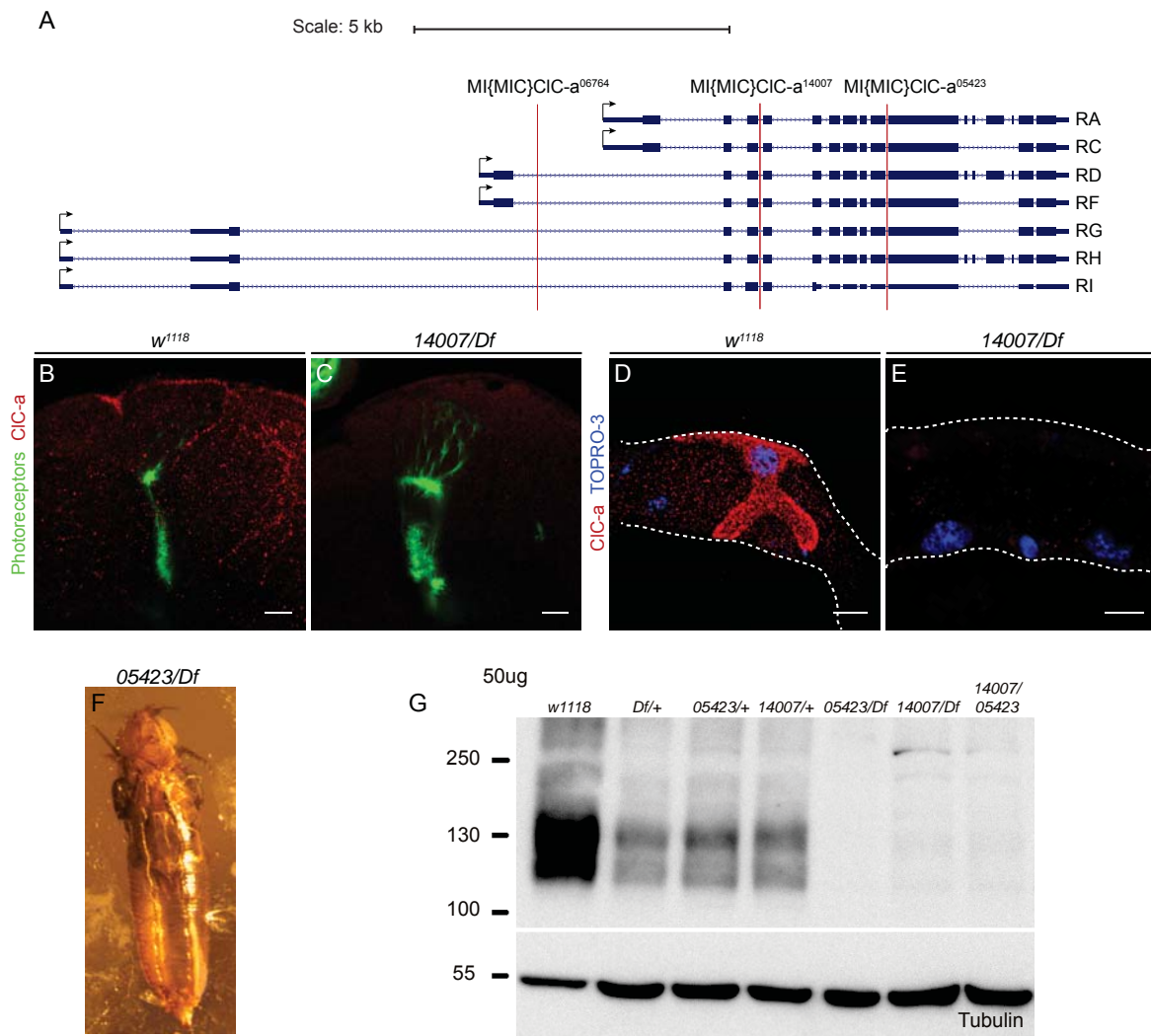


**Figure 23. *CIC-a* MiMIC mutants are strong loss of function alleles.** (A) MiMIC insertion locations in the *CIC-a* locus. Three alleles are available in coding introns of the *CIC-a* locus. Only *05423* and *14007* insertions affect all isoforms, while insertions at the *06764* allele will only affect some of them. (B, C) *CIC-a* antibody staining at late L3 stage in wild type (B) and *14007/Df* mutants (C). The expression pattern observed in the optic lobe did not appear in mutants. (D, E) *CIC-a* antibody staining at adult malpighian tubules in wild type (D) and *14007/Df* mutants (E). Stellate cells do not show any detectable *CIC-a* expression. (F) Trapped *05423/Df* escaper. 79,54% of escapers of this allelic combination get trapped at emerging from the pupal case or died immobile on the food. (G) Western blot of protein extraction from adult heads. 50  $\mu$ g of protein extraction was loaded. Scale bars represent 10  $\mu$ m.

Based on our genetic analyses and the mutant phenotypes (see in the next section) we could order the allelic combinations by strength:  $05423^{CIC-aGal4} > 05423/Df > 14007/Df = 05423^{CIC-aGal4}/14007 > 05423/14007 > 14007/14007$ . It was difficult to obtain enough  $05423^{CIC-aGal4}/Df$  or  $05423/Df$  animals, hence we mainly used *14007/Df* and  $05423^{CIC-aGal4}/14007$  flies in our experiments. These two allelic combinations behave in a very similar way and mutant animals were easier to obtain. The 24 hours delay at pupariation of these two allelic combinations, was also observed at larval stages. For example, the L3 stage can be divided

in early, mid and late stage. In wild type and heterozygote control animals, photoreceptor innervation beginning and pupariation take place at mid L3 (96h AEL) and late L3 stage (120h AEL) respectively. However, in mutant animals, photoreceptor innervation started at 120h AEL and pupariation at 144h AEL. To compare control and mutant animals in the same larval stage we have taken into account this delay, and, for simplicity, from now on we will refer to it as early L3: 96h AEL, mid L3: 120h AEL and late L3: 144h AEL when referring to mutant animals.

In summary, we have characterized the first *CIC-a* mutant alleles and found them to be strong loss of function alleles.



## **CHAPTER II:**

Phenotypic analysis  
of *C/C-a* mutants





## Mutations in *CIC-a* result in smaller brains with photoreceptor guidance defects

We first dissected adult brains to check whether some apparent developmental phenotype was observed, due to *CIC-a* expression at larval stage. We realized, that *CIC-a* mutant brains seemed smaller. In  $05423^{CIC-aGal4}/Df$  flies, the strongest allelic combination, both the optic lobes and central brains were smaller compared to heterozygote controls (Figure 24A,B). For  $05423^{CIC-aGal4}/14007$ , the differences were not as big for the central brain, but optic lobes were clearly smaller (Figure 24A,B).

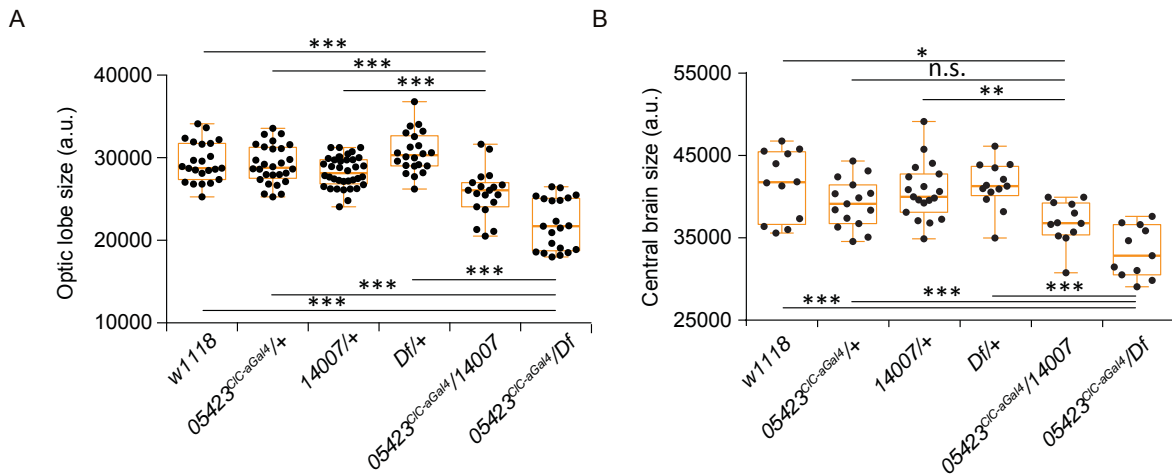


**Figure 24. *CIC-a* mutants have smaller brains.** (A, B) Box-plots showing adult optic lobe (A) and central brain (B) size in control heterozygotes and different *CIC-a* mutant allelic combinations. Mutants have smaller brains. The data are in arbitrary units (a.u.). P values were calculated with the non-parametric Mann-Whitney test. \* $p < 0,05$ , \*\* $p < 0,01$ , \*\*\* $p < 0,001$ .

Optic lobe size was dramatically affected and *CIC-a* expression was detected in a boundary in close contact with photoreceptors. Therefore, we next focused on photoreceptor axonal projections. It is a well-characterized system and developmental defects are easy to detect.

In wild-type adult optic lobes, R8 and R7 photoreceptor axons from the oldest ommatidia, located at the posterior edge of the eye, enter through the posterior lamina, traverse the outer optic chiasm and project into the anterior-most medulla (Figure 25A). R8 and R7 photoreceptor axons from the anterior region of the eye extend through the anterior lamina and the outer chiasm before entering the posterior medulla (Figure 25A). All R7 and R8 photoreceptor axons enter the medulla neuropil from its distal face and their projections align in a stereotyped array forming a retinotopic map. R1-R6 photoreceptor axons always project into the lamina neuropil (Figure 25D) (Reviewed in Clandinin and Zipursky 2002).

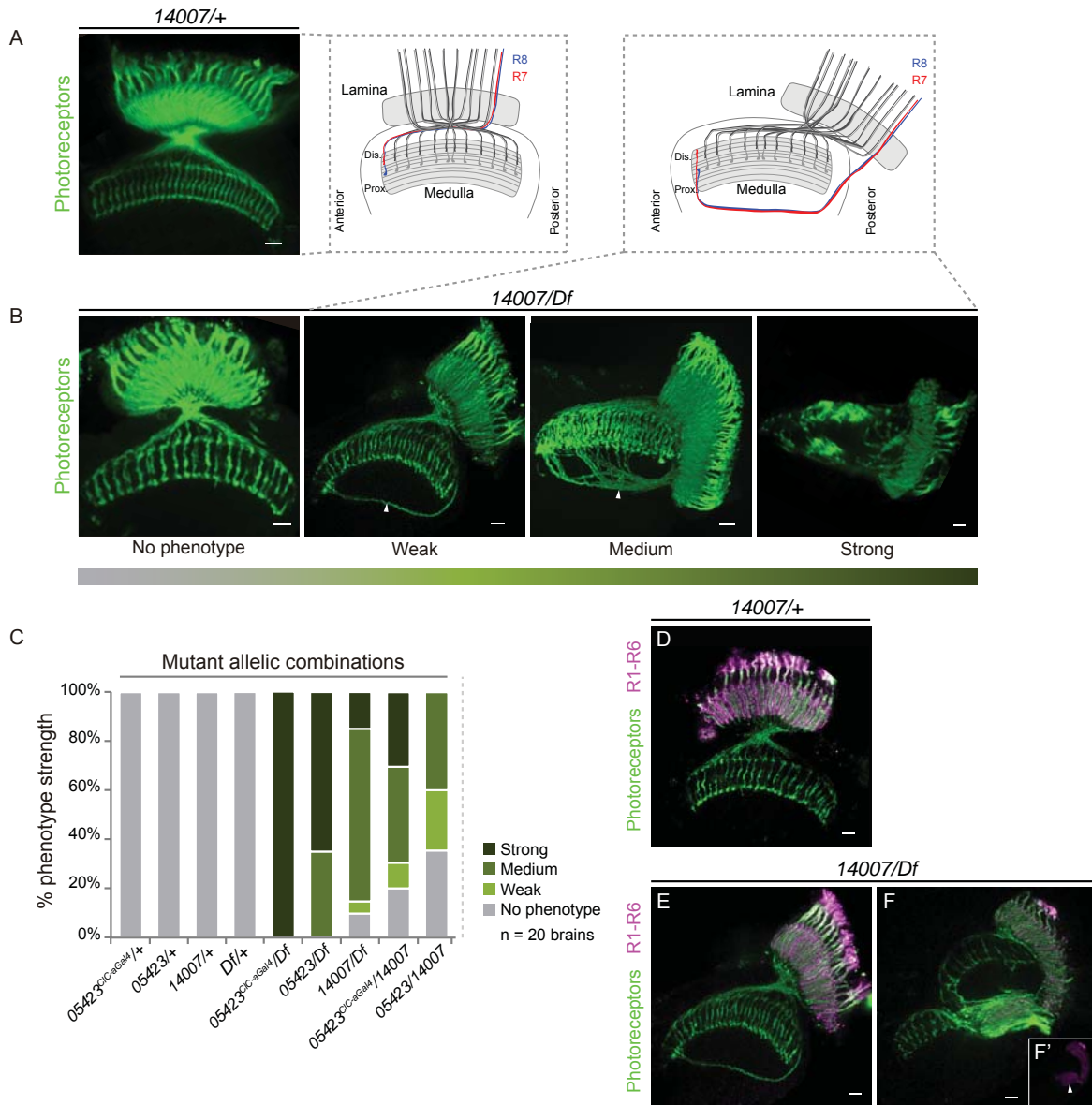


**Figure 25. *CIC-a* mutant photoreceptor guidance phenotypes.** (A) A wild type array of photoreceptors (24B10, green) with an illustration. R8 (blue) and R7 (red) photoreceptor axons from the oldest ommatidia, located at the posterior edge of the eye, enter through the posterior lamina, traverse the outer optic chiasm and project into the anterior-most medulla from its distal face. (B) *CIC-a* mutant photoreceptor classification in order of strength, including an illustration. Weak phenotypes show one to three thin misprojected axon bundles entering the medulla proximally (arrowheads), while in medium phenotypes at least three thicker misprojected bundles are present. In the strongest phenotypes a severe disruption of photoreceptor axons is observed. Weak and medium images are Z projections to show the complete trajectory of the bundles. (C) Phenotype percentages based on severity shown in (B) of different allelic combinations. Heterozygotes do not show any phenotype, whereas different allelic combinations vary in the phenotype expressivity, due to the nature of the alleles. (D) R1 to R6 axons labeled by *Rh1Gal4* (magenta) stop in the lamina, never arriving to the medulla. (E, F) While in weak and medium phenotypes R1-R6 target correctly to the lamina (E), in strong phenotypes they are mistargeted to the medulla (arrowhead in (F')). (E) is a Z projection. Scale bars represent 10  $\mu$ m.

*C/C-a* mutant adult optic lobes showed photoreceptor guidance defects (Figure 25B). These defects were classified by severity in three categories. The strongest phenotypes were characterized by a severe disruption of photoreceptor array organization. Most of R7 and R8 axons bypassed the outer chiasm, projected along the posterior edge of the medulla neuropil turning anteriorly, and extended for variable distances before innervating the medulla neuropil from its proximal face (Figure 25B). Additionally, the lamina neuropil was misplaced posteriorly and part of R1-R6 axons, which were identified using the *Rh1Gal4* line, were also misprojecting into the medulla, from the posterior edge (Figure 25F). In medium phenotypes, the photoreceptor array looked mostly wild-type, however, at least three posterior to anterior thick bundles of photoreceptor axons were present, following the same trajectory as bundles in the strong phenotype (Figure 25B). In this case the R1-R6 axons looked wild type and projected to the lamina (Figure 25E). Finally, in the weakest phenotypes just one to three posterior to anterior thin misprojected bundles were seen (Figure 25B).

As mutants were strong loss of function alleles but not nulls, the expressivity of these three degrees of phenotypes varied for different allelic combinations. The phenotypes were stronger in *05423<sup>C/C-aGal4</sup>/Df* and *05423/Df*, followed by *14007/Df*, *05423<sup>C/C-aGal4</sup>/14007*, and *05423/14007* (Figure 25C). This expressivity perfectly matches with characterized allele classification. We did not observe any phenotype for any of the heterozygotes (Figure 25C).

To better understand axonal targeting of misguided R7 and R8 photoreceptors, we took advantage of R8 labeling *Rh6lacZ* and R7 labeling *Rh4EGFP*. In a wild type situation, R8s project to the M3 layer in the medulla (Figure 26C), and the R7s to M6 (Figure 26A). In mutants, 84% of misguided R7s were projecting to the M6 layer in the medulla (Figure 25B,E), their correct target layer (n = 49 of 58), 14% were mistargeted to the M3 layer (n=8 of 58) and 2% to the M1 layer (n=1 of 58). R7 axonal targeting was mostly unaltered. On the contrary, 76,82% of R8s were mistargeted to the M1 layer (n = 116 of 151) (Figure D,E) and just a 23,13% of them projected correctly to M3 (n = 35 of 151).

R7 and R8 photoreceptors start innervating the medulla at larval stages, projecting to a temporary layer. This process is asynchronous, so different R7 and R8s arrive to the temporary layer at different times. Once all photoreceptors are positioned in their temporary layer, at 40h APF, the second targeting phase starts. All R7 and R8s synchronously target to their final layers, the R8 to M3 and the R7 to M6 (Figure 25F). It has been shown that R8s actively move to their final target, while the R7s passively move while the medulla keeps growing (Reviewed in Plazaola-Sasieta et al. 2017). Interestingly, at 40h APF, when R7 and R8 axons are in their respective temporary layers, misguided R8 axons were still targeting correctly (Figure 25G). We hypothesize, that when movement to their final target starts, these cells cannot be detached from their temporary layer and stayed there. R7 targeting is not affected, as axons stabilize in their temporary layer and are pushed due to the medulla growth.

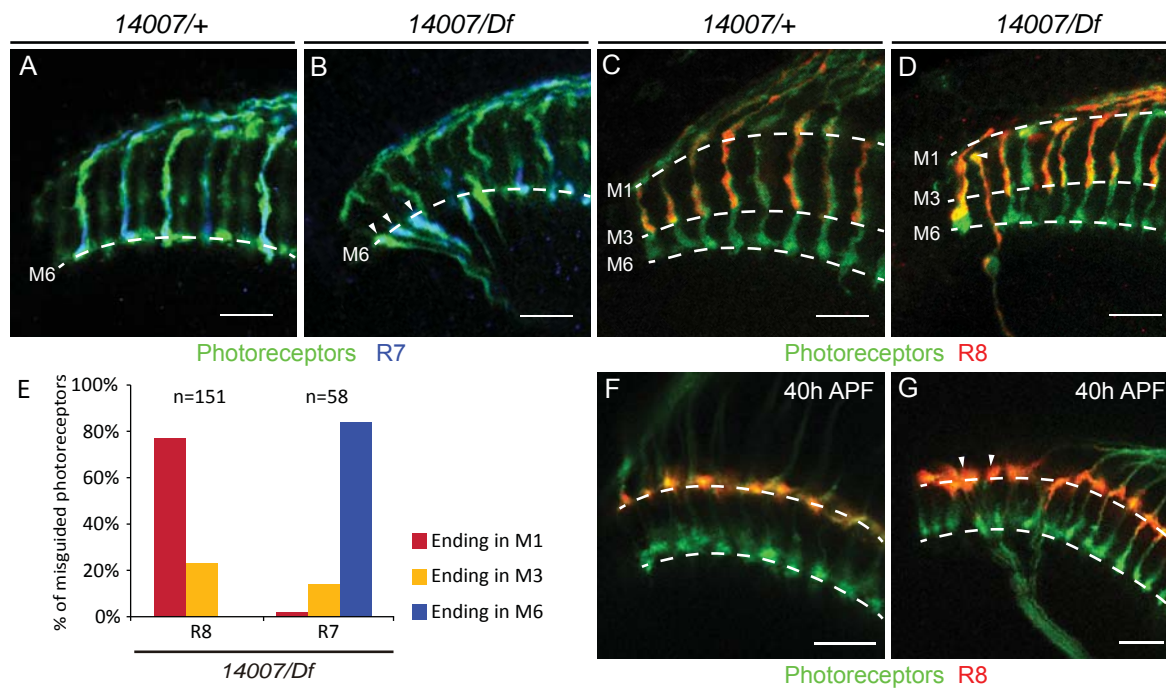


**Figure 26. R8s targeting defects.** (A,B) R7 (*Rh4EGFP*, blue) targeting in the medulla in control and *14007/Df* mutants. In wild type R7 axons target to the M6 layer entering the medulla distally (A). Misprojected R7 axons in *CIC-a* mutants enter the medulla proximally and target correctly to M6 (B, arrowheads). (C,D) R8 (*Rh6lacZ*, red) targeting in the medulla in wild type and *14007/Df* mutants. R8 axons in wild type enter the medulla distally and target to the M3 layer (C), while in mutants misprojected R8 axons mistarget to the M1 layer, entering the medulla proximally (D, arrowhead). (E) Target counting of misprojected R8 and R7 axons in *14007/Df* mutants. (F,G) At 40h APF, mistargeted R8s (*sensGal4*, *UASutrGFP*, red) project correctly to their temporary layer. Scale bars represent 10  $\mu$ m.

### **CIC-a is required in glia for a normal brain size and photoreceptor guidance**

In order to confirm the requirement of *CIC-a* in glia, we performed cell type specific knock down and rescue experiments.

We knocked down *CIC-a* with RNAi using the *05423<sup>CIC-aGal4</sup>* and, exclusively in glial cells, with the pan-glial driver *RepoGal4* (a Gal4 enhancer trap into the *repo* locus). In both cases, the *CIC-a* knock down phenocopied the photoreceptor phenotypes seen in mutant animals (Figure 27A). In addition, we used an alternative technique called *deGradFP* (Caussinus et al. 2012) to specifically knock down the gene in glia. It consisted in an anti-GFP nanobody mediated GFP-tagged protein knock-down. We expressed the anti-GFP nanobody in glia with *RepoGal4* in homozygous *CIC-aGFP* flies. As *CIC-aGFP* tags the gene at the endogenous locus, all *CIC-a* protein are tagged. *deGradFP* knock down experiments in glia also phenocopied photoreceptor phenotypes (Figure 27B).

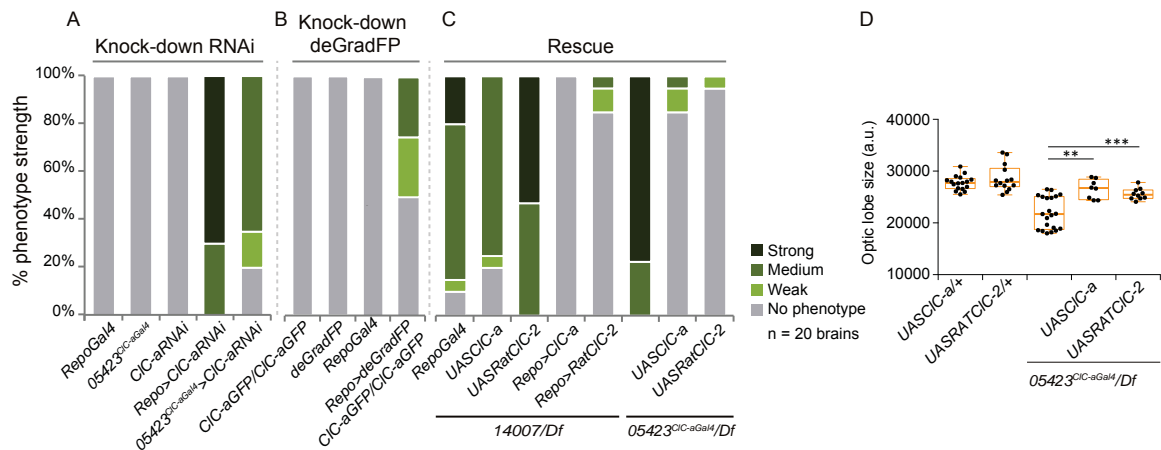


**Figure 27. *CIC-a* is required in glia for a correct guidance of photoreceptor and proper optic lobe size.** (A) Phenotype percentages in RNAi knock down of *CIC-a* by *05423<sup>CIC-aGal4</sup>* and *RepoGal4*. Both knock down experiments phenocopy photoreceptor phenotypes. Controls do not show any phenotype. (B) Phenotype percentages in knock down of *CIC-a* using the deGradFP technique in a homozygous *CIC-aGFP* background. It phenocopies photoreceptor phenotypes. Controls do not show any phenotype. (C) Phenotype percentages in rescue experiments for photoreceptor phenotypes. Expression of *CIC-a* or *RatCIC-2* cDNA in glia by *RepoGal4* is sufficient to rescue photoreceptor phenotypes. Expression of *05423<sup>CIC-aGal4</sup>* also rescues the phenotypes. (D) Box plots showing rescue experiment for the optic lobe size expressing *CIC-a* or *RatCIC-2* cDNA under *05423<sup>CIC-aGal4</sup>* in *CIC-a* mutants. Adult optic lobe size is rescued to wild type levels. P values were calculated with the non-parametric Mann-Whitney test. \*\*p<0,01, \*\*\*p<0,001.

In order to rescue optic lobe size and photoreceptor phenotypes in whole animal mutants, we created two different transgenic lines: *UASCIC-a* and *UASRatCIC-2*. They allowed us to do rescue experiments, expressing *Drosophila*'s *CIC-a* or *CIC-a*'s Rat homologue *CIC-2* cDNA in the desired tissue using the Gal4/UAS system. Rescue experiments were carried out with the same two drivers as before: *05423<sup>CIC-aGal4</sup>* and glia specific *RepoGal4*. The expression of *CIC-a* or *RatCIC-2* cDNA with *05423<sup>CIC-aGal4</sup>* rescued the brain size (Figure 27D) and photoreceptor phenotypes (Figure 27C). Expression of cDNAs in glia also rescued photoreceptor phenotypes (Figure 27C). Interestingly, in all rescue experiments we performed, the developmental delay was also rescued. The rescues with Rat *CIC-2* suggests that *CIC-a* properties have been conserved during evolution.

To discard any requirement of *CIC-a* in photoreceptors, we knocked down *CIC-a* and performed rescue experiments, specifically in photoreceptors, using the pan-photoreceptor driver *GMRGal4*, a GAL4, under the control of a glass multiple reporter (GMR) promoter. We could not observe any photoreceptor phenotype in the knock down (Figure 28) or any rescue in the rescue experiments (Figure 28).

To be completely sure that *CIC-a* is not necessary in photoreceptors, we also performed clonal analysis. The *MARCM* technique was used to (Lee and Luo 1999) generate positively marked sparsed homozygous mutant clones in the eye (Annex 2). Alternatively, by *EGUF-*

*hid* technique (Stowers and Schwarz 1999), we generated eyes composed exclusively from homozygous mitotic clones (Annex 2). We could not observe any phenotype in photoreceptors in any of the cases (Annex 2).

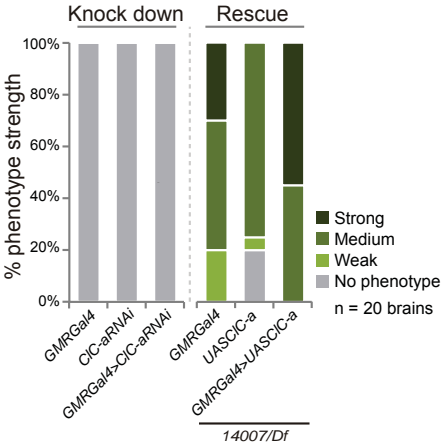


**Figure 28. Photoreceptor phenotypes are non-autonomous.** Phenotype percentages in *CIC-a* knock down and rescue experiments mediated by a photoreceptor specific *GMRGal4*. The knock down did not phenocopy guidance phenotypes and expression of *CIC-a* in photoreceptors did not rescue the phenotypes.

Thus, together with the lack of *CIC-a* expression in photoreceptors, our results indicated that *CIC-a* was required in glia and that photoreceptor guidance defects in *CIC-a* mutants were non-autonomous.

## **CHAPTER III:**

Brain size and proliferative  
defects in *C/C-a* mutants





## Cortex glial cells wrap neuroepithelia and neuroblasts in mutants

In order to elucidate how mutations in *CIC-a* resulted in smaller brains we first assessed the morphology of cortex glia in *CIC-a* mutants. Therefore, we labeled the glial cell membranes (*UAS-mCD8GFP*) and nuclei (*UAS-H2BRFP*) with *05423<sup>CIC-aGal4</sup>* in controls and *05423<sup>gal4</sup>/14007* mutants. Cortex glial processes were still in close contact with the OPC and IPC in mutants through larval development (Figure 29A,B,E,F). Mature neurons were also individually wrapped and the trophospongium seemed unaltered in both, the optic lobe and central brain (Figure 29C,G). Central brain neuroblasts and lineages were encased in chambers as in control animals (Figure 29D,H).

We concluded that mutations in *CIC-a* did not result in major morphological changes of the cortex glial membrane scaffold. However, it suggests that it would affect their physiology.

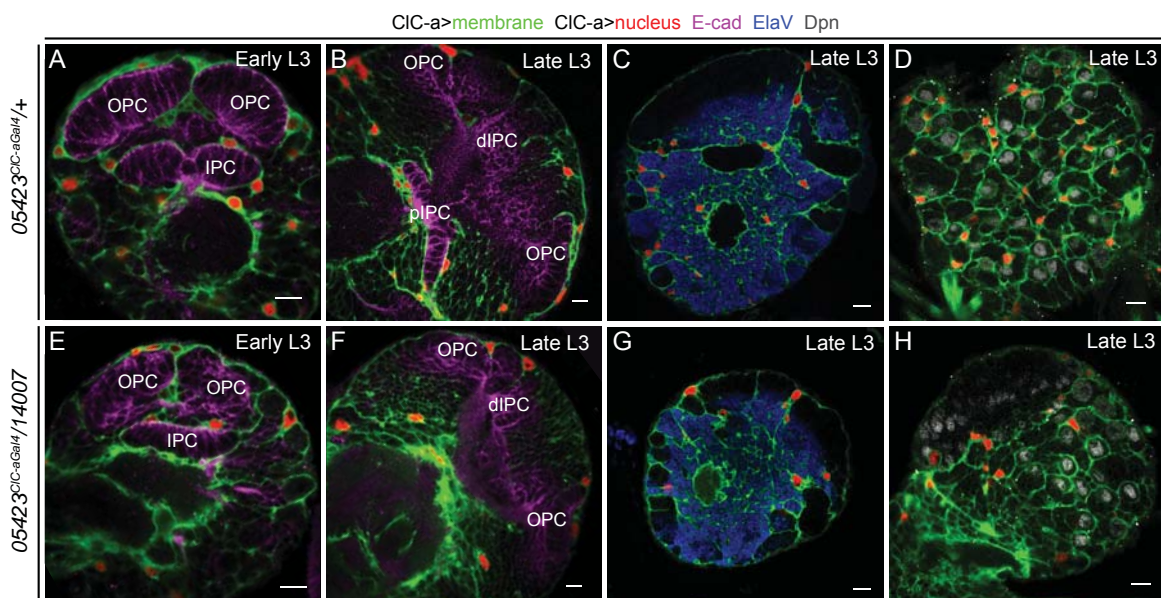


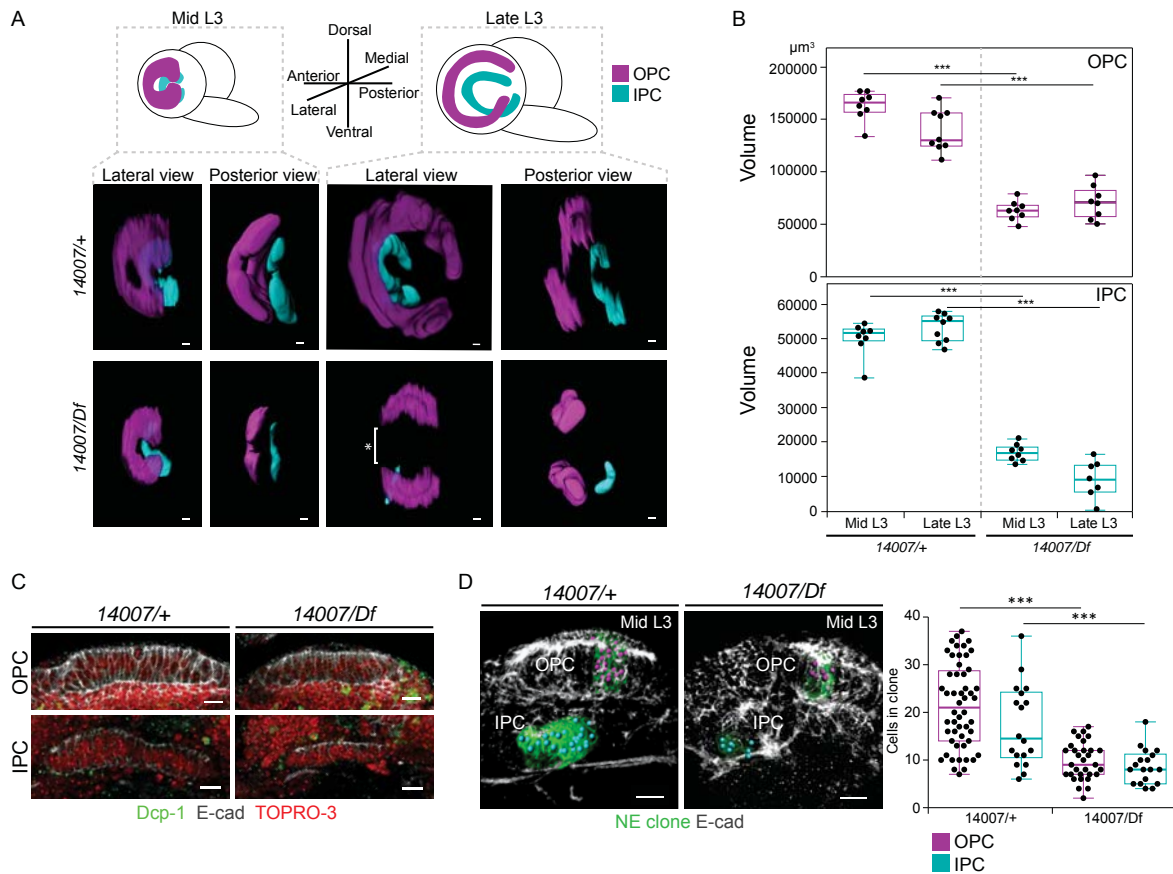
**Figure 29. Cortex glial morphology remain unaltered in *CIC-a* mutants.** In all figures *05423<sup>CIC-aGal4</sup>* mediated membrane (*UAS-mCD8GFP*, green) and nuclei (*UAS-H2BRFP*, red) labeling are shown. (A,B,E,F) In early (E) and late L3 (F) mutants, neuroepithelia (E-cad, magenta) are surrounded by cortex glial cells as it is the case in controls (A, B). (C,G) Neurons (ElaV, blue) are surrounded by cortex glial membranes at late L3 stage in controls (C) and mutants (G). (D,F) Neuroblasts (Dpn, grey) are isolated in individual cortex glial chambers in controls (D) and mutants (H). dIPC, distal inner proliferation center; IPC, inner proliferation center; OPC, outer proliferation center; pIPC, proximal inner proliferation center. Scale bars represent 10  $\mu$ m.

## *CIC-a* is required for neuroepithelial expansion

Cortex glia is part of neuroepithelia and the neuroblast niche, and it has been shown, that they integrate external, nutritional, and possible neuroblast signals that mediate the formation of the cortex glia scaffold (Spéder and Brand 2018). These functions seem to be unaltered in *CIC-a* mutants, as the trophospongium seems to develop correctly. Cortex glia was also shown to be essential for neurogenesis (Morante et al. 2013) and their processes

are in close contact with the OPC and IPC, the major contributors to the optic lobe size. Defects in these neuroepithelia could be the reason of smaller adult optic lobes. Hence, we decided to look for phenotypes in them.

Neuroepithelia grow by symmetric division from a pool of few cells. By doing so, they are positioned along the dorso-ventral axis, having a crescent shape, with an opening pointing posteriorly. At late L2 stage, the neuroepithelial cells start to divide asymmetrically. In the OPC, cells at the lateral edge give rise to lamina neurons, whereas the ones on the medial edge generate neuroblasts that will produce optic lobe neurons. While asymmetric divisions continue, the neuroepithelium keeps dividing symmetrically, increasing the pool of cells that would derive in neuroblasts. Once symmetrical divisions stop and the wave of differentiation continues, the OPC will start reducing in size and disappear in early pupal stages, when it is all converted into precursors and neuroblasts. A similar process takes place in the IPC.



We first measured OPC and IPC neuroepithelia size, based on the antibody labeling of the adhesion protein *E-cadherin*. We manually segmented the neuroepithelia and obtained 3D reconstruction (Figure 30A). We segmented the OPC from the transition zone to the lamina precursor cells. Regarding the IPC, which is subdivided into d-IPC, p-IPC, and s-IPC, we just segmented the p-IPC and s-IPC, as the d-IPC is not a neuroepithelium. We concluded that both neuroepithelia are significantly smaller in *14007/Df* mutants at mid and late L3 (Figure 30A,B). Although at mid L3 the shape of the neuroepithelia was the same, they were already clearly smaller (Figure 30A,B). Interestingly, in late L3, in most cases the OPC appeared as two separate dorsal and ventral domains with the central part absent (Figure 30A), normally described to be the *Vsx* positive region. Similarly, the p-IPC was also missing and we could just observe a piece of the s-IPC (Figure 30A).

We wondered, whether the reduction in size of neuroepithelia were due to an increase in cell death. To test that, we stained the larval brains with the apoptotic marker *Dcp-1*. We could not observe any apoptotic cell neither in controls nor in *14007/Df* mutants in both the OPC and the IPC (Figure 30C). So, the absence of cell death in this tissue suggest, that proliferation defects could be the responsible for smaller neuroepithelia.

In order to check, whether proliferation of proliferative tissues was affected in mutants, we performed clonal analysis. Using the *MARCM* technique, we generated positively labeled clones in wild type and whole animal *14007/Df* mutants. We induced clones in L2 stage, while the neuroepithelia were still expanding, and dissected the brains at mid L3, 48 hours after induction. To assess symmetric division inside the neuroepithelia, we counted clones that were composed exclusively of neuroepithelial cells and did not start to differentiate into neuroblasts. On the one hand, the clones in controls, where cortex glia expressed *CIC-a*, contained a median of 21 cells in the OPC and 14,5 cells in the IPC (Figure 30D). On the other hand, clones in *14007/Df* mutants, where cortex glia were not expressing *CIC-a*, the size of the clones was significantly reduced with a median number of 9 and 8 cells for the OPC and IPC respectively (Figure 30D). Thus, *CIC-a* is necessary in the cortex glial niche for neuroepithelial expansion.

This reduction on neuroepithelial proliferation could also be the origin of the disruption of the OPC and the disappearance of the d-IPC observed at late L3 stages. An imbalance between symmetrical proliferation of the neuroepithelium and neuroepithelium to neuroblast transition, could explain the early disappearance of these. In the OPC, the wave of proneural gene expression that sweep the neuroepithelium and signal its transition to asymmetrically dividing neuroblasts is well described. We observed that this process was taking place, as we identified Deadpan positive neuroblasts in the remaining portions of the neuroepithelium and in the region, where neuroepithelium was absent (Figure 31A,C). This means that neuroblasts kept differentiating until quite recently in the area. Indeed, in some brains, we could see a thinner OPC in the anterior region, a previous step before disappearing (Figure 31B). We did not further focus on why a disbalance between symmetric neuroepithelial proliferation and neuroepithelium to neuroblast transition is more evident in specific regions of the OPC and IPC.

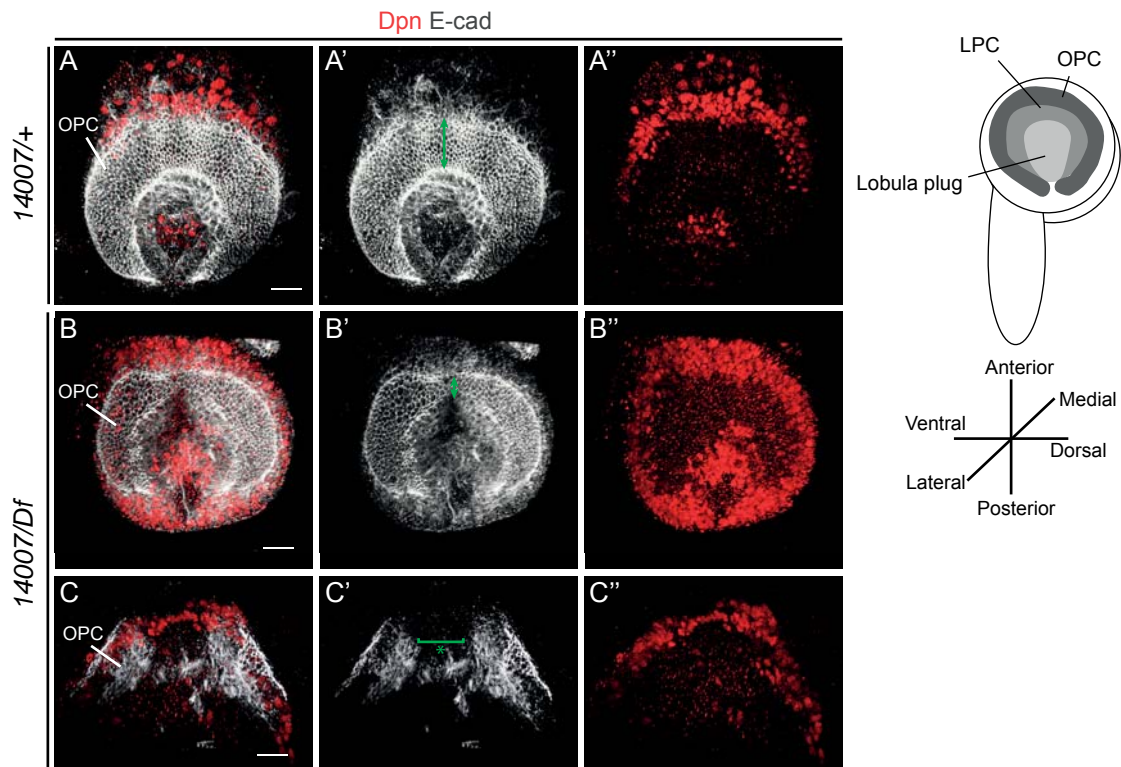


**Figure 31. The anterior OPC is absent in late L3 *CIC-a* mutants.** (A) A lateral view of the OPC (E-cad, grey) in controls at late L3 stage. Neuroblasts (Dpn, red) are being differentiated in the medial edge of the neuroepithelium. Arrows indicate the thickness of the posterior OPC. (B, C) Lateral views of the OPC in *14007/Df* mutants at late L3 stage. In (B) the anterior OPC is present, but it is thinner than in controls (arrows). In (C) the anterior OPC is absent (bracket). In both cases, the anterior area is full of neuroblasts, suggesting they kept differentiating from the OPC until recently. All the images are 3D. Scale bars represent 10  $\mu\text{m}$ .

### ***CIC-a* expression is required for neuroblast proliferation and neuronal survival**

Brain size also depends on the capacity of neuroblasts to divide and generate neurons. We wondered, whether proliferation by asymmetric divisions of neuroblasts was also reduced, as neuroblasts in the central brain and the ones generated from the OPC in the optic lobe were also wrapped by *CIC-a*<sup>+</sup> cortex glia. Due to the difficulty of obtaining single neuroblast clones in the optic lobe, being sufficiently apart from each other, we focused on assessing proliferation of central brain type I neuroblasts. For that, we used the same clone induction protocol as for neuroepithelial clones. Neuroblast clones in the controls had a median number of 34 cells (Figure 32A) and clones in the mutant background were reduced in size, having a median of 26 cells (Figure 32A). We also observed more Dcp-1 puncta per volume in mutant brains, compared to controls (Figure 32B). This suggests that the reduction in clone size could be due to a combination of cell death and proliferation defects, as we already described how neuroepithelial proliferation is affected.

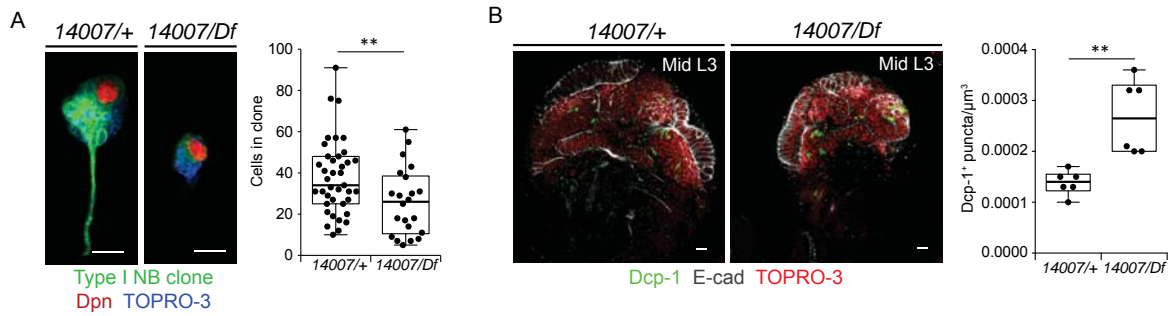


**Figure 32. CIC-a is required for neuroblast proliferation and neuronal survival.** (A) 3D reconstructions of MARCM clones (green) in type I neuroblasts of the central brain, induced at L2 stage and recovered at mid L3 stage (48 hours). The neuroblast is the Dpn<sup>+</sup> cell (red) and nuclei are labeled by TOPRO-3 (blue). The graphic represents the number of nuclei the clones have in control and *14007/Df* mutants. In mutants, the clone size is reduced. (B) Dcp-1 staining (green) in larval brains in controls and *14007/Df* mutants. Neuroepithelia are labeled by E-cad (grey) and nuclei by TOPRO-3 (red). The graphic represents the Dcp-1<sup>+</sup> puncta per volume in controls and *14007/Df* mutants. Cell death is increased in *CIC-a* mutants. P values were calculated using the non-parametric Mann-Whitney test. \*\* $p < 0,01$ . Scale bars represent 10  $\mu\text{m}$ .

In summary, we concluded that *CIC-a* in glia affects proliferation of neuroepithelia and probably also affects neuroblast division. Moreover, the increased cell death outside the neuroepithelia in mutants suggests, that *CIC-a* is required in glia for neuronal survival. Consistent with these conclusions and with adult brains being smaller, the size and growth rate of larval hemispheres through L3 stage was reduced in mutant animals (Figure 33). At early L3, brain hemispheres were similar in size (Figure 33), but from then on, the differences increased. From early to mid L3 stage, the brain hemisphere diameter grew 50 $\mu\text{m}$  in controls, while 30 $\mu\text{m}$  in *CIC-a* mutants (Figure 33). From mid to late L3 stage, in controls the growth was of 60 $\mu\text{m}$  and 40 $\mu\text{m}$  in mutants (Figure 33).

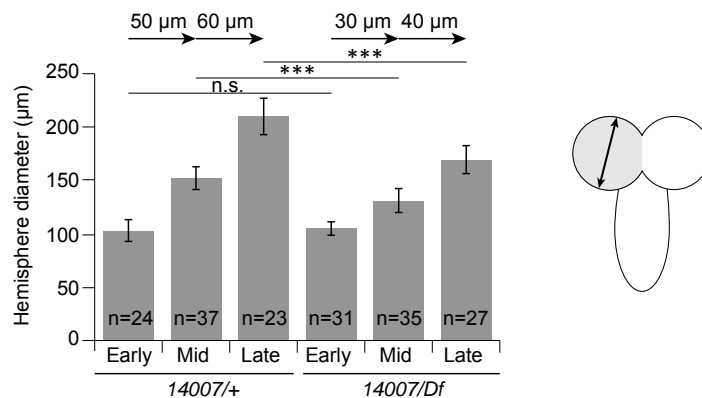


**Figure 33. Size and growth rate of the larval hemispheres is reduced in mutants.** The diameter of larval hemispheres is shown at early, mid and late L3 stage in control and *14007/Df* mutants. P values were calculated using the parametric T-student test. Error bars indicate Standard Deviation. n.s.>0,05, \*\*\* $p < 0,001$ .



## **CHAPTER IV:**

Photoreceptor phenotypes and  
guidepost glial cells





## **A subset of CIC-a<sup>+</sup> glial cells, which suffer a strong reduction in mutant animals, act as guidepost cells for photoreceptors**

To better understand the non-autonomous photoreceptor phenotypes in relation to the identified glial barrier between the developing lamina and lobula plug at late L3 stage, we performed a detailed developmental analysis of the region in control and mutant animals. To this purpose, we monitored the development of the boundary and the types of glia contributing to it starting from L2 stage. In previous studies, a small population of centrally located glia has been described, which preceded the arrival of photoreceptor axons in the lamina (Perez and Steller 1996; Dearborn and Kunes 2004), but a detailed description was lacking in those studies.

At L2 stage in controls, OPC and IPC neuroepithelia were still in contact and no glial cells were observed between them (see Figure 1). At this stage, the lobula plug is not developed yet. During early and mid L3 brains, a population of CIC-a<sup>+</sup> glial nucleus, with lower expression than cortex glia, progressively positioned in the expanding region between the OPC and IPC (Figure 34A,B). We called them boundary glia. Another CIC-a<sup>-</sup> glial population was also positioned distal to these cells (Figure 34A,B). We identified the CIC-a<sup>-</sup> glial cells as satellite glial cells (sg) using the *R43H01* line (Pfeiffer et al. 2008; Edwards et al. 2012). This driver had been described to specifically label satellite glia together with wrapping glia at late L3 (Figure 35B). We described, that the driver was expressed in satellite glial cells already at early L3 stage (Figure 35A). Boundary glia, a seemingly homogeneous population, differentiate into two cell types in late L3 brains: the outer chiasm glia (Xg<sub>o</sub>) and palisade glia (a glial type never described before) (Figure 34C,D). The palisade glia positioned in the same plane as the cortex glia projection and the Xg<sub>o</sub>, forming a continuous glial barrier. We do not know whether palisade glia are maintained until adult stage or not.

We next focused on the transition from boundary glia to Xg<sub>o</sub> and palisade glia. We observed, that in brains where just one ommatidial row of photoreceptors innervated the brain, boundary glia was looking like a homogeneous population sitting at the base of the cortex glia projection (Figure 34N). They had close contact with first innervating R8s (Figure 34N,O). However, in slightly older brains, where more ommatidial rows of photoreceptors innervated, we could observe cellular rearrangements. The majority of boundary glial cells started to position at the base of the lamina plexus (where R1-6 axons stop), creating a row (Figure 34P,Q) and few of them migrated distally. This row of boundary glial cells will become in Xg<sub>o</sub> and it will be the future outer chiasm. It seems that these cells have a strong relation with innervating photoreceptors.

Although we classified Xg<sub>o</sub> and palisade glia into two glial types by morphology and location, it could be that they are not genetically that different, since both were labeled using a previously described Xg<sub>o</sub> specific *R25A01* line (Pfeiffer et al. 2008; Edwards et al. 2012) (Figure 35C).

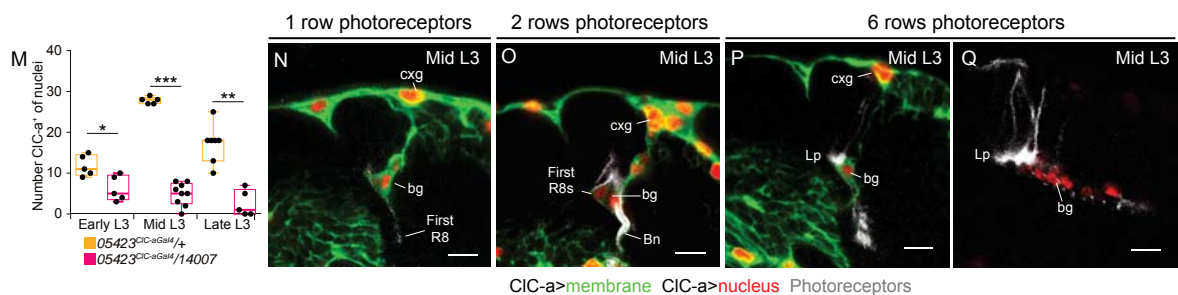
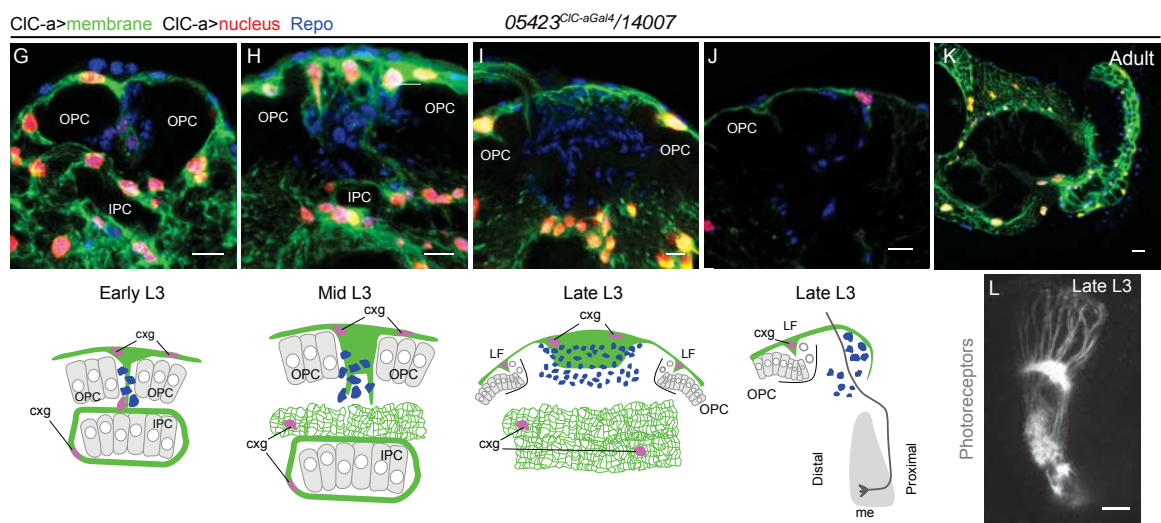
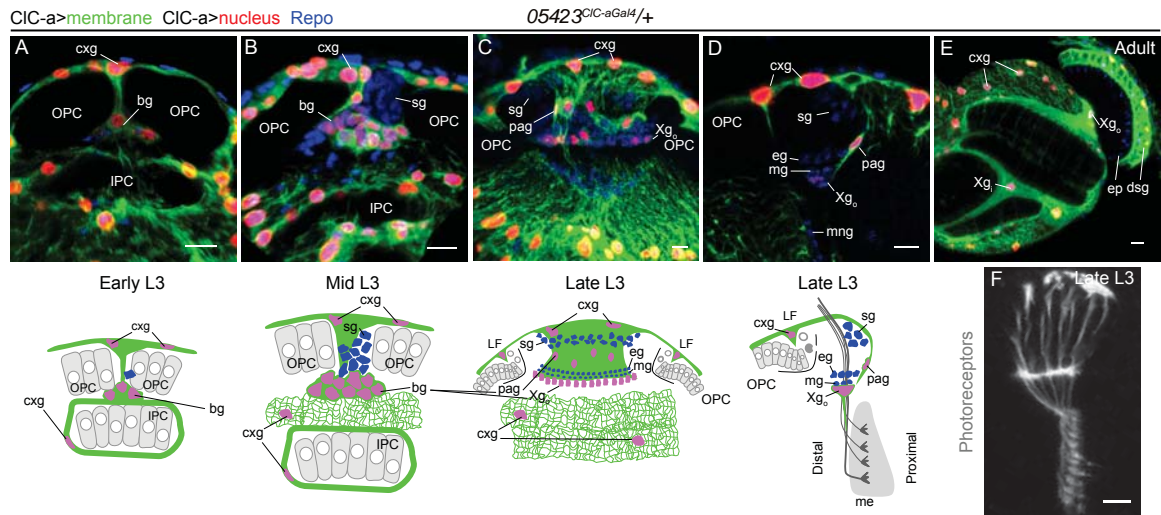


**Figure 34. A subset of CIC-a<sup>+</sup> glial cells, showing strong reduction in mutant animals, act as guidepost cells for photoreceptors.** 05423<sup>CIC-aGal4</sup> mediated membrane (*UAS-mCD8GFP*, green) and nuclei (*UAS-H2BRFP*, red) labeling is shown in all images, together with glial nuclei (Repo, blue) or photoreceptors (24B10, grey). (A-D) Development of the glial barrier in the developing control optic lobe from early L3 to late L3 with its schematics, in frontal views (A-C) and horizontal view (D). (B) and (C) are 3D images. A CIC-a<sup>+</sup> boundary glia is positioning and converting into Xg<sub>s</sub> and palisade glia during development. (E) Adult optic lobe of a control, with a well-organized chiasm. (F) Control larval photoreceptors. All R7 and R8 axons go through the chiasm and arrive to the medulla from its distal face. (G-J) Development of the glial barrier in the developing mutant optic lobe from early L3 to late L3 with its schematics, in frontal (G-I) and horizontal views (J). (G), (H) and (I) are 3D images. Few or no CIC-a<sup>+</sup> glia are observed in the glial barrier. (K) Adult optic lobe of a mutant with disorganized chiasm. (L) Mutant larval photoreceptors. Due to the reduction in boundary glia, some R7 and R8 axons skip the chiasm and arrive to the medulla from its proximal face. (M) Box plots showing CIC-a<sup>+</sup> nuclei counting in

the barrier in controls and mutants. Mutants show a strong reduction. (N-Q) Cellular rearrangements with the beginning of photoreceptor innervation. First R8s have close contact with boundary glia. Rows of photoreceptors were inferred by rows of 24B10<sup>+</sup> rows in the imaginal disc. Bn, Bolwig's nerve; bg, boundary glia; cxg, cortex glia; dsgr, distal satellite glia; ep, epithelial glia; LF, lamina furrow; Lp, lamina plexus; mg, marginal glia; mng, medulla neuropil glia; OPC, outer proliferation center; pag, palisade glia; IPC, inner proliferation center; sg, satellite glia; Xg<sub>i</sub>, inner chiasm glia; Xg<sub>o</sub>, outer chiasm glia. P values were calculated using the non-parametric Mann-Whitney test. \*p<0,05, \*\*p<0,01, \*\*\*p<0,001. Scale bars represent 10 μm.

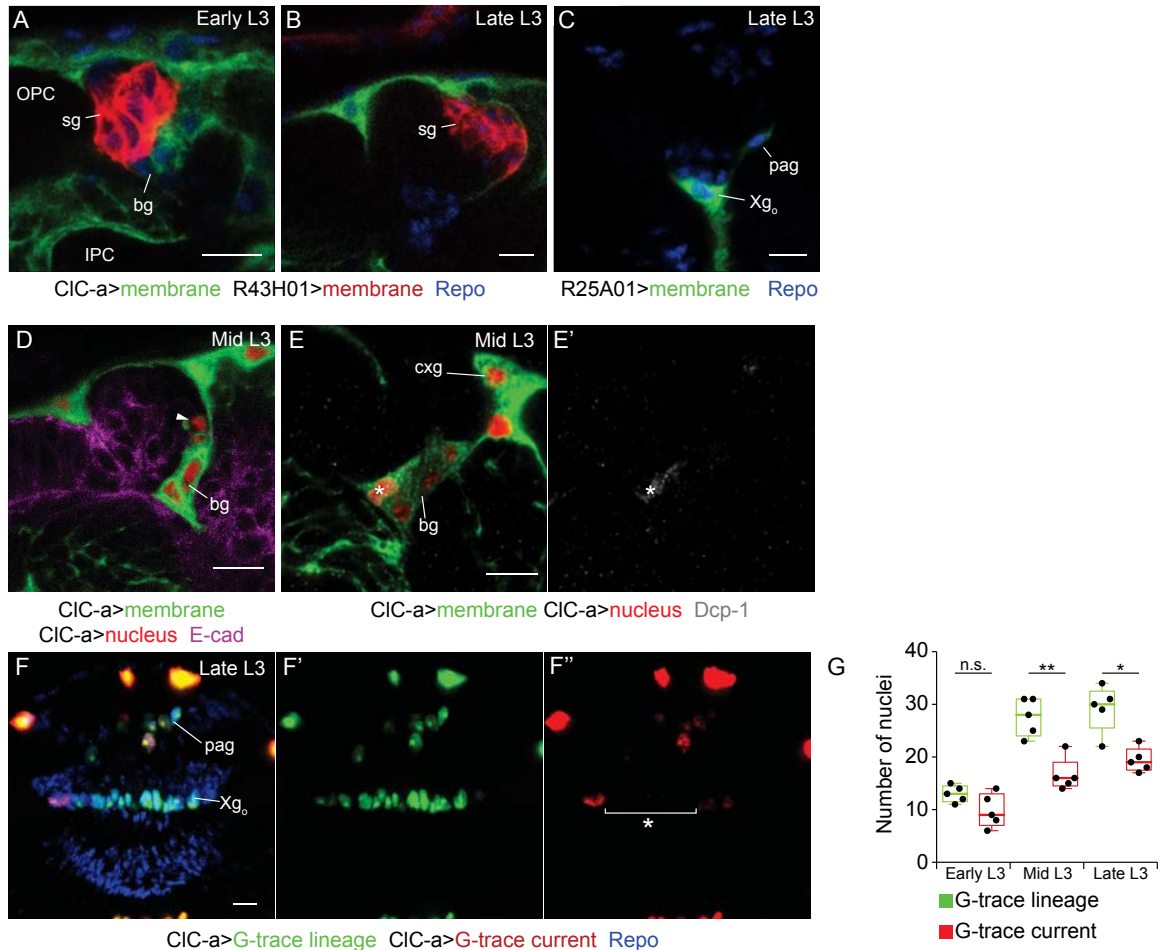


**Figure 35. Developmental details of the glial barrier.** (A,B) Satellite glia specific *R43H01LexA* (red) and *05423<sup>CIC-aGal4</sup>* (green) mediated membrane labeling at early and late L3. The *CIC-a*<sup>-</sup> glial population in the glial barrier at early L3, are satellite glial cells. (C) *R25A01Gal4* labels both Xg<sub>o</sub> and palisade glia. (D,E) Some boundary glial cells go through apoptosis when cellular rearrangements start at mid L3. Apoptotic bodies can be seen in (D) (arrow), and Dcp-1<sup>+</sup> boundary glial cells in (E) (asterisk). (F-G) G-trace lineage tracing by *05423<sup>CIC-aGal4</sup>* in a frontal view of the optic lobe at late L3. Green shows *CIC-a* lineage tracing, while *CIC-a* current expression is shown in red. Glial nuclei are labeled by Repo (blue). Some cells stopped expressing *CIC-a* at late larval stages (bracket). In (G) box plot depicting the counting of G-trace nuclei. bg, boundary glia; cxg, cortex glia; IPC, inner proliferation center; OPC, outer proliferation center; pag, palisade glia; sg, satellite glia; Xg<sub>o</sub>, outer chiasm glia. P values were calculated using the non-parametric Mann-Whitney test. n.s.> 0,05, p<0,05, \*\*p<0,01. Scale bars represent 10 μm.

Quantification of *CIC-a*<sup>+</sup> glia in control brains showed how their numbers increased from early to mid L3 stage and there was a slight drop at late L3. We wondered whether this drop was due to cell death or because of a dip in expression. We could observe very few *CIC-a*<sup>+</sup> apoptotic bodies at mid L3 in some brains (Figure 35D), hence some boundary glial cells go through apoptosis. Using an antibody against apoptotic marker Dcp-1, we could observe 1-2 boundary glial cells labeled and committed to die (Figure 35E). G-TRACE lineage tracing experiments (a *Gal4* technique for real-time and clonal expression) (Evans et al. 2009), using the *05423<sup>CIC-a gal4</sup>*, showed how cells, that had expressed *CIC-a* in mid L3 were present in the tissue, but were not expressing the reporter at late L3 (Figure 35F,G), meaning a dip in expression. We suggest that the few apoptotic events are a refinement due to cellular rearrangements and not a major apoptotic event.

Interestingly, when we assessed the integrity of the described glial barrier in *14007/05423<sup>CIC-aGal4</sup>* mutant brains, we observed, that while the number of boundary glia present in early L3 was the same as in controls (Figure 34G-J,M), the number of these cells did not increase at later stages (Figure 34G-J,M). Hence, there was a strong reduction in boundary glial cells during development.

In previous studies, it was suggested that some outer and inner chiasm glia were generated before L3 (Tix et al. 1997). Interestingly, it was described, that  $Xg_0$  derive from a central brain type II neuroblast lineage DL1 (Viktorin et al. 2013). Immediately following the generation of the glia in the central brain, during the second half of larval development, the DL1 lineage-derived glia migrate into the optic lobe entering between the posterior borders of the IPC. Once in the optic lobe, they differentiate into three identified types of optic lobe glial cells, inner chiasm glia, outer chiasm glia, and cortex glia (Viktorin et al. 2013; Ren et al. 2018). They detected DL1 derived glial cells in the optic lobe for the first time at around 66-72h AEL (late L2-early L3) and kept migrating until 84-90h AEL (just prior to mid L3). The appearance of boundary glial cells at early L3 stage and the increase in numbers until mid L3 matches perfectly. To confirm, boundary glial cells were coming from DL1 lineage, we took advantage of the *R38H02Gal4* line, which represent a neurotactin enhancer fragment (Jenett et al. 2012), and it was used by Viktorin and colleagues (Viktorin et al. 2013) to generate DL1 clones. A lineage tracing experiment using the G-trace technique with this driver, allowed stochastic, but very specific labeling of DL1 progeny throughout postembryonic development. Indeed, we could observe glial cells migrating from central brain to the optic lobe (Figure 36A) at early L3 stage, and outer chiasm glial cells at mid-late L3 (Figure 36B). We concluded, that boundary glia was derived from central brain type II neuroblast lineage DL1.

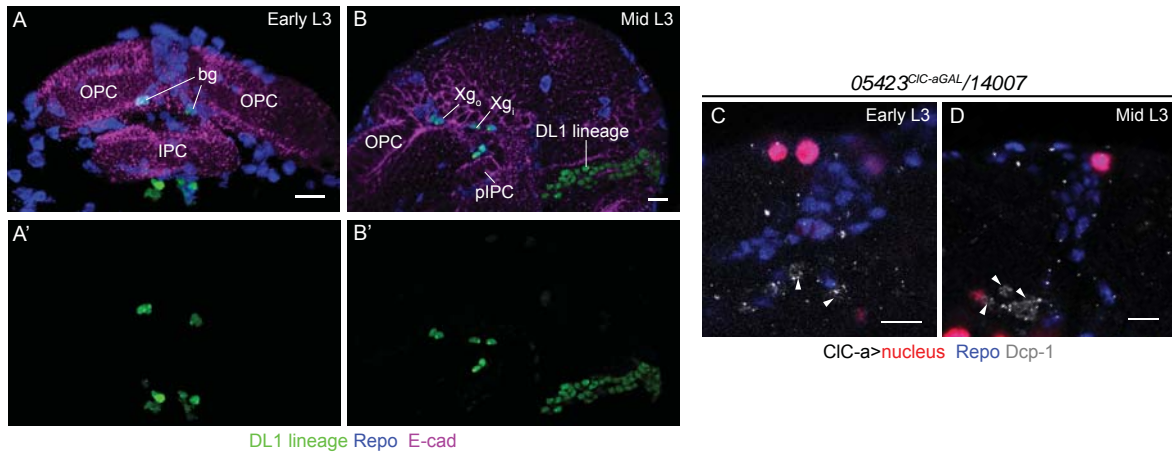


**Figure 36. Boundary glia migration and cell death in the barrier.** (A,B) DL1 lineage nuclei (green) combining the *38H02Gal4* with G-trace, at early and late L3. Neuroepithelia are labeled with E-cad (magenta) and glial nuclei with Repo (blue). (A) is a 3D image, neuroepithelia were segmented and E-cad signal is masked to avoid background noise. (C,D) Dcp-1 staining (grey) in early and mid L3 glial barriers. No Dcp-1<sup>+</sup> glial nuclei (Repo, blue) was observed in the glial barrier. Arrows show some Dcp-1<sup>+</sup> apoptotic neurons. bg, boundary glia; IPC, inner proliferation center; OPC, outer proliferation center; pIPC, proximal inner proliferation center; Xg<sub>i</sub>, inner chiasm glia; Xg<sub>o</sub>, outer chiasm glia. Scale bars represent 10 μm.

It could be, that boundary glial cells in *CIC-a* mutants reached to the optic lobe and died soon after migration. To test that, we performed Dcp-1 staining to see whether we observe dying glial cells in the area. No apoptotic glial cells were detected in the region (Figure 36C,D), which indicated that just very few boundary glial cells reached the optic lobe in mutants, suggesting, that their differentiation or migration could be affected.

We next wondered how the strong reduction in boundary glial cells affected the photoreceptors. As previously mentioned, R8s from the first rows of ommatidia projected into the posterior part of the field of LPC, and their axons were found very close to boundary glia as they continued to the medulla (Figure 34F). On the contrary, in mutant brains the absence of boundary glia resulted in posterior R8 axons, skipping the outer chiasm and innervating the medulla from its proximal face (Figure 34L).

### ***slit* mutants have similar photoreceptor guidance phenotypes**

To gain further insight into the relation of the reduction of boundary glia and photoreceptor phenotypes, we checked the literature trying to find similar phenotypes. We found that *slit* mutants showed very similar photoreceptor phenotypes at both larval (Figure 37A,C) and adult stages (Figure 37B,D).

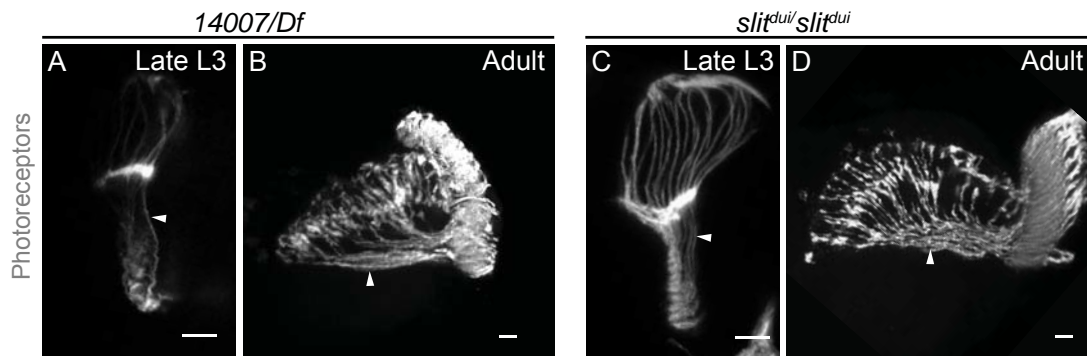


**Figure 37. *slit* mutants show similar photoreceptor guidance phenotypes compared to CIC-a mutants.** (A, B) Larval (A) and adult (B) photoreceptor (24B10, grey) phenotypes in CIC-a mutants. (C, D) Larval (C) and adult (D) photoreceptor (GMR-GFP, grey) phenotypes in *slit<sup>dui</sup>/slit<sup>dui</sup>* mutants. Arrows show misguided axons reaching the medulla from its proximal face. Scale bars represent 10  $\mu$ m.

It has been proposed, that Slit and Robo-family repulsive signals, act to maintain the distinct cellular composition of the lamina and the lobula cortex, maintaining the boundary between populations of non-intermingling cells. Slit seems to be required in the lamina, to prevent the inappropriate invasion of Robo expressing neurons from the lobula cortex and controlling photoreceptor axonal guidance (Taylor et al. 2004). Furthermore, it has been described that the Robo-3 receptor is expressed specifically and transiently in R8 growth cones, when innervating the brain. Most posterior R8 axons extend along a border of glial cells, demarcated by the expression of *slit*, a Robo3 secreted ligand (Pappu et al. 2011). These studies suggest a clear role of Slit-Robo signaling required for correct photoreceptor axon guidance, which is important for maintaining a boundary between compartments. However, nobody has described the cell types contributing to the boundary in detail, and the expression of *slit* in these cells in relation to photoreceptor innervation.

### The glial barrier expresses *slit* at the time of photoreceptor innervation

We already described the glial cell types, that contribute to the glial boundary between the population of non-intermingling cells in the lamina and lobula plug. Next, we took advantage of a tagged *slit-GFP* reporter, which was derived from a MiMIC insertion in the *slit* locus, to describe its expression in the barrier. The Slit full length protein can be cleaved into a large N-terminal (Slit-N) and a short C-terminal (Slit-C) fragment. These various forms of Slit show different activities and functions. For example, mammalian Slit-FL and Slit-N are more tightly associated with the cell surface, whereas Slit-C is mostly diffused into the extracellular space (Brose et al. 1999). The GFP tag in this *slit-GFP* reporter line was located between aminoacids 398-399, in the second LRR repeat, hence in the Slit-N terminal. This allowed us to identify the cells that expressed *slit*, as GFP was attached to the membrane of these cells and not diffused. As this reporter was not previously used in other studies, we compared

its expression to the well-known *slit-LacZ* (*slit*<sup>05428</sup>) nuclear reporter in cells described to express *slit* (Figure 38C,D). In the ventral nerve cord, both *slit-GFP* and *slit-LacZ* labeled the midline glia (Figure 38A,C). In the optic lobe, the reporters were expressed in Xg<sub>o</sub> and some medulla neurons (Figure 38B,D), as described in literature (Tayler et al. 2004; Suzuki et al. 2016). We concluded that this reporter was reporting Slit expression correctly.

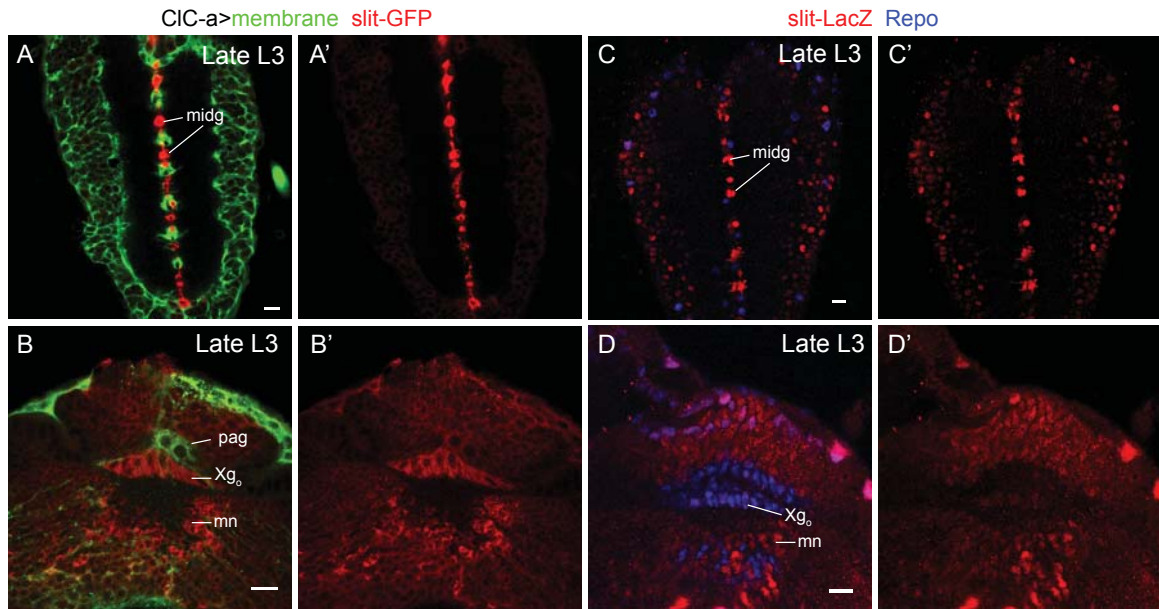


**Figure 38. *slit-GFP* confirms described *slit* expression.** (A,B) *slitGFP* expression (red) in VNC (A) and in frontal view of a larval optic lobe (B). *slitGFP* is expressed in midline glia, Xg<sub>o</sub> and medulla neurons. (C,D) *slit-LacZ* nuclear expression (red) in VNC (C) and in frontal view of a larval optic lobe (D). Both reporters are expressed in the same described cells. midg, midline glia; mn, medulla neuron; pag, palisade glia; Xg<sub>o</sub>, outer chiasm glia. Scale bars represent 10 μm.

Focusing on the glial barrier, we found that at early L3 stage, before photoreceptor innervation, *slit* was expressed in satellite glial cells, but not in boundary glia (Figure 39A). Importantly, at the time when photoreceptor innervation starts at mid L3 stage, both satellite and boundary glia expressed the repulsive signal (Figure 39B). Thus, first innervating R8s will encounter a glial barrier, where all glial types are Slit<sup>+</sup>. In late L3 stage, *slit* was also expressed in satellite glia, and boundary glia derived outer chiasm glia and palisade glia (Figure 39C).

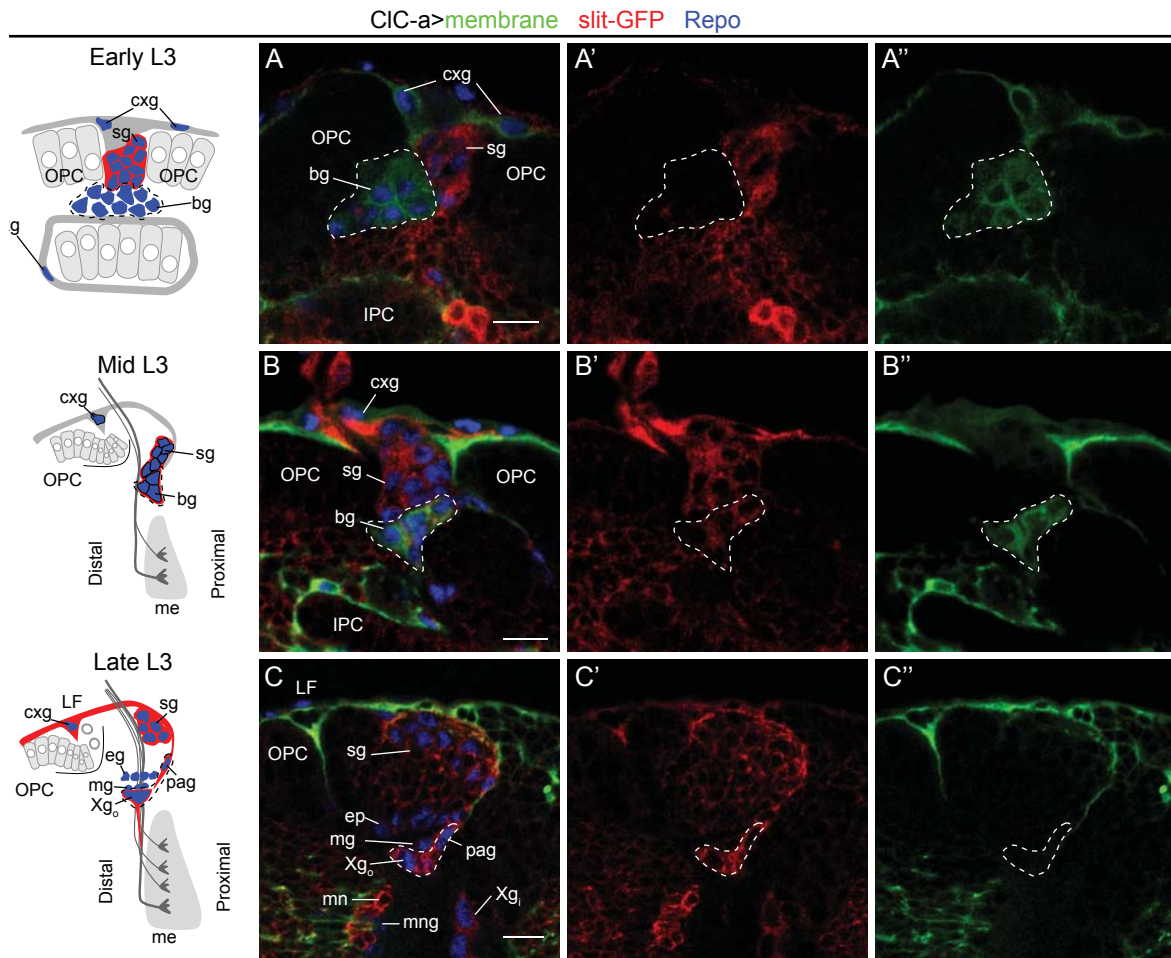


**Figure 39. *slit* is expressed in the glial barrier during photoreceptor innervation.** (A-C) *slit* expression (*slitGFP*, red) during glial barrier development, from early to late L3 stage. Glial nuclei are labeled with Repo (blue) and boundary and cortex glia with  $05423^{CIC-aGal4}$  mediated membrane (*UAS-mCD8GFP*, green) labeling. Boundary glia are outlined in (A) and (B) and  $Xg_0$  and palisade glia in (C). Schematics show *slit* expressing cells in red. In (C)  $Xg_0$  and palisade glia do not express *CIC-a* due to the dip in expression that happens in late L3 stage. bg, boundary glia; cxg, cortex glia; ep, epithelial glia; IPC, inner proliferation center; LF, lamina furrow; mn, medulla neuron; mng, medulla neuropil glia; mg, marginal glia; OPC, outer proliferation center; pag, palisade glia; sg, satellite glia;  $Xg_i$ , inner chiasm glia;  $Xg_0$ , outer chiasm glia. Scale bars represent 10  $\mu$ m.

### Reduced *slit* expression in the glial barrier phenocopies axon guidance defects in *CIC-a* mutants

Slit expression in boundary glia led us to ask whether Slit is required in this glial type, and whether removing the repulsive signal from these cells could phenocopy *CIC-a* mutant photoreceptor phenotypes. This would explain, why the strong reduction of this glial type led to guidance defects. We used a previously described Slit RNAi to knock down the gene in cortex and boundary glia, with  $05423^{CIC-aGal4}$ . 40% of the brains showed exactly the same photoreceptor phenotypes as in *CIC-a* mutants (Figure 40A). In order to increase the strength of the *slit* knock down, we repeated the experiment in a heterozygous background for a *slit<sup>dui</sup>* mutation. This mutation is characterized by removing *slit* expression only from



the optic lobe (Tayler et al. 2004). In this case, 70% of the brains showed exactly the same guidance phenotypes (Figure 40A). Thus, we can conclude, that Slit is necessary in boundary glia for correct photoreceptor axon guidance.

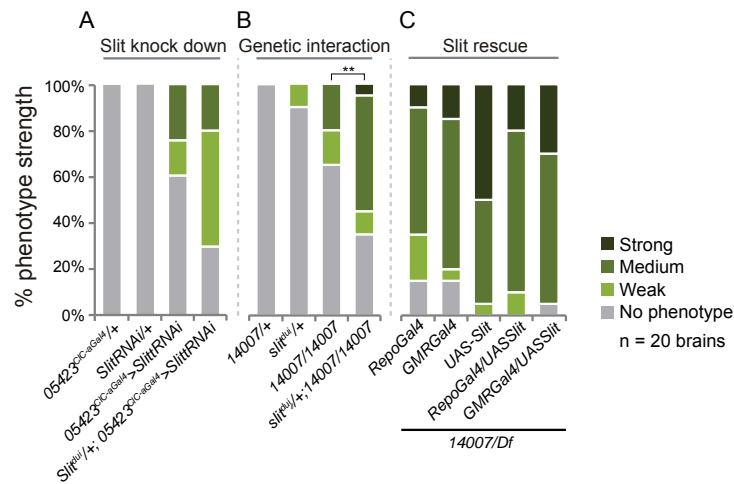


**Figure 40. Slit is necessary in boundary glia for correct photoreceptor guidance.** (A) Phenotype percentages in *slit* RNAi knock down in boundary glia. *slit* was knocked down in a *slit* wild type and a *slit*<sup>dl1</sup> heterozygous background. (B) Phenotype percentages in genetic interaction between *CIC-a* and *slit*. The removal of one copy of *slit* significantly increased the percentage of 14007/14007 photoreceptor phenotypes. (C) Phenotype percentages in rescue experiment by the overexpression of *slit* cDNA with *RepoGal4* and *GMRGal4* in 14007/*Df* mutant background. The increase of Slit concentration in the area did not rescue the photoreceptor phenotypes. P values were calculated using the non-parametric Mann-Whitney test. \*\*p<0,01.

Interestingly, when removing a copy of *slit* in *CIC-a* mutant 14007/14007, which originally displayed a relatively low percentage of phenotypes, we observed a significant increase of brains having axon guidance defects, changing from 35% to 65% (Figure 40B). Therefore we concluded that *CIC-a* and *slit* genetically interact.

It has been described that providing Slit to the area, overexpressing it in glia, or photoreceptors themselves was enough to rescue Slit mutant phenotypes (Tayler et al. 2004). We wondered, whether increasing Slit concentration in the region would rescue *CIC-a* mutant phenotypes, and make the photoreceptor take the correct path. We increased Slit concentration in 14007/*Df* allelic combination. We expressed the Slit cDNA via two different reporters: in the remaining glia, with *RepoGal4* and in photoreceptors, using *GMRGal4*. We could not rescue photoreceptor phenotypes at all (Figure 40C), so we concluded that a correct assembly of the Slit<sup>+</sup> glial barrier is necessary for normal photoreceptor axon guidance.

Together, this observations show that Slit is necessary in boundary glia, for correct photoreceptor guidance. Also, we concluded that the strong reduction of boundary glia in *CIC-a* mutants would affect axon guidance, disrupting the Slit expressing barrier.

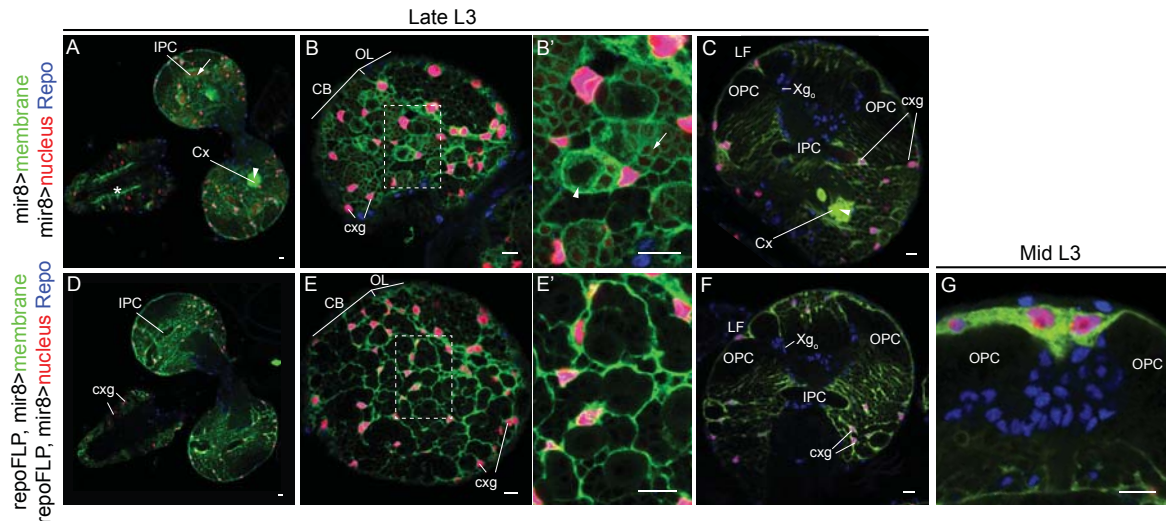


**Figure 41. *mir8Gal4* expression is restricted to cortex glia based on an intersectional strategy.** (A-C) *mir8Gal4* expression (membranes, green; nuclei, red) in the late L3 brain. Glial nuclei are labeled with Repo (blue). Apart from cortex glia, it is expressed in non-glial cells, such as, VNC neurons (asterisk in A), neurons of the mushroom body (arrowhead A,C), parts of the IPC (arrow in A), neuroblasts (arrowhead in B'), and other neurons (arrow in B'). (D-F) *mir8Gal4* expression combined with the *RepoFLP* strategy. Non-glial cell expression disappeared and only cortex glia expresses the driver. Xg<sub>o</sub> or other neuropil glia (C, F) do not express the driver. (G) The glial barrier int mid L3 stage. *mir8Gal4* is not expressed in boundary glia. CB, central brain; Cx, calyx; cxg, cortex glia; LF, lamina furrow; OL, optic lobe; OPC, outer proliferation center; IPC, inner proliferation center; Xg<sub>o</sub>, outer chiasm glia. Scale bars represent 10  $\mu$ m.

### CIC-a is sufficient in cortex glia for the generation of guidepost cells in the central brain and their positioning in the optic lobe

Next, we focused on how *CIC-a* mutations resulted in the reduction of boundary glia in the optic lobe. Boundary glia migrates to the optic lobe from central brain lineage DL1, which is encased by *CIC-a*<sup>+</sup> glial processes. Previously we already described, that *CIC-a* might be required for neuroblast divisions. At the same time, boundary glia itself expresses *CIC-a*. In order to assess the requirement of *CIC-a* for the described phenotypes in boundary glia itself or in cortex glia, we did another rescue experiment expressing *CIC-a* cDNA.

This time we used the previously mentioned cortex glia labeling *mir8Gal4* driver. Apart from cortex glia, this driver was also expressed in non-glial cells (Figure 41A-C). To restrict its expression to glia, we used an intersectional strategy. We combined the driver with a *tub>gal80>* and *repoFLP6:2*. The flippase is expressed exclusively in glia, were it removes the FRT-flanked Gal80 from DNA, allowing the Gal4 to work only in *mir8* expressing glia (Figure 41D-F). We confirmed, that *mir8Gal4* was not expressed in boundary glia, Xg<sub>o</sub>, or any neuropil glia (Figure 41F,G).

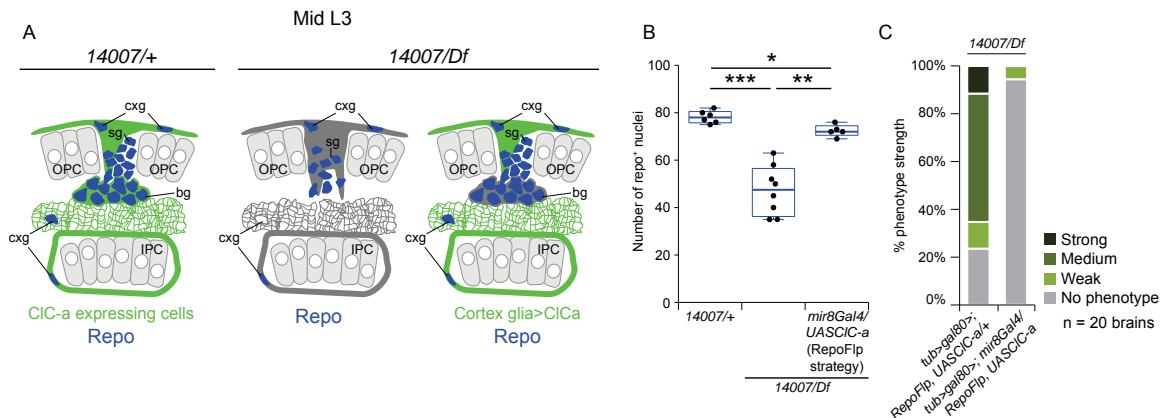


**Figure 42. *CIC-a* expression in cortex glia rescues boundary glia reduction and photoreceptor phenotypes.** (A) Illustration, showing the design of the rescue experiment. In controls, cortex glia and boundary glia expresses *CIC-a* (green), while in mutants, none of them does. In the rescue experiment, *CIC-a* is only expressed in cortex glia. (B) Box plots showing glial cell number in the barrier region. While in mutants, numbers of glial cells decrease hugely, their numbers are rescued through expression of the channel in cortex glia. (C) Photoreceptor phenotype percentages in the *mir8Gal4* rescue experiment. Photoreceptor phenotypes are rescued. P values were calculated using the non-parametric Mann-Whitney test. \* $p < 0,05$ , \*\* $p < 0,01$ , \*\*\* $p < 0,001$ .

Since we were not able to specifically label boundary glia in this experiment, (the only way to label them specifically was using the *05423<sup>CIC-aGal4</sup>*), we counted Repo<sup>+</sup> cells in the barrier in mid L3 stage, just when the first photoreceptors innervate the brain. This includes boundary and satellite glia. In mutants, compared to controls, the number of glial cells in the barrier was reduced to half, due to the strong reduction in boundary glia (Figure 42B). Expression of *CIC-a*, exclusively in cortex glia, resulted in an almost complete rescue of the number of glial cells present in the barrier region in mid L3 (Figure 42B). Furthermore, photoreceptor phenotypes were also rescued (Figure 42C). Surprisingly, it seems, that autonomous *CIC-a* expression in boundary glia is not necessary for these cells, to migrate from their point of origin in the central brain to the optic lobe.

Overall, the boundary glia decrease is a secondary consequence of the removal of *CIC-a* from cortex glia. *CIC-a* could be required in cortex glia to promote the generation of boundary glia from the DL1 neuroblast, or their migration to the optic lobe, and/or their survival.

### Migration of boundary glia could be affected due to DL1 lineage mispositioning

The majority of central brain neuroblasts are type I neuroblasts (approximately 90 in each hemisphere) and they are located in all brain regions. On the contrary, there are only eight type II neuroblasts, which are located in the dorso-posterior side of each hemisphere. *R9D11-CD4-tdtomato* reporter (Pfeiffer et al. 2008; Han et al. 2011) labels selectively all type II lineages (Figure 43A). Six of them (DM1-6) are located at the posterior-medial

edge and are distributed in a dorso-ventral row. The other two localize at a more lateral position (DL1-2) and are usually close to each other (Figure 43A). It is not possible to differentiate between DL1 and DL2 lineages just based on location or secondary axon tract (SAT) trajectory (Pereanu and Hartenstein 2006; Viktorin et al. 2013), so we will name them together as DL1-2.

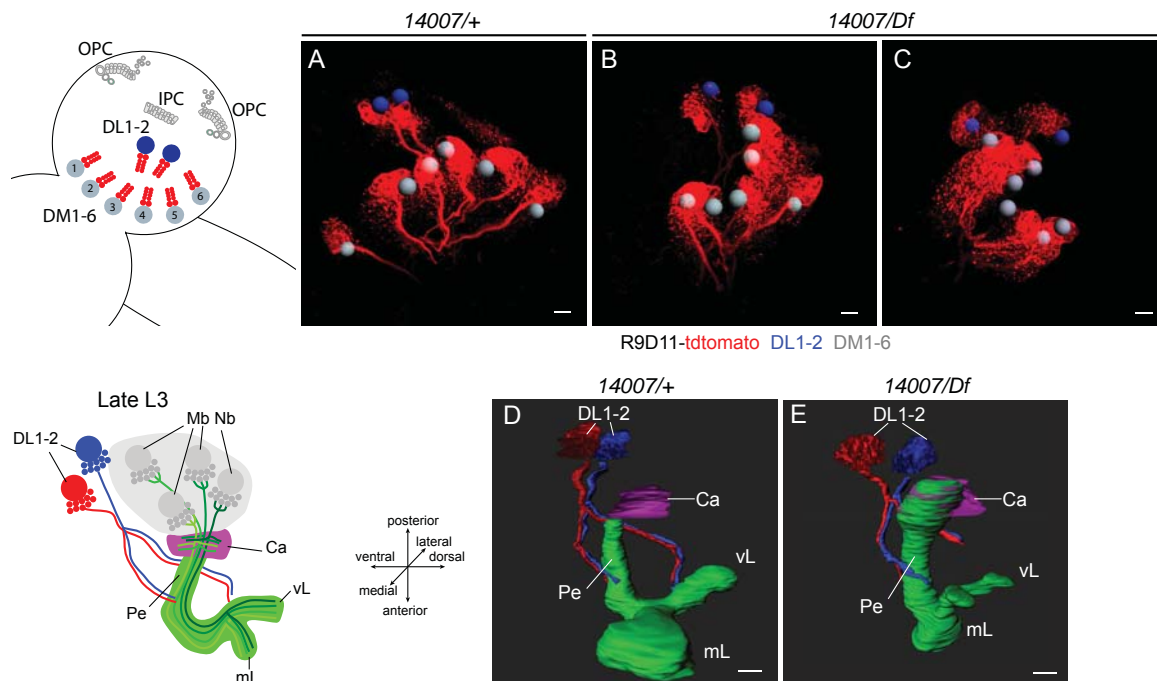


**Figure 43. Boundary glia reduction could be a consequence of DL1 mispositioning.** (A-C) 3D images showing type II lineages (R9D11-tdtomato, red) in control (A) and *14007/Df* mutants (B,C), with a schematic showing the wild type distribution of lineages. DM1-6 neuroblasts are shown in grey and DL1-2 neuroblasts in blue. (D,E) 3D reconstructions showing DL1-2 axon tracts (blue and red) in controls (D) and mutants (E) at late L3. The illustration shows wild type DL1-2 axon tracts and mushroom body. The calyx is shown in magenta and the mushroom body peduncle and the lobes in green (segmented from FasII staining). Ca, calyx; Pe, peduncle; vL, vertical lobe, mL, medial lobe; Mb Nb, Mushroom body neuroblasts. Scale bars represent 10 µm.

DL1 lineage is present in *CIC-a* mutants (Figure 43B,C) and we observed defects in the distribution of type II lineages in some few *14007/Df* mutants. In some of those affected brains DL1-2 lineages were usually separated from each other, and one of them was usually in contact with DM4-5 (Figure 43B,C). In others, DM1-6 lineages were moved laterally, in contact with DL1-2, and lost the ordered location they had in the wild type (Figure 43B,C). Although we saw variability between the brains, it was clear that mutants showed type II lineage organization defects. DL1 derived boundary glial cells migrate to the optic lobe between the posterior borders of the IPC and all of these migrating glial cells are interconnected by cellular processes, some of which also extended to the cluster of DL1 derived neuronal cells in the central brain (Viktorin et al. 2013). The IPC is defective in mutants and sometimes DL1 lineage has different relative positions respect to the IPC.

Thus, aberrant location of DL1 lineage could affect to a normal boundary glial migration to the optic lobe.

Next, we wondered whether lineage distribution problems were affecting DL1-2 secondary axon tract (SAT) trajectory. DL1-2 axon tracts are the equivalent to the CP2/3 axon tracts (Pereanu and Hartenstein 2006; Viktorin et al. 2013) and their trajectories are well established. As a landmark, we labeled the mushroom body neuropil by an antibody against Fasciclin II (FasII), a cell adhesion molecule. As far as we could follow the tracts, we could not observe any defects in their trajectories in reference to the mushroom body neuropil in *14007/Df* mutants (Figure 43D,E). However, we could observe severe phenotypes in the mushroom body by Fas II staining (Figure 43E), which will be described further in the text.

### Boundary glia generation could be affected by proliferation defects in DL1 lineage

Next, we sought to characterize proliferation defects in DL1 lineage. Type I neuroblasts divide asymmetrically, to generate a ganglion mother cell (GMC), that will give rise to two differentiated cells. However, type II neuroblasts divide asymmetrically, but instead of generating a GMC, they generate a transit amplifying intermediate neural progenitor (INP). It undergoes a series of transcriptional changes to become a mature INP. Mature INPs continue to divide asymmetrically, 3-5 times (Bello et al. 2008), generating a self-renewed INP and a GMC that divides once more, to generate two differentiated neurons or glial cells. After that, mature INPs disappear.

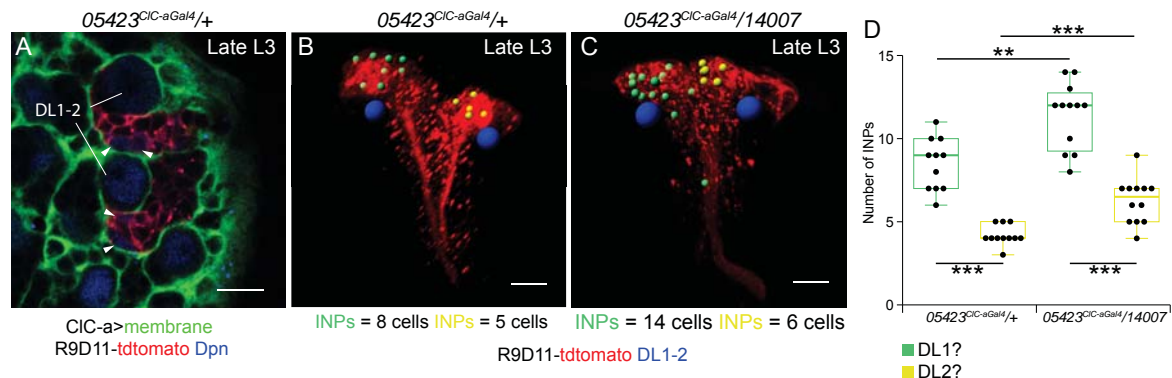


**Figure 44. Boundary glia reduction could be a consequence of decreased proliferation in DL1 lineage.**

(A) DL1-2 lineages (*R9D11tdtomato*, red) with their respective mature INPs (arrowheads), encased in cortex glial chambers (green). Neuroblasts and mature INPs are labeled with Dpn antibodies (blue). (B,C) 3D images showing DL1-2 lineages (*R9D11tdtomato*, red). DL1-2 neuroblasts are shown in blue and INPs, corresponding to each lineage, in green and yellow respectively. There is always a lineage which has more INPs. (D) Box plot showing INP numbers for predicted DL1-2 lineages. Mutant DL1-2 lineages have more INPs compared to controls. P values were calculated using the non-parametric Mann-Whitney test. \*\*p<0,01, \*\*\*p<0,001. Scale bars represent 10  $\mu$ m.

Our initial approach was to compare control to mutant DL1 clones. However, even though the clonal analysis protocol used in our study was very similar to the one used in other studies, where type II clones were analyzed, which are identified by the presence of INPs (*Dpn* positive cells in the lineage), we hardly obtained any type II clone (2 out of 116 analyzed clones), and none of them was in DL1.

As an alternative, we use the number of INPs in a lineage as a read out for proliferation. Mature INPs can be easily detected by immunostaining against the transcription factor *Deadpan* (*Dpn*), which labels their nucleus. Together with *Dpn*, we labeled type II lineages with *R9D11tdtomato* and cortex glia with *05423<sup>CIC-aGal4</sup>* (Figure 44A). Cortex glia processes separate the lineages in different chambers and labeling them allowed us to identify INPs belonging to the specific lineage, when lineages were touching. Although we could not distinguish between the DL1 and DL2 lineages in wild type condition, there was always one of the DL1 or DL2 lineages, that contained more mature INPs than the other. Hence, we used this difference in INP numbers to predict different lineages between DL1 and DL2. Interestingly, both lineages in *14007/05423<sup>CIC-aGal4</sup>* mutants contained more INPs compared to controls (Figure 44B-D). An increase in INPs would suggest, that the increase has no relation to a decreased proliferation, but proliferative defects could explain this increase: INPs could have a slower division rate, increasing their life expectancy, which would result in their accumulation. INP position or morphology in the lineages was not affected.

Thus, given that we also observed proliferation defects in neuroepithelial cells, we suggest that reduced mitotic activity of INPs could be one of the causes for the strong reduction of boundary glia. We should not forget, that overall cell death in the larval brain was increased in *CIC-a* mutants, so it could also be, that less boundary glia are generated and the decrease is enhanced by cell death. Although we showed that boundary glia does not die in the optic lobe, the glia's destiny, it could be, that some of the boundary glia die, soon after being generated in the central brain.

### **Mushroom body neurons also show guidance defects**

We previously mentioned, that FasII staining showed strong phenotypes in the mushroom body in *CIC-a* mutants. Although we did not perform specific experiments to describe these phenotypes in detail, we benefit from other experiments and pay attention to the mushroom body when possible.

The four mushroom body neuroblasts are special type I neuroblasts, which never enter quiescence, during the transition from embryo to larva. The neurons differentiated from these neuroblasts project to the mushroom body. The mushroom body is an easily distinguishable neuropil, comprising thousands of neurons (Kenyon cells). It consists of the neuronal cell bodies, followed by a cup-shaped protrusion called the calyx, where neurons send dendrites

to (Figure 45). The axons continue through the peduncle and finally bifurcate in two lobes, pointing vertical or medially (Figure 45). Newly differentiated Kenyon cells project their axons through the middle of the peduncle.

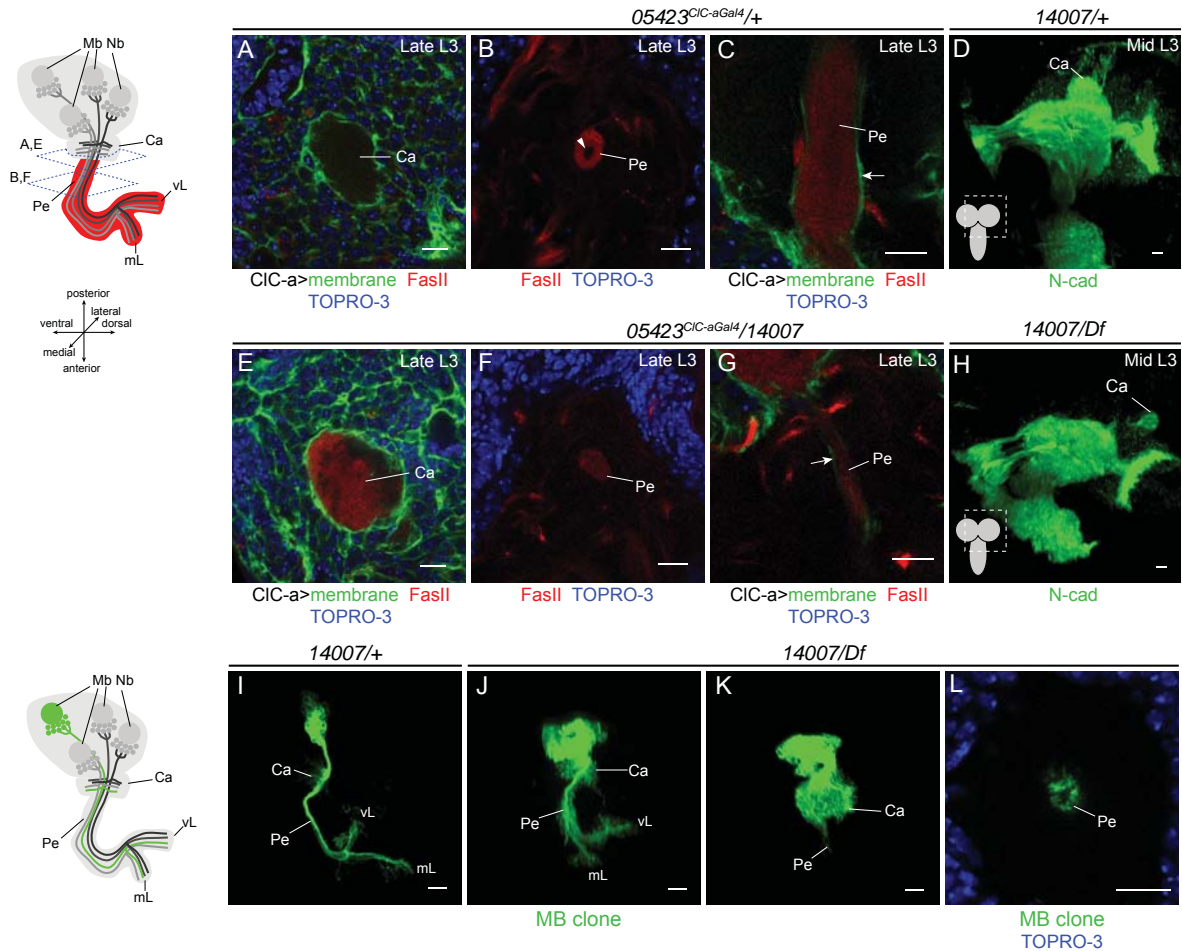


**Figure 45. Neurons of the mushroom body show guidance defects.** (A, E) A transversal cut at the level of the calyx. While in controls (A) the calyx does not show any FasII labeled MB neuronal axons, in mutants (E) a lot of FasII<sup>+</sup> axons misproject to the calyx. Nuclei are labeled in blue (TOPRO-3) and CIC-a<sup>+</sup> membranes in green (*05423<sup>CIC-aGal4</sup>* mediated *UASmCD8GFP* expression). (B,F) A transversal cut at the level of the peduncle. In controls (B) a FasII<sup>+</sup> area, which belong to new differentiated neuronal axons, is observed in the middle of the peduncle (arrowhead). In mutants (F) all peduncles seem homogeneous. (C, G) A sagittal cut at the peduncle. The peduncle is wrapped by CIC-a<sup>+</sup> ensheathing glia (arrows) in controls (C) and mutants (G). The peduncle is thinner in mutants. (D-H) 3D images of whole larval hemispheres at mid L3 stage, stained by N-cad (green). The calyx is mispositioned to the surface in mutants (H), compared to controls (D). (I-L) 3D images of MB neuroblast clones (green). In controls (I) just some few dendrites of MB neurons are observed in the calyx and the peduncle is thin, as new neurons on the clone project through the middle of it. In mutants, a medium phenotype (J) shows an increased staining in the calyx, while the peduncle is much thicker and disorganized. New differentiated neurons in the clone go through the peduncle from its exterior part (L). In stronger phenotypes (K), all axons stopped at the calyx, and the peduncle is not visible. Ca, calyx; Pe, peduncle; vL, vertical lobe, mL, medial lobe; Mb Nb, Mushroom body neuroblasts. Scale bars represent 10  $\mu$ m.

The cell adhesion molecule Fasciclin II (FasII) is highly expressed in the oldest mushroom body neurons and labels the peripheral region of the peduncle and the lobes, but not the calyx (Figure 45A,B). The strongest phenotypes showed strong FasII signaling in the calyx (Figure 45E), whereas the peduncle and the lobes were weakly labeled, the peduncle being thinner (Figure 45F,G). It seemed that mushroom body neuron axons were misprojecting to the calyx without going through the peduncle. Also, in the peduncle, FasII signaling was homogeneous, labeling peripheral and internal regions (Figure 45F). Hence, newly differentiated neurons (FasII negative) do not project their axons through the middle of the peduncle. Using N-cad staining, which labels different neuropils, we also identified mispositioning of the calyx to the surface, far from other central brain neuropils (Figure 45D,H).

MB neuroblast *MARCM* clones induced at L2 stage and collected at mid L3 stage in *14007/Df* mutants, allowed us to describe these defects in more detail. Phenotypes could be classified in two groups by severity. We observed that in the strongest phenotypes, Kenyon cell axons stopped in the calyx, without going through the peduncle (Figure 45K). In weaker phenotypes, some stopped in the calyx, but the majority went through the peduncle (Figure 45J). Interestingly, peduncle internal organization was also disrupted, since new axons did not go through the middle of it, but entered from the peripheral region (Figure 45L). Whether these phenotypes are related to the described proliferation defects or not, is yet to be elucidated.

The mushroom body is separated from the rest of the brain by a thin sheath of glia lamellae, a kind of ensheathing glia which is *CIC-a*<sup>+</sup>. To explain these phenotypes, we wondered whether this glia lamellae was still ensheathing the peduncle in *CIC-a* mutants. Interestingly, in some preliminary experiments in *14007/Df* mutants, we could not observe any detectable defects in the ensheathing glia surrounding the peduncle. This is just an observation and additional experiments are required to conclude whether the morphology of these glia is wild type. Furthermore, other glial types, being in close relation with the mushroom body, could also be affected.

Thus, guidance phenotypes are not exclusive to photoreceptors in *CIC-a* mutants, as they affect mushroom body neurons. As some of the mushroom body glia is generated from DM2, DM3, DM5 and DM6 type II neuroblasts (Ren et al. 2018), it could be, that in the same way as boundary glia, other neuropil glial types of the mushroom body are also decreased, affecting neuronal guidance.

Even though, we did not assess proliferation defects in those type II neuroblasts, in other experiments, we occasionally observed encasing defects in some *14007/05423<sup>CIC-aGal4</sup>* mutant brains. Two type II neuroblasts could be in the same cortex glial chamber (Figure 46B,C). In each brain the pair of affected neuroblasts was different; DM1-DM2, DM2-DM3 or DM4-DM5 neuroblast pairs clustered together in the same cortex glial chamber (Figure



46B,C). However, DL1-2 neuroblasts did not show this phenotype. Hence, cortex glial encasing of some type II neuroblasts was not happening correctly in the central brain, but more information needs to be obtained to know, whether these defects could somehow affect the lineage.

In summary, it could be, that in the same way as boundary glia decrease affects photoreceptor guidance, other neuronal guidance is affected as well.

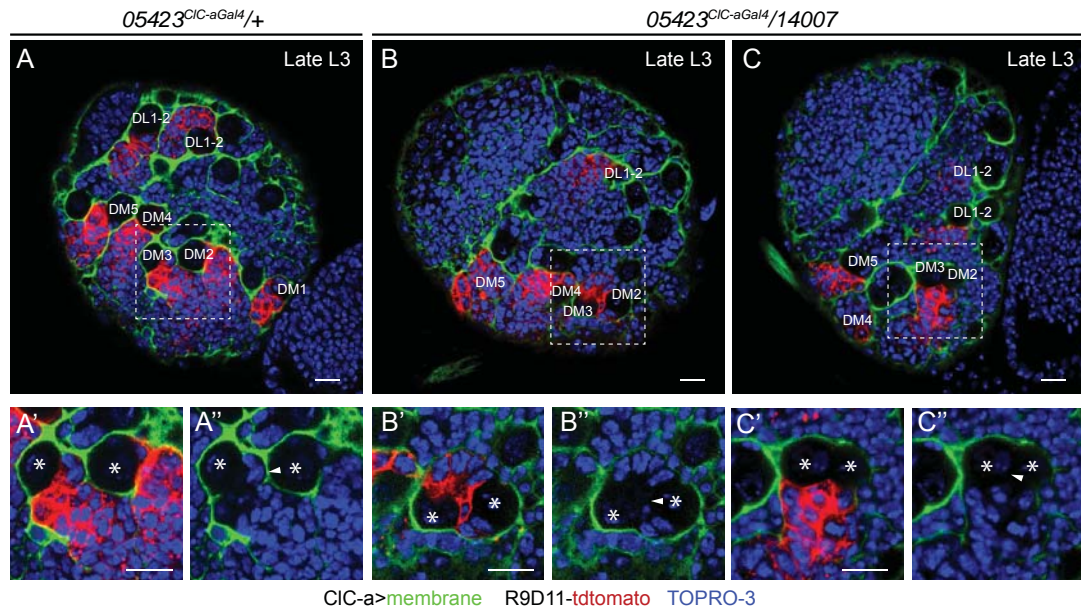


**Figure 46. Cortex glia, showing DM type II neuroblast encasing defects.** (A-C) Surface of the central brain in a control (A) and mutant (B,C). Cortex glial membranes (*05423<sup>CIC-aGal4</sup>* mediated *UASmCD8GFP* expression, green) encase individual type II neuroblasts and its lineages (*R9D11tdtomato*, red). Nuclei are labeled with TOPRO-3 (blue). In controls, a cortex glial process could be observed (A', A''), separating DM2 and DM3 neuroblasts (arrowhead). In mutants, no cortex glial processes between DM2 and DM3 neuroblasts are observed (arrowhead) (B', B'', C', C''). Since the images for controls and mutants are taken at different depths, the mutant brains seem bigger, but they are not. Neuroblasts are marked with an asterisk. Scale bars represent 10  $\mu\text{m}$ .



# **DISCUSSION**



Ion channels, of all kinds, are expressed in glia and even though they are mainly responsible for regulating glial homeostasis, they also directly regulate the well-being of surrounding cells. This is due to their ability of controlling extracellular ionic concentration as well as secretion and uptake of different organic compounds. Regarding the mammalian mature CNS, knowledge about the relation between ion channels in glia and neuronal behavior is growing, with few studies investigating the roles of ion channels in glia in the developing CNS. The results of this work contribute to the understanding of how chloride channels can affect the development of neural tissue, controlling the niche microenvironment during neurogenesis.

### **CIC-a as a key channel in the glial niche for neural progenitor proliferation**

In the mammalian mature CNS CIC-2 is expressed in neurons and glial populations, such as, astrocytes and oligodendrocytes (Nobile et al. 2000; Sík et al. 2000; Blanz et al. 2007b; Ratte and Prescott 2011). Our results demonstrate, that its fly homologue CIC-a is expressed in glia not only in the mature CNS, but also in the developing one, while neuronal expression was not detected. Interestingly, only some types of glia express the channel. To obtain a detailed description, we tested and described new tools for CIC-a expression assessment; a CIC-a protein tagged by GFP (*CIC-aGFP*) and a Gal4 line (*05423<sup>CIC-aGAL4</sup>*), both under the control of CIC-a regulatory sequences. From early development to adulthood, CIC-a is expressed in cortex glia and some types of ensheathing glial cells. Astrocyte-like glia, which has fine membrane processes close to synapses, does not express it.

The first described *CIC-a* mutants (*05423* and *14007*) had smaller brains and allowed us to investigate the consequences of removing the channel from the developing CNS. The lack of CIC-a in cortex glia, unveiled the non-autonomous influence of the channel in these glia, and especially on the development of the neuroepithelia. We concluded, that CIC-a is non-autonomously required for neuroepithelial proliferation. The central brain neuroblast lineage growth rate also decreased, although an overall higher cell death levels in mutant brains makes it difficult to conclude whether this is a consequence of neuroblast proliferative defects, less neuronal survival, or both. Interestingly, we observed an accumulation of INPs in DL1-2 type II lineages. This accumulation cannot be explained by dying INPs, but could be explained by reduced division rates and increased life expectancy of INPs. Therefore, these findings suggest, that apart from increased cell death, there might also be proliferative defects in the central brain. To elucidate whether proliferative defects are also responsible for decreased neuroblasts growth rate, *MARCM* clones could be induced in mutants, blocking cell death. Cell death could be blocked by overexpression of the baculovirus P35 (Hay et al. 1994) and the loss of Gal80 in clonal cells would allow P35 expression specifically in them. If there were proliferative defects, the clones would still be smaller after blocking cell death.

Some studies indicate, that cortex glial cells are in close contact with neural progenitors and

are responsible for creating a niche microenvironment for neuroepithelial cells (Morante et al. 2013) and neuroblasts (Dumstrei et al. 2003; Bailey et al. 2015). Our study also supports, that cortex glia is part of the *Drosophila* NSC niche. Historically, glia in contact with the OPC has been classified as surface glia, until Morante and colleagues (Morante et al. 2013) demonstrated, that a third glial layer belonging to cortex glial cells exists. However, there is still controversy in the field, as some studies have been published afterwards referring to this glial layer as surface glia (Coutinho-Budd et al. 2017). This is due to the atypical flat morphology of surface-associated cortex glial cells. Our observations corroborate, that this glial layer belongs to cortex glial cells. Furthermore, we identified CIC-a as necessary in this cortex glial niche to non-autonomously maintain growth of neuroepithelial cells and probably neuroblasts as well.

It is believed, that ion channels provide the basis for generating bioelectric signals, that intrinsically control migration, proliferation, and differentiation in a variety of stem cells (Reviewed in Li and Deng 2011). Therefore, the niche microenvironment should have the required ionic balance. To our knowledge, this is the first described example of a chloride channel necessary in neurogenic niche cells to extrinsically regulate stem cell proliferation. This confirms the importance of ionic homeostasis regulation in stem cell niches.

### **Central brain neuroblast derived glial cells act as guidepost cells for neuronal guidance**

Apart from studying stem cell proliferation defects, we also described the photoreceptor guidance phenotypes in *CIC-a* mutants and tried to identify the cause of these.

We first described adult photoreceptor phenotypes in detail and classified them by severity. This allowed us to define the strength of different allelic combinations. Some R7 and R8 photoreceptors were misguided during their targeting to the medulla. We showed, that they skipped the chiasm and reached the medulla from its proximal face. Afterwards, knock down and rescue experiments specifically in glia showed, that the *CIC-a* is required in glia, in agreement with its expression pattern. Thus, photoreceptor phenotypes are non-autonomous.

As the guidance defects had a developmental origin, we moved to the larval brain trying to identify the phenotype cause, and described, in detail, glial cell interaction with photoreceptors during brain innervation. We found that a glial barrier compartmentalizing the optic lobe was present in the targeting area of photoreceptors. This was composed by two glial populations, *CIC-a*<sup>-</sup> and *CIC-a*<sup>+</sup>, and cortex glial membrane processes. The *CIC-a*<sup>-</sup> cells become the known satellite glial cells at later larval stages and proximal satellite glial cells in the adult. The proximal satellite glia, together with the distal satellite glia, is classified as part of the lamina's cortex glia at adult stages (Kremer et al. 2017). However,

the proximal satellite glia is the only cortex glial type, that does not express *CIC-a*. It could be, that in adults, the functions proximal satellite glia accomplish are different from the other cortex glial cell functions.

The *CIC-a*<sup>+</sup> cells in the glial barrier, which we named boundary glia, turned out to be the precursors of two cell types, the outer chiasm glia and a new glial type, termed by us as palisade glia. Boundary glial cells are in close contact with first innervating photoreceptors and express the repulsive signal *slit* at innervation start. We linked the guidance phenotypes to a strong reduction of boundary glial cells in *CIC-a* mutants, since Slit signaling, necessary for correct photoreceptor guidance, is disrupted in these situations. We also showed that *CIC-a* is sufficient in cortex glia to rescue the decrease in boundary glial cells and photoreceptor phenotypes in *CIC-a* mutants. Therefore, *CIC-a* is not required for glial barrier correct positioning or photoreceptor guidance, in boundary glia, and its reduction is a secondary effect. Interestingly, the function *CIC-a* might accomplish in boundary glia or other ensheathing glia are still unknown.

It has been described that Xg<sub>o</sub> cells migrate from the central brain and belong to the DL1 neuroblast lineage (Viktorin et al. 2013; Ren et al. 2018). We demonstrated that the boundary glial cells, being Xg<sub>o</sub> precursors, are indeed coming from DL1 neuroblasts, and tried to decipher the origin of the strong reduction of those glial cells.

Although we could not conclude the cause of reduction, with certainty, we came up with two hypotheses, which could be complementary. On the one hand, the disorganization of type II lineages in the central brain, together with defects in the IPC, led us to hypothesize that the migration of boundary glia could be altered. On the other hand, the accumulation of INPs in DL1-2 lineages suggests, that in the same way as in neuroepithelia, proliferation could be decreased in those lineages, creating less boundary glial cells. An *ex vivo* analysis would be the best to answer this question. DL1 clone derived cells could be tracked *ex vivo* in cultured brains, where migration defects, generation of new cells and dying cells in the lineage could be easily assessed. The proliferation rate of neuroblasts could be assessed in the same way. Interestingly, a new technique, that allows creating individual clones for each type II neuroblast lineage (Ren et al. 2018), have been developed this year, and could be used for *ex vivo* experiments.

Furthermore, a study described the requirement of the Babo/Smad2 pathway in neuroblasts for correct proliferation and brain growth, as well as defects in photoreceptor axonal guidance. Mutants showed slower neuroblast proliferation and photoreceptor phenotypes were non-autonomous (Zhu et al. 2008). This previous link between neuroblast proliferation and photoreceptor guidance phenotypes is very interesting. However, due to a lack of detailed description of these guidance phenotypes in this study, we do not know whether the guidance phenotypes would be similar to the *CIC-a* ones. If those phenotypes were similar, this finding could support the idea, that proliferation defects are the main reason of reduction of boundary glia.

Guidance defects are not exclusive to photoreceptors in *CIC-a* mutants. Neurons of the mushroom body misproject to the calyx, instead of going through the peduncle, and if they do, they go through the outer part of it, instead of going through the middle. Also, in the strongest phenotypes, the calyx is mispositioned to the surface. When Spindler and colleagues (Spindler et al. 2009) overexpressed the pro-apoptotic proteins Hid and Reaper with *Nrv2Gal4*, they created what they called a glial-less brain. In those brains the surface glia is wild type, but they killed cortex and neuropil glial cells. In glial-less brains the mushroom body was frequently misshaped, since superficial calyx and glia elimination caused abnormal mushroom body fasciculation (Spindler et al. 2009). In an interesting way, DM2, DM3, DM5, and DM6 type II neuroblasts give glial offspring, that cover the mushroom body (Calyx, Peduncle) between other neuropils (Ren et al. 2018). It could be, that glia differentiated from the rest of type II lineages and necessary for neuropil compartmentalization are also affected, in a similar way as glia derived from DL1 lineage is strongly decreased. However, to answer this question, a detailed description of the mushroom body glia would be necessary through all developmental stages. A recent study described the adult glia in contact with the mushroom body (Kremer et al. 2017), and suggests, that developmental stage descriptions of the mushroom body glia would not be easy to obtain, as a lot of different kind of glia are present in this complex structure. Interestingly, we could observe some encasing problems of the DM type II neuroblasts, including the glia giving ones. It remains unknown if and how this behavior could affect proliferation. Encasing problems were not observed in DL1-2 lineages, proposing that these defects are an additional phenotype unrelated to proliferative defects. As done for the DL1-2 lineages, INPs of the DM type II lineages could be counted, to see whether accumulation of INPs also occurs in those lineages. Photoreceptor and mushroom body neuron guidance phenotypes could be only two guidance examples and some other neurons that need neuroblast derived guidepost cells for their correct axonal guidance could be affected.

### **Towards the physiological mechanism of *CIC-a***

Although we identified the requirement of *CIC-a* in cortex glia, the physiological mechanism of the channel is yet to be elucidated. We carried out some exploratory experiments, trying to address functional details. *CIC-a*, the same way as mammalian *CIC-2*, have an inwardly rectifying current (chloride leaves the cell), activated during hyperpolarized conditions (Jeworutzki et al. 2012). In mammals, the GLIALCAM subunit activates *CIC-2* at positive potentials (chloride enters the cell), however, the subunit is not conserved in *Drosophila*. Interestingly, *CIC-a* can suffer naturally occurring RNA editing in the “gating” glutamate (E269G) (Stapleton et al. 2006), which activates the channel also at positive potentials. It has been shown, that this activation at positive potentials is necessary in glia for the K<sup>+</sup> buffering process (Reviewed in Estévez et al. 2018). At this point, we wondered which *CIC-a* properties were required in cortex glia. As mentioned in the results section, *CIC-a* and *CIC-2*



expression in glia was sufficient to rescue all observed phenotypes. Hence, it seems, that the activation of the channel at negative potentials (chloride leaves the cell) is enough to rescue the phenotypes. A rescue with the edited version of CIC-a (E269G) in glia was also enough to completely rescue the photoreceptor guidance phenotypes, so the activation of the channel, also at positive potentials, did not alter its necessary function.

#### *Extracellular fluid regulation*

Chloride channels have usually been related to cell volume regulation, including glial cells. For example, VRAC channel activity is crucial for restoring astrocyte cell volume after a hypotonic shock (Hoffmann et al. 2009). In *Drosophila*, two of the few studied channels in glia,  $K^+/Cl^-$  cotransporter Kcc and  $Na^+/K^+/2Cl^-$  cotransporter Ncc69, maintain osmotic homeostasis, avoiding fluid accumulation between glia and axons (Leiserson and Keshishian 2011; Rusan et al. 2014). CIC-2 has been related to glial volume regulation in mammals as well, as its removal causes fluid accumulation leading to myelin vacuolization (Reviewed in Estévez et al. 2018). However, we could not detect any cell swelling or vacuoles in the *CIC-a* mutant brain; and cortex glia seems to maintain its trophospongium morphology, without any fluid accumulation. Since we only dissected adult fly brains of 1-2 days of age, it could be, that brain vacuoles appear in older flies.

#### *Membrane potential regulation*

The first hypothesis we had, was that the lack of CIC-a could be altering the glial membrane potential. The hypothetical function of the channel could be to take chloride out in compensation for cell membrane hyperpolarization. So the lack of CIC-a would led to membrane hyperpolarization. We overexpressed the mammalian potassium channel Kir2.1 in cortex glia to test whether glial membrane hyperpolarization could phenocopy photoreceptor phenotypes. The overexpression of this channel will increase potassium efflux and, thus, the membrane will hyperpolarize. Membrane hyperpolarization did not have any effect on photoreceptor guidance. The bacterial sodium channel NaChBac, which has the opposite effect than Kir2.1, increases sodium influx, hence depolarizing the membrane. Overexpressing NaChBac in *CIC-a* mutants we tried to rescue *CIC-a* photoreceptor phenotypes, but we could not see any rescue at all Hence, it seems that membrane potential alterations cannot phenocopy or rescue *CIC-a* phenotypes. These channels are normally used to block or activate neurons (Reviwed in Hodge 2009) and it could be that in glia the channels were not working as expected.

### *Secretion regulation*

Another hypothesis was, that the lack of CIC-a could be impairing glial secretion of some necessary factors for stem cell proliferation. It has been described, that cortex glial are secreting cells (Morante et al. 2013; Coutinho-Budd et al. 2017) and secretion is usually regulated by an increase of intracellular calcium. Therefore, chloride homeostasis impairment could affect  $\text{Ca}^{2+}$  regulation. The first exploratory experiment we did to test this hypothesis was an overexpression of a dominant negative Shibire dynamin ( $\text{SHI}^{\text{DN}}$ ) (Moline et al. 1999) using the mir8-repoflp strategy, which would block secretion in cortex glial cells. We chose the photoreceptor phenotypes as a readout. Surprisingly, photoreceptors showed very similar guidance phenotypes as *CIC-a* mutants. However, unlike in *CIC-a* mutants, cortex glia at mid and late L3 stages increased in volume and their membrane processes were much thicker, mainly affecting the thickness of surface-associated cortex glia. The morphological differences observed in cortex glia by  $\text{SHI}^{\text{DN}}$  suggest, that most probably photoreceptor phenotypes appeared due to reasons different from that in *CIC-a* mutants.

We also did a small RNAi screening of proteins known to regulate  $\text{Ca}^{2+}$  induced secretion in other tissues (such as, Rab3, IP3R, RyR, Unc13...), but we could not find any downregulated protein, which would recapitulate photoreceptor guidance phenotypes. It could be, that the selected candidates were not expressed in cortex glia. For example, a recent study demonstrated that Rab3 is not expressed in cortex glia (Coutinho-Budd et al. 2017). In any case, IP3R and RyR  $\text{Ca}^{2+}$  channels, the unique channels responsible for  $\text{Ca}^{2+}$  release from the endoplasmatic reticulum in  $\text{Ca}^{2+}$  induced secretion, did not show any phenotype in photoreceptors or general brain development. Therefore, the secretion in cortex glia is hardly controlled by calcium and other secretory machinery might be used.

### *Extracellular pH regulation*

Most  $\text{Cl}^-$  channels are also permeable for other anions, including amino acids and other organic and inorganic anions. A study in *C. elegans* demonstrated that the CIC  $\text{Cl}^-$  channel CLH-1 is highly permeable for  $\text{HCO}_3^-$  and mediates  $\text{HCO}_3^-$  uptake. At neutral extracellular pH, the cell would take up  $\text{HCO}_3^-$  via CLH-1. When extracellular acidification occurs, CLH-1 would mediate  $\text{HCO}_3^-$  efflux, to compensate for the protons (Figure 47A) (Grant et al. 2015). In fact, CLH-1 shows homology to and has electrophysiological properties similar to the mammalian CIC-2  $\text{Cl}^-$  channel. Assays in *Xenopus* oocytes done by our collaborators from Raul Estevez's group concluded that CIC-a and CIC-2 are not able to transport  $\text{HCO}_3^-$ . However, CIC-2 opens in response to extracellular acidification (Jordt and Jentsch 1997). This activation might be required to regulate  $\text{HCO}_3^-$  transport by creating a  $\text{Cl}^-$  recycling pathway for  $\text{HCO}_3^-/\text{Cl}^-$  exchangers (Bösl et al. 2001). Assays in *Xenopus* oocytes also concluded, that CIC-a activity is also sensitive to pH. It could be, that the lack of CIC-a in cortex glia would lead to a more acidic extracellular pH, due to deficient  $\text{Cl}^-$  recycling for

$\text{HCO}_3^-/\text{Cl}^-$  exchangers (Figure 47B). There are two  $\text{HCO}_3^-/\text{Cl}^-$  exchangers that could play this role in *Drosophila*, *Ndae1* and *CG8177*. It would be very interesting to investigate whether the exchangers are expressed in cortex glia and if they are, identify whether mutants have similar developmental phenotypes as described for CIC-a. Also, an experiment to assess pH in *CIC* mutants could be done. Genetically encoded pH-indicators (GEPHIs) (Rossano et al. 2013) could be used in *in vivo* experiments, such as pHluorin, which changes fluorescence color depending on the pH.

The extracellular acidification could affect neuroepithelial and neuroblast proliferation, and decrease neuronal survival. Several studies in several tissues describe the relation between pH and proliferation (Carswell and Papoutsakis 2000; Flinck et al. 2018), including cancer metabolism (Persi et al. 2018). Also, changes in pH can alter differentiation of different cell types (Bernard et al. 2006; Teo et al. 2014; Ulmschneider et al. 2016) and even affect oligodendrocyte precursor viability, migration, and differentiation (Jagielska et al. 2013). Thus, extracellular acidification could also affect boundary glial differentiation, migration, or viability.

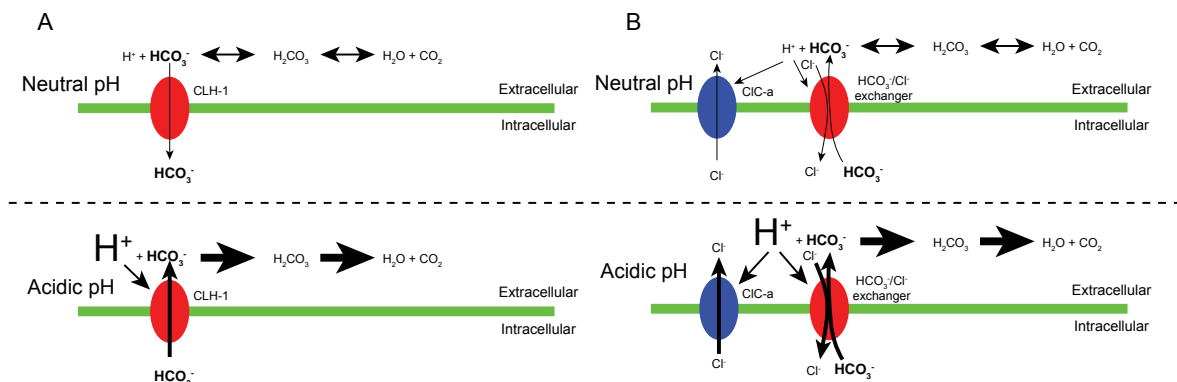


**Figure 47. Hypothetical physiological mechanism of CIC-a.** (A) Proposed role of glial-expressed CLH-1 in *C. elegans* in intracellular and extracellular pH buffering. At neutral pH, the cell accumulates  $\text{HCO}_3^-$  through CLH-1. Upon extracellular acidification, which tends to deplete extracellular  $\text{HCO}_3^-$  via conversion to  $\text{CO}_2$  and  $\text{H}_2\text{O}$ , CLH-1 may be activated and mediate  $\text{HCO}_3^-$  efflux to neutralize the extracellular space. (Modified from Grant et al., 2015). (B) Proposed role of CIC-a. In cases of acidic extracellular pH, CIC-a would release chloride to compensate positive charges, which in turn would create an increased extracellular chloride concentration. This chloride would be used by the exchanger, taking out  $\text{HCO}_3^-$  molecules, buffering the acidification.

### CIC-a in the mature nervous system, possible functions

CIC-a plays a role during CNS development, but we detected the channel is also expressed in cortex glia and different ensheathing glia in the mature CNS. In *Drosophila*, the mature CNS does not show any sign of neurogenesis. Therefore, CIC-a may play a different role. Ion channels have been shown to regulate seizure susceptibility (Leiserson et al. 2010; Melom and Littleton 2013; Rusan et al. 2014) and, with some controversy, mutations in mammalian *CICN2* have also been linked to epilepsy (Saint-Martin et al. 2009). While carrying out

some other exploratory experiments, we could use the same flies to test whether the lack of CIC-a has any effect in seizures susceptibility. We used transgenic flies expressing TrpA1, a temperature-sensitive Ca<sup>2+</sup> channel, under the control of a UAS promoter (UAS-TrpA1; Hamada et al. 2008). Prior studies overexpressing TrpA1 in cortex glia demonstrated that this manipulation resulted in acute and robust seizure activity in neurons, with epileptic behavior observed in both, larval and adult flies (Melom and Littleton 2013). *05423<sup>CIC-aGal4</sup>/UAS-TrpA1* controls and *05423<sup>CIC-aGal4</sup>/14007, UAS-TrpA1* mutants, were raised at 21°C, to avoid TrpA1 activation during development, since it activates at 29°C. Adult flies were transferred to new vials and moved to a 29°C chamber to activate the channel. We could observe how little by little both controls and mutants started to have seizures until they were fully paralyzed and fell in food. We could not observe any differences between controls and mutants at this point. Surprisingly, when we took the vials at room temperature (25°C), the recovery time of mutants was altered. While control flies were all recovered and walking after 60 seconds, *CIC-a* mutants needed more than 210 seconds to fully recover. We do not know whether this phenotype is due to a CIC-a role in recovering membrane potential after seizure or a secondary effect of the defective development of the mutant brain. The same experiment should be repeated conditionally removing the channel only in adult, having a normally developed brain. The best way for conditionally removing CIC-a only in adult would be to create a transgenic line having the *CIC-a* gene (or part of it) in a FRT cassette and at adult stages remove it by inducible FLP expression.

### Biological relevance of the study

Almost all *phyla* present a *CIC-a* homologue, but little is known about the processes the channel is involved in. In mammals, CIC-2 was mostly studied in relation to MLC leukoencephalopathy disease, in which CIC-2 functions attached to the GLIALCAM subunit and participates in charge compensation during K<sup>+</sup> buffering process. CIC-2 chloride uptake is necessary for potassium positive charge compensation. GLIALCAM regulates CIC-2 localization to cell-cell junctions and changes its physiological properties (Reviewed in Estevez et al. 2018). However, GLIALCAM is not conserved in insects and we demonstrated that in the fly's brain the chloride needs to leave the cell, so the knowledge we obtained about its homologue in fly hardly makes any contribution to the understanding of its role in K<sup>+</sup> buffering.

However, it could contribute to the understanding of other CIC-2 functions. Human patients with mutations in CIC-2 also show mental symptoms, such as, learning disabilities and retardation (Depienne et al. 2013; Di Bella et al. 2014; Hanagasi et al. 2015). It could be, that mutations in *CICN2* affect the development of the CNS in a similar way as identified in the fly. Rat CIC-2 completely rescued *CIC-a* mutant phenotypes in *Drosophila*, so the CIC-a properties needed for its function in glia are conserved in mammals. Curiously, although we

tried to rescue *CIC-a* phenotypes using the human *CIC-2*, we did not observe any rescue. Our collaborators from Raul Estévez's group, who work with mammalian channels, informed us that the human *CIC-2* does not move as easily to the membrane as the rat *CIC-2*, which could explain the absence of rescue. Indeed, the human *CIC-2* was almost not detected in glial membranes when overexpressed in *Drosophila* glia.

Furthermore, the *CIC-a* regulation of niche ionic homeostasis could be conserved in other non-neural niches. Humans showing decreased vision and infertility have been observed as well. In agreement with these findings, mice *CICN2* mutants also show a post-natal retinal degeneration and azoospermia (Bösl et al. 2001; Edwards et al. 2010). In mammalian testis, *CIC-2* is necessary in Sertoli cells, a cell type that creates a niche for germinal stem cells. These cells secrete a potassium rich fluid, but also provide lactate as an essential nutrient for the germ cells (Jutte et al. 1982). In the retina, *CIC-2* is necessary in the retinal pigment epithelia (RPE), an epithelium, that creates the optimal microenvironment for photoreceptors. Even though it does not represent a niche and proliferation is not happening, the rationale is similar. In both cases, it has been suggested that *CIC-2* would be necessary for transepithelial transport, although a role in extracellular pH regulation could be another plausible hypothesis. Both cases are very interesting, as different studies suggest that photoreceptor and germinal stem cell degeneration are non-autonomous. Hence, *CIC-2* would be necessary in the surrounding cells, which regulate the microenvironment for stem cell and photoreceptor survival. This reminds us of our observations in the fly brain, in which *CIC-a* is necessary in the cortex glial niche for the correct maintenance of neuroepithelia, neuroblasts, and neurons.

Thus, it could be that *CIC-a* and *CIC-2* have similar functions in tissues where a specific microenvironment is created by niche cells or supporting cells. The chloride channel is required in these cells for the correct proliferation or survival of different cell types. Although, used in different tissues, this mechanism seems to be conserved across different phyla.

## General overview

The hypothetical  $\text{Cl}^-$  recycling pathway for  $\text{HCO}_3^-/\text{Cl}^-$  exchangers and pH control in the glial niche by CIC-a (Figure 48), would be necessary for neuroepithelial and neuroblast proliferation. A proper proliferation rate is needed in the DL1 neuroblast for giving rise to migratory glia that acts as guidepost cells for photoreceptors (Figure 48). Guidepost cells for other neurons, and derived from other neuroblasts, could also be required in the same way.

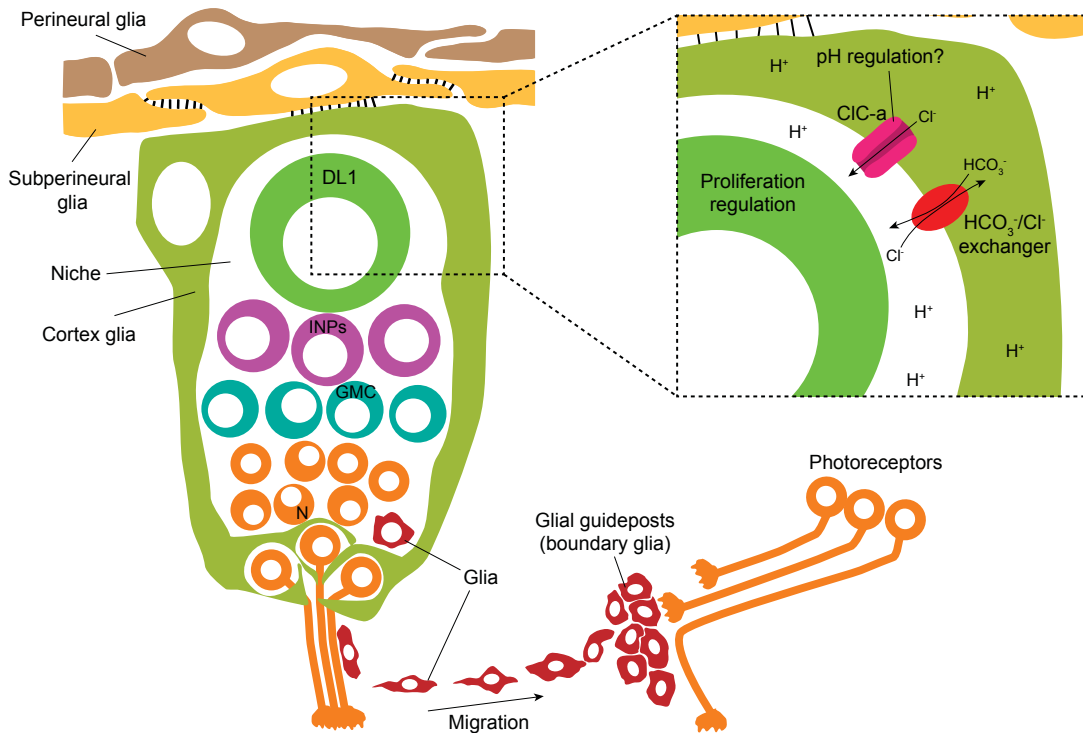


**Figure 48. Model of CIC-a function in the glial niche.** Scheme of the DL1 neuroblast niche and its lineage, as well as the possible role of CIC-a in pH regulation. Although the neuroepithelia niche is not depicted, the function would be the same. DL1 derived migratory glia creates a barrier which is not crossed by photoreceptors. GMC, ganglion mother cell; INPs, intermediate neural progenitors; N, neuron.

# CONCLUSIONS





As a summary of this work, we described how the chloride channel *CIC-a* is required for CNS development.

Specific conclusions:

- *CIC-a* is expressed exclusively in some types of glia during development, from early larva to the adult, specifically in cortex glia and different types of ensheathing glia.
- Described *CIC-a* mutants (*Mi(MIC)CIC-a<sup>05423</sup>* and *Mi(MIC)CIC-a<sup>14007</sup>*) are strong loss of function alleles.
- We identified two main non-autonomous phenotypes in *CIC-a* mutants: smaller brains and photoreceptor guidance phenotypes.
- *CIC-a* is required in the cortex glial niche for the correct proliferation of neuroepithelia and probably neuroblasts as well. Also, it is required in cortex glia for neuronal survival.
- The lack of *CIC-a* in cortex glia non-autonomously reduces the number of cells of a specific glial guidepost population necessary for the correct photoreceptor axonal guidance.
- *CIC-a* is also required for the wiring of mushroom body neurons, suggesting that proliferation defects could be widespread to different NB lineages



# **BIBLIOGRAPHY**



## A

- Achour S Ben, Pont-Lezica L, Béchade C, Pascual O. 2010. Is astrocyte calcium signaling relevant for synaptic plasticity? *Neuron Glia Biol* **6**: 147–155.
- Apitz H, Salecker I. 2015. A region-specific neurogenesis mode requires migratory progenitors in the Drosophila visual system. *Nat Neurosci* **18**: 46–55.

## B

- Bailey AP, Koster G, Guillermier C, Hirst EMA, MacRae JI, Lechene CP, Postle AD, Gould AP. 2015. Antioxidant Role for Lipid Droplets in a Stem Cell Niche of Drosophila. *Cell* **163**: 340–353. <http://dx.doi.org/10.1016/j.cell.2015.09.020>.
- Barres BA. 2008. The Mystery and Magic of Glia: A Perspective on Their Roles in Health and Disease. *Neuron* **60**: 430–440.
- Battista D, Ferrari CC, Gage FH, Pitossi FJ. 2006. Neurogenic niche modulation by activated microglia: transforming growth factor  $\beta$  increases neurogenesis in the adult dentate gyrus. *Eur J Neurosci* **23**: 83–93.
- Bayraktar OA, Boone JQ, Drummond ML, Doe CQ. 2010. Drosophila type II neuroblast lineages keep Prospero levels low to generate large clones that contribute to the adult brain central complex. *Neural Dev* **5**.
- Bello BC, Izergina N, Caussinus E, Reichert H. 2008. Amplification of neural stem cell proliferation by intermediate progenitor cells in Drosophila brain development. *Neural Dev* **3**.
- Bernard F, Vanhoutte P, Bennisroune A, Labourdette G, Perraut M, Aunis D, Gaillard S. 2006. pH is an intracellular effector controlling differentiation of oligodendrocyte precursors in culture via activation of the ERK1/2 pathway. *J Neurosci Res* **84**: 1392–1401.
- Bezzi P, Carmignoto G, Pasti L, Vesce S, Rossi D, Rizzini BL, Pozzan T, Volterra A. 1998. Prostaglandins stimulate calcium-dependent glutamate release in astrocytes. *Nature* **391**: 281–285.
- Bi MM, Hong S, Zhou HY, Wang HW, Wang LN, Zheng YJ. 2014. Chloride channelopathies of CIC-2. *Int J Mol Sci* **15**: 218–49.
- Billups D, Marx M-C, Mela I, Billups B. 2013. Inducible Presynaptic Glutamine Transport Supports Glutamatergic Transmission at the Calyx of Held Synapse. *J Neurosci* **33**: 17429–17434.
- Bjornsson CS, Apostolopoulou M, Tian Y, Temple S. 2015. It takes a village: Constructing the neurogenic niche. *Dev Cell* **32**: 435–446.

- Black JA, Liu S, Waxman SG. 2009. Sodium channel activity modulates multiple functions in microglia. *Glia* **57**: 1072–1081.
- Blanz J, Schweizer M, Auberson M, Maier H, Muenscher A, Hübner C a, Jentsch TJ. 2007a. Leukoencephalopathy upon disruption of the chloride channel CIC-2. *J Neurosci* **27**: 6581–9.
- Blanz J, Schweizer M, Auberson M, Maier H, Muenscher A, Hubner CA, Jentsch TJ. 2007b. Leukoencephalopathy upon Disruption of the Chloride Channel CIC-2. *J Neurosci* **27**: 6581–6589.
- Bockenbauer D, Feather S, Stanescu HC, Bandulik S, Zdebik AA, Reichold M, Tobin J, Lieberer E, Sterner C, Landouere G, et al. 2009. Epilepsy, Ataxia, Sensorineural Deafness, Tubulopathy, and KCNJ10 Mutations. *N Engl J Med* **360**: 1960–1970.
- Bond AM, Ming G, Song H. 2015. Adult Mammalian Neural Stem Cells and Neurogenesis: Five Decades Later. *Cell Stem Cell* **17**: 385–395.
- Boone JQ, Doe CQ. 2008. Identification of Drosophila type II neuroblast lineages containing transit amplifying ganglion mother cells. *Dev Neurobiol* **68**: 1185–1195.
- Bösl MR, Stein V, Hübner C, Zdebik a a, Jordt SE, Mukhopadhyay a K, Davidoff MS, Holstein a F, Jentsch TJ. 2001. Male germ cells and photoreceptors, both dependent on close cell-cell interactions, degenerate upon CIC-2 Cl(-) channel disruption. *EMBO J* **20**: 1289–99.
- Bowman SK, Rolland V, Betschinger J, Kinsey KA, Emery G, Knoblich JA. 2008. The Tumor Suppressors Brat and Numb Regulate Transit-Amplifying Neuroblast Lineages in Drosophila. *Dev Cell* **14**: 535–546.
- Brabletz S, Bajdak K, Meidhof S, Burk U, Niedermann G, Firat E, Wellner U, Dimmler A, Faller G, Schubert J, et al. 2011. The ZEB1/miR-200 feedback loop controls Notch signalling in cancer cells. *EMBO J* **30**: 770–782.
- Brand AH, Perrimon N. 1993. Targeted gene expression as a means of altering cell fates and generating dominant phenotypes. *Development* **118**: 401–15.
- Brody T, Odenwald WF. 2000. Programmed Transformations in Neuroblast Gene Expression during Drosophila CNS Lineage Development. *Dev Biol* **226**: 34–44.
- Brose K, Bland KS, Kuan HW, Arnott D, Henzel W, Goodman CS, Tessier-Lavigne M, Kidd T. 1999. Slit proteins bind robo receptors and have an evolutionarily conserved role in repulsive axon guidance. *Cell* **96**: 795–806.

## C

- Cabrero P, Terhzaz S, Romero MF, Davies S a, Blumenthal EM, Dow J a T. 2014. Chloride channels in stellate cells are essential for uniquely high secretion rates in neuropeptide-stimulated *Drosophila* diuresis. *Proc Natl Acad Sci U S A* **111**: 14301–6.
- Camp AJ. 2012. Intrinsic Neuronal Excitability: A Role in Homeostasis and Disease. *Front Neurol* **3**.
- Carmignoto G, Haydon PG. 2012. Astrocyte calcium signaling and epilepsy. *Glia* **60**: 1227–1233.
- Carswell KS, Papoutsakis ET. 2000. Extracellular pH affects the proliferation of cultured human T cells and their expression of the interleukin-2 receptor. *J Immunother* **23**: 669–74.
- Caussinus E, Kanca O, Affolter M. 2012. Fluorescent fusion protein knockout mediated by anti-GFP nanobody. *Nat Struct Mol Biol* **19**: 117–121.
- Chatton JY, Magistretti PJ, Barros LF. 2016. Sodium signaling and astrocyte energy metabolism. *Glia* **64**: 1667–1676.
- Chell JM, Brand AH. 2010. Nutrition-responsive glia control exit of neural stem cells from quiescence. *Cell* **143**: 1161–1173.
- Cheng LY, Bailey AP, Leever SJ, Ragan TJ, Driscoll PC, Gould AP. 2011. Anaplastic lymphoma kinase spares organ growth during nutrient restriction in *drosophila*. *Cell* **146**: 435–447.
- Chung W-S, Allen NJ, Eroglu C. 2015. Astrocytes Control Synapse Formation, Function, and Elimination. *Cold Spring Harb Perspect Biol* **7**: a020370.
- Cid LP, Montrose-Rafizadeh C, Smith DI, Guggino WB, Cutting GR. 1995. Cloning of a putative human voltage-gated chloride channel (CIC-2) cDNA widely expressed in human tissues. *Hum Mol Genet* **4**: 407–13.
- Clandinin TR, Zipursky SL. 2002. Making connections in the fly visual system. *Neuron* **35**: 827–41.
- Coutinho-Budd JC, Sheehan AE, Freeman MR. 2017. The secreted neurotrophin spätzle 3 promotes glial morphogenesis and supports neuronal survival and function. *Genes Dev* **31**: 2023–2038.
- Craner MJ, Damarjian TG, Liu S, Hains BC, Lo AC, Black JA, Newcombe J, Cuzner ML, Waxman SG. 2005. Sodium channels contribute to microglia/macrophage activation and function in EAE and MS. *Glia* **49**: 220–229.

## D

- Datta S. 1995. Control of proliferation activation in quiescent neuroblasts of the *Drosophila* central nervous system. *Development* **121**: 1173–1182.
- Davis RL. 1993. Mushroom bodies and drosophila learning. *Neuron* **11**: 1–14.
- Dearborn R, Kunes S. 2004. An axon scaffold induced by retinal axons directs glia to destinations in the *Drosophila* optic lobe. *Development* **131**: 2291–2303.
- Denholm B, Hu N, Fauquier T, Caubit X, Fasano L, Skaer H. 2013. The tiptop/teashirt genes regulate cell differentiation and renal physiology in *Drosophila*. *Development* **140**: 1100–1110.
- Depienne C, Bugiani M, Dupuits C, Galanaud D, Touitou V, Postma N, van Berkel C, Polder E, Tollard E, Darios F, et al. 2013. Brain white matter oedema due to CLC-2 chloride channel deficiency: An observational analytical study. *Lancet Neurol* **12**: 659–668.
- Di Bella D, Pareyson D, Savoiaro M, Farina L, Ciano C, Caldarazzo S, Sagnelli A, Bonato S, Nava S, Bresolin N, et al. 2014. Subclinical leukodystrophy and infertility in a man with a novel homozygous CLCN2 mutation. *Neurology* **83**: 1217–1218.
- Dibaj P, Kaiser M, Hirrlinger J, Kirchhoff F, Neusch C. 2007. Kir4.1 channels regulate swelling of astroglial processes in experimental spinal cord edema. *J Neurochem* **103**: 2620–2628.
- Ding R, Weynans K, Bossing T, Barros CS, Berger C. 2016. The Hippo signalling pathway maintains quiescence in *Drosophila* neural stem cells. *Nat Commun* **7**: 1–12.
- Djukic B, Casper KB, Philpot BD, Chin L-S, McCarthy KD. 2007. Conditional Knock-Out of Kir4.1 Leads to Glial Membrane Depolarization, Inhibition of Potassium and Glutamate Uptake, and Enhanced Short-Term Synaptic Potentiation. *J Neurosci* **27**: 11354–11365.
- Duffy JB, Harrison DA, Perrimon N. 1998. Identifying loci required for follicular patterning using directed mosaics. *Development* **125**: 2263–71.
- Dumstrei K, Wang F, Hartenstein V. 2003. Role of DE-cadherin in neuroblast proliferation, neural morphogenesis, and axon tract formation in *Drosophila* larval brain development. *J Neurosci* **23**: 3325–3335.

## E

- Ebens AJ, Garren H, Cheyette BNR, Zipursky SL. 1993. The *Drosophila* anachronism locus: A glycoprotein secreted by glia inhibits neuroblast proliferation. *Cell* **74**: 15–27.
- Edgar JM, Garbern J. 2004. The myelinated axon is dependent on the myelinating cell for support and maintenance: Molecules involved. *J Neurosci Res* **76**: 593–598.



- Edwards MM, Marín de Evsikova C, Collin GB, Gifford E, Wu J, Hicks WL, Whiting C, Varvel NH, Maphis N, Lamb BT, et al. 2010. Photoreceptor degeneration, azoospermia, leukoencephalopathy, and abnormal RPE cell function in mice expressing an early stop mutation in *CLCN2*. *Invest Ophthalmol Vis Sci* **51**: 3264–72.
- Edwards TN, Nuschke AC, Nern A, Meinertzhagen IA. 2012. Organization and metamorphosis of glia in the *Drosophila* visual system. *J Comp Neurol* **520**: 2067–2085.
- Egger B, Boone JQ, Stevens NR, Brand AH, Doe CQ. 2007. Regulation of spindle orientation and neural stem cell fate in the *Drosophila* optic lobe. *Neural Dev* **2**.
- Egger B, Gold KS, Brand AH. 2010. Notch regulates the switch from symmetric to asymmetric neural stem cell division in the *Drosophila* optic lobe. *Development* **137**: 2981–2987.
- Estévez R, Elorza-Vidal X, Gaitán-Peñas H, Pérez-Rius C, Armand-Ugón M, Alonso-Gardón M, Xicoy-Espauella E, Sirisi S, Arnedo T, Capdevila-Nortes X, et al. 2018. Megalencephalic leukoencephalopathy with subcortical cysts: A personal biochemical retrospective. *Eur J Med Genet* **61**: 50–60.
- Evans CJ, Olson JM, Ngo KT, Kim E, Lee NE, Kuoy E, Patananan AN, Sitz D, Tran PT, Do MT, et al. 2009. G-TRACE: Rapid Gal4-based cell lineage analysis in *Drosophila*. *Nat Methods* **6**: 603–605.

## F

- Featherstone DE. 2011. Glial solute carrier transporters in *drosophila* and mice. *Glia* **59**: 1351–1363.
- Filosa JA, Bonev AD, Straub S V, Meredith AL, Wilkerson MK, Aldrich RW, Nelson MT. 2006. Local potassium signaling couples neuronal activity to vasodilation in the brain. *Nat Neurosci* **9**: 1397–1403.
- Flinck M, Kramer SH, Pedersen SF. 2018. Roles of pH in control of cell proliferation. *Acta Physiol* **223**: 1–17.
- Flores CA, Niemeyer MI, Sepúlveda F V, Cid LP. 2006. Two splice variants derived from a *Drosophila melanogaster* candidate CIC gene generate CIC-2-type Cl<sup>-</sup> channels. *Mol Membr Biol* **23**: 149–56.
- Fuller MT, Spradling AC. 2007. Male and Female *Drosophila* Germline Stem Cells: Two Versions of Immortality. *Science (80- )* **316**: 402–404.

## G

- Gaitán-Peñas H, Gradogna A, Laparra-Cuervo L, Solsona C, Fernández-Dueñas V, Barrallo-Gimeno A, Ciruela F, Lakadamyali M, Pusch M, Estévez R. 2016. Investigation of LRRRC8-Mediated Volume-Regulated Anion Currents in *Xenopus* Oocytes. *Biophys J* **111**: 1429–1443.

- Galic MA, Riazi K, Pittman QJ. 2012. Cytokines and brain excitability. *Front Neuroendocrinol* **33**: 116–125.
- Girouard H, Bonev AD, Hannah RM, Meredith A, Aldrich RW, Nelson MT. 2010. Astrocytic endfoot Ca<sup>2+</sup> and BK channels determine both arteriolar dilation and constriction. *Proc Natl Acad Sci* **107**: 3811–3816.
- Grant J, Matthewman C, Bianchi L. 2015. A Novel Mechanism of pH Buffering in *C. elegans* Glia: Bicarbonate Transport via the Voltage-Gated CIC Cl<sup>-</sup> Channel CLH-1. *J Neurosci* **35**: 16377–16397.
- Grosskortenhaus R, Pearson BJ, Marusich A, Doe CQ. 2005. Regulation of Temporal Identity Transitions in *Drosophila* Neuroblasts. *Dev Cell* **8**: 193–202.

## H

- Hamada FN, Rosenzweig M, Kang K, Pulver SR, Ghezzi A, Jegla TJ, Garrity PA. 2008. An internal thermal sensor controlling temperature preference in *Drosophila*. *Nature* **454**: 217–220.
- Han C, Jan LY, Jan Y-N. 2011. Enhancer-driven membrane markers for analysis of nonautonomous mechanisms reveal neuron-glia interactions in *Drosophila*. *Proc Natl Acad Sci* **108**: 9673–9678.
- Hanagasi HA, Bilgiç B, Abbink TEM, Hanagasi F, Tüfekçioğlu Z, Gürvit H, Başak N, van der Knaap MS, Emre M. 2015. Secondary paroxysmal kinesigenic dyskinesia associated with CLCN2 gene mutation. *Parkinsonism Relat Disord* **21**: 544–546.
- Hartenstein V. 2011. Morphological diversity and development of glia in *Drosophila*. *Glia* **59**: 1237–1252.
- Hartenstein V, Campos-Ortega J a. 1984. Early neurogenesis in wild-type *Drosophila melanogaster*. *Wilhelm Roux's Arch Dev Biol* **193**: 308–325.
- Hartenstein V, Rudloff E, Campos -Ortega JA. 1987. The pattern of proliferation of the neuroblasts in the wild-type embryo of *Drosophila melanogaster*. *Roux's Arch Dev Biol* **196**: 473–485.
- Hartenstein V, Younossi-Hartenstein A, Lekven A. 1994. Delamination and Division in the *Drosophila* Neuroectoderm: Spatiotemporal Pattern, Cytoskeletal Dynamics, and Common Control by Neurogenic and Segment Polarity Genes. *Dev Biol* **165**: 480–499.
- Haubensak W, Attardo A, Denk W, Huttner WB. 2004. From The Cover: Neurons arise in the basal neuroepithelium of the early mammalian telencephalon: A major site of neurogenesis. *Proc Natl Acad Sci* **101**: 3196–3201.

- Hay BA, Wolff T, Rubin GM. 1994. Expression of baculovirus P35 prevents cell death in *Drosophila*. *Development* **120**: 2121–9.
- Heisenberg M. 1998. What do the mushroom bodies do for the insect brain? an introduction. *Learn Mem* **5**: 1–10.
- Hindle SJ, Bainton RJ. 2014. Barrier mechanisms in the *Drosophila* blood-brain barrier. *Front Neurosci* **8**.
- Hodge JLL. 2009. Ion channels to inactivate neurons in *Drosophila*. *Front Mol Neurosci* **2**.
- Hofbauer A, Campos-Ortega JA. 1990. Proliferation pattern and early differentiation of the optic lobes in *Drosophila melanogaster*. *Roux's Arch Dev Biol* **198**: 264–274.
- Hoffmann EK, Lambert IH, Pedersen SF. 2009. Physiology of Cell Volume Regulation in Vertebrates. *Physiol Rev* **89**: 193–277.
- Homem CCF, Knoblich JA. 2012. *Drosophila* neuroblasts: a model for stem cell biology. *Development* **139**: 4297–4310.
- Hoyle G. 1986. Glial cells of an insect ganglion. *J Comp Neurol* **246**: 85–103.
- Hoyle G, Williams M, Phillips C. 1986. Functional morphology of insect neuronal cell-surface/glial contacts: The trophospongium. *J Comp Neurol* **246**: 113–128.
- Huber S, Braun G, Schröppel B, Horster M. 1998. Chloride channels CIC-2 and ICIn mRNA expression differs in renal epithelial ontogeny. *Kidney Int Suppl* **67**: S149-51.

## I

- Isshiki T, Pearson B, Holbrook S, Doe CQ. 2001. *Drosophila* Neuroblasts Sequentially Express Transcription Factors which Specify the Temporal Identity of Their Neuronal Progeny. *Cell* **106**: 511–521.
- Ito K, Awano W, Suzuki K, Hiromi Y, Yamamoto D. 1997. The *Drosophila* mushroom body is a quadruple structure of clonal units each of which contains a virtually identical set of neurones and glial cells. *Development* **124**: 761–71.
- Ito K, Hotta Y. 1992. Proliferation pattern of postembryonic neuroblasts in the brain of *Drosophila melanogaster*. *Dev Biol* **149**: 134–148.
- Ito K, Urban J, Technau GM. 1995. Distribution, classification, and development of *Drosophila* glial cells in the late embryonic and early larval ventral nerve cord. *Roux's Arch Dev Biol* **204**: 284–307.

## J

- Jagielska A, Wilhite KD, van Vliet KJ. 2013. Extracellular Acidic pH Inhibits Oligodendrocyte Precursor Viability, Migration, and Differentiation. *PLoS One* **8**.
- Jenett A, Rubin GM, Ngo T-TB, Shepherd D, Murphy C, Dionne H, Pfeiffer BD, Cavallaro A, Hall D, Jeter J, et al. 2012. A GAL4-Driver Line Resource for Drosophila Neurobiology. *Cell Rep* **2**: 991–1001.
- Jeworutzki E, López-Hernández T, Capdevila-Nortes X, Sirisi S, Bengtsson L, Montolio M, Zifarelli G, Arnedo T, Müller CS, Schulte U, et al. 2012. GlialCAM, a protein defective in a leukodystrophy, serves as a CIC-2 Cl(-) channel auxiliary subunit. *Neuron* **73**: 951–61.
- Jordt S-E, Jentsch T. 1997. Molecular dissection of gating in the CIC-2 chloride channel. *EMBO J* **16**: 1582–1592.
- Jutte NH, Jansen R, Grootegoed JA, Rommerts FF, Clausen OP, van der Molen HJ. 1982. Regulation of survival of rat pachytene spermatocytes by lactate supply from Sertoli cells. *J Reprod Fertil* **65**: 431–8.

## K

- Kahanovitch U, Cuddapah VA, Pacheco NL, Holt LM, Mulkey DK, Percy AK, Olsen ML. 2018. MeCP2 Deficiency Leads to Loss of Glial Kir4.1. *Eneuro* **2**: ENEURO.0194-17.2018.
- Kambadur R, Koizumi K, Stivers C, Nagle J, Poole SJ, Odenwald WF. 1998. Regulation of POU genes by castor and hunchback establishes layered compartments in the Drosophila CNS. *Genes Dev* **12**: 246–260.
- Kanai MI, Kim M-J, Akiyama T, Takemura M, Wharton K, O'Connor MB, Nakato H. 2018. Regulation of neuroblast proliferation by surface glia in the Drosophila larval brain. *Sci Rep* **8**: 3730.
- Kang KH, Reichert H. 2015. Control of neural stem cell self-renewal and differentiation in Drosophila. *Cell Tissue Res* **359**: 33–45.
- Karres JS, Hilgers V, Carrera I, Treisman J, Cohen SM. 2007. The Conserved microRNA MiR-8 Tunes Atrophin Levels to Prevent Neurodegeneration in Drosophila. *Cell* **131**: 136–145.
- Kawamori H, Tai M, Sato M, Yasugi T, Tabata T. 2011. Fat/Hippo pathway regulates the progress of neural differentiation signaling in the Drosophila optic lobe. *Dev Growth Differ* **53**: 653–667.
- Kearney JB, Wheeler SR, Estes P, Parente B, Crews ST. 2004. Gene expression profiling of the developing Drosophila CNS midline cells. *Dev Biol* **275**: 473–492.

- Kim J-B. 2014. Channelopathies. *Korean J Pediatr* **57**: 1.
- Kirischuk S, Héja L, Kardos J, Billups B. 2015. Astrocyte sodium signaling and the regulation of neurotransmission. *Glia* **64**: 1655–1666.
- Knoblich JA. 2010. Asymmetric cell division: Recent developments and their implications for tumour biology. *Nat Rev Mol Cell Biol* **11**: 849–860.
- Kremer MC, Jung C, Batelli S, Rubin GM, Gaul U. 2017. The glia of the adult *Drosophila* nervous system. *Glia* **65**: 606–638.
- Kress GJ, Mennerick S. 2009. Action potential initiation and propagation: Upstream influences on neurotransmission. *Neuroscience* **158**: 211–222.
- Kucheryavykh Y V., Kucheryavykh LY, Nichols CG, Maldonado HM, Baksi K, Reichenbach A, Skatchkov SN, Eaton MJ. 2007. Downregulation of Kir4.1 inward rectifying potassium channel subunits by RNAi impairs potassium transfer and glutamate uptake by cultured cortical astrocytes. *Glia* **55**: 274–281.
- Kuffler SW, Nicholls JG. 1966. The physiology of neuroglial cells. *Ergeb Physiol* **57**: 1–90.
- Kuffler SW, Nicholls JG, Orkand RK. 1966. Physiological properties of glial cells in the central nervous system of amphibia. *J Neurophysiol* **29**: 768–787.
- Kuffler SW, Potter DD. 1964. Glia in the leech central nervous system: physiological properties and neuron-glia relationship. *J Neurophysiol* **27**: 290–320.

## L

- Lee T, Luo L. 1999. Mosaic analysis with a repressible cell marker for studies of gene function in neuronal morphogenesis. *Neuron* **22**: 451–461.
- Leiserson WM, Forbush B, Keshishian H. 2010. *Drosophila* glia use a conserved cotransporter mechanism to regulate extracellular volume. *Glia* **59**: 320–332.
- Leiserson WM, Keshishian H. 2011. Maintenance and regulation of extracellular volume and the ion environment in *Drosophila* larval nerves. *Glia* **59**: 1312–1321.
- Li G-R, Deng X-L. 2011. Functional ion channels in stem cells. *World J Stem Cells* **3**: 19.
- Li X, Erclik T, Bertet C, Chen Z, Voutev R, Venkatesh S, Morante J, Celik A, Desplan C. 2013. Temporal patterning of *Drosophila* medulla neuroblasts controls neural fates. *Nature* **498**: 456–462.
- Lutter D, Ullrich F, Lueck JC, Kempa S, Jentsch TJ. 2017. Selective transport of neurotransmitters and –modulators by distinct volume-regulated LRRC8 anion channels. *J Cell Sci* jcs.196253.

## M

- Ma Z, Stork T, Bergles DE, Freeman MR. 2016. Neuromodulators signal through astrocytes to alter neural circuit activity and behaviour. *Nature* **539**: 428–432.
- Magistretti PJ, Pellerin L. 1999. Cellular mechanisms of brain energy metabolism and their relevance to functional brain imaging. *Philos Trans R Soc B Biol Sci* **354**: 1155–1163.
- Melom JE, Littleton JT. 2013. Mutation of a NCKX Eliminates Glial Microdomain Calcium Oscillations and Enhances Seizure Susceptibility. *J Neurosci* **33**: 1169–1178.
- Mi Hwang E, Kim E, Yarishkin O, Ho Woo D, Han K-S, Park N, Bae Y, Woo J, Kim D, Park M, et al. 2014. A disulphide-linked heterodimer of TWIK-1 and TREK-1 mediates passive conductance in astrocytes. *Nat Commun* **5**: 3227.
- Middleton RE, Pheasant DJ, Miller C. 1996. Homodimeric architecture of a ClC-type chloride ion channel. *Nature* **383**: 337–40.
- Miyata T, Kawaguchi A, Saito K, Kawano M, Muto T, Ogawa M. 2004. Asymmetric production of surface-dividing and non-surface-dividing cortical progenitor cells. *Development* **131**: 3133–45.
- Mohyeldin A, Garzón-Muvdi T, Quiñones-Hinojosa A. 2010. Oxygen in Stem Cell Biology: A Critical Component of the Stem Cell Niche. *Cell Stem Cell* **7**: 150–161.
- Moline MM, Southern C, Bejsovec A. 1999. Directionality of wingless protein transport influences epidermal patterning in the Drosophila embryo. *Development* **126**: 4375–84.
- Morante J, Vallejo DM, Desplan C, Dominguez M. 2013. Conserved miR-8/miR-200 defines a glial niche that controls neuroepithelial expansion and neuroblast transition. *Dev Cell* **27**: 174–187.
- Morrison SJ, Spradling AC. 2008. Stem Cells and Niches: Mechanisms That Promote Stem Cell Maintenance throughout Life. *Cell* **132**: 598–611.
- Morsali D, Bechtold D, Lee W, Chauhdry S, Palchaudhuri U, Hassoon P, Snell DM, Malpass K, Piers T, Pocock J, et al. 2013. Safinamide and flecainide protect axons and reduce microglial activation in models of multiple sclerosis. *Brain* **136**: 1067–1082.
- Mothet J-P, Pollegioni L, Ouanounou G, Martineau M, Fossier P, Baux G. 2005. Glutamate receptor activation triggers a calcium-dependent and SNARE protein-dependent release of the gliotransmitter D-serine. *Proc Natl Acad Sci* **102**: 5606–5611.
- Murray CB, Morales MM, Flotte TR, McGrath-Morrow SA, Guggino WB, Zeitlin PL. 1995. ClC-2: a developmentally dependent chloride channel expressed in the fetal lung and downregulated after birth. *Am J Respir Cell Mol Biol* **12**: 597–604.

Muthukumar AK, Stork T, Freeman MR. 2014. Activity-dependent regulation of astrocyte GAT levels during synaptogenesis. *Nat Neurosci* **17**: 1340–1350.

## N

Nagarkar-Jaiswal S, Deluca SZ, Lee PT, Lin WW, Pan H, Zuo Z, Lv J, Spradling AC, Bellen HJ. 2015a. A genetic toolkit for tagging intronic MiMIC containing genes. *Elife* **4**: 2–9.

Nagarkar-Jaiswal S, Lee P-T, Campbell ME, Chen K, Anguiano-Zarate S, Cantu Gutierrez M, Busby T, Lin W-W, He Y, Schulze KL, et al. 2015b. A library of MiMICs allows tagging of genes and reversible, spatial and temporal knockdown of proteins in *Drosophila*. *Elife* **4**: 1–28.

Newman EA. 2001. Propagation of intercellular calcium waves in retinal astrocytes and Müller cells. *J Neurosci* **21**: 2215–23.

Ngo KT, Wang J, Junker M, Kriz S, Vo G, Asem B, Olson JM, Banerjee U, Hartenstein V. 2010. Concomitant requirement for Notch and Jak/Stat signaling during neuro-epithelial differentiation in the *Drosophila* optic lobe. *Dev Biol* **346**: 284–295.

Niemeyer M, Yusef Y. 2004. Functional evaluation of human CIC-2 chloride channel mutations associated with idiopathic generalized epilepsies. *Physiol ...* **26**: 74–83.

Nobile M, Pusch M, Rapisarda C, Ferroni S. 2000. Single-channel analysis of a CIC-2-like chloride conductance in cultured rat cortical astrocytes. *FEBS Lett* **479**: 10–4.

Noctor SC, Martínez-Cerdeño V, Ivic L, Kriegstein AR. 2004. Cortical neurons arise in symmetric and asymmetric division zones and migrate through specific phases. *Nat Neurosci* **7**: 136–144.

## O

Olsen ML, Higashimori H, Campbell SL, Hablitz JJ, Sontheimer H. 2006. Functional expression of Kir4.1 channels in spinal cord astrocytes. *Glia* **53**: 516–528.

Olsen ML, Sontheimer H. 2009. Ionic Channels in Glia. *Encycl Neurosci* 237–247.

Orkand RK, Nicholls JG, Kuffler SW. 1966. Effect of nerve impulses on the membrane potential of glial cells in the central nervous system of amphibia. *J Neurophysiol* **29**: 788–806.

## P

Pappalardo LW, Samad OA, Black JA, Waxman SG. 2014. Voltage-gated sodium channel Na<sub>v</sub> 1.5 contributes to astrogliosis in an in vitro model of glial injury via reverse Na<sup>+</sup> / Ca<sup>2+</sup> exchange. *Glia* **62**: 1162–1175.

- Pappu KS, Morey M, Nern A, Spitzweck B, Dickson BJ, Zipursky SL. 2011. Robo-3--mediated repulsive interactions guide R8 axons during *Drosophila* visual system development. *Proc Natl Acad Sci U S A* **108**: 7571–6.
- Parpura V, Basarsky TA, Liu F, Jeftinija K, Jeftinija S, Haydon PG. 1994. Glutamate-mediated astrocyte–neuron signalling. *Nature* **369**: 744–747.
- Pascual A, Pr at T. 2001. Localization of Long-Term Memory Within the *Drosophila* Mushroom Body. *Science (80- )* **294**: 1115–1117. h
- Pearson BJ, Doe CQ. 2003. Regulation of neuroblast competence in *Drosophila*. *Nature* **425**: 624–628.
- Pereanu W, Hartenstein V. 2006. Neural Lineages of the *Drosophila* Brain: A Three-Dimensional Digital Atlas of the Pattern of Lineage Location and Projection at the Late Larval Stage. *J Neurosci* **26**: 5534–5553.
- Pereanu W, Spindler S, Cruz L, Hartenstein V. 2007. Tracheal development in the *Drosophila* brain is constrained by glial cells. *Dev Biol* **302**: 169–180.
- Perez-Gomez R, Slovakova J, Rives-Quinto N, Krejci A, Carmena A. 2013. A Serrate-Notch-Canoe complex mediates essential interactions between glia and neuroepithelial cells during *Drosophila* optic lobe development. *J Cell Sci* **126**: 4873–4884.
- Perez SE, Steller H. 1996. Migration of glial cells into retinal axon target field in *Drosophila melanogaster*. *J Neurobiol* **30**: 359–373.
- Persi E, Duran-Frigola M, Damaghi M, Roush WR, Aloy P, Cleveland JL, Gillies RJ, Ruppin E. 2018. Systems analysis of intracellular pH vulnerabilities for cancer therapy. *Nat Commun* **9**: 2997.
- Persson A-K, Estacion M, Ahn H, Liu S, Stamboulian-Platel S, Waxman SG, Black JA. 2014. Contribution of sodium channels to lamellipodial protrusion and Rac1 and ERK1/2 activation in ATP-stimulated microglia. *Glia* **62**: 2080–2095.
- Pfeiffer BD, Jenett A, Hammonds AS, Ngo T-TB, Misra S, Murphy C, Scully A, Carlson JW, Wan KH, Lavery TR, et al. 2008. Tools for neuroanatomy and neurogenetics in *Drosophila*. *Proc Natl Acad Sci U S A* **105**: 9715–9720.
- Plazaola-Sasieta H, Fern andez-Pineda A, Zhu Q, Morey M. 2017. Untangling the wiring of the *Drosophila* visual system: developmental principles and molecular strategies. *J Neurogenet* **31**.
- Poon CLC, Mitchell KA, Kondo S, Cheng LY, Harvey KF. 2016. The Hippo Pathway Regulates Neuroblasts and Brain Size in *Drosophila melanogaster*. *Curr Biol* **26**: 1034–1042.
- Poroca DR, Pelis RM, Chappe VM. 2017. CIC channels and transporters: Structure, physiological functions, and implications in human chloride channelopathies. *Front Pharmacol* **8**: 1–25.



Prokop A, Technau GM. 1991. The origin of postembryonic neuroblasts in the ventral nerve cord of *Drosophila melanogaster*. *Development* **111**: 79–88.

## Q

Qiu Z, Dubin AE, Mathur J, Tu B, Reddy K, Miraglia LJ, Reinhardt J, Orth AP, Patapoutian A. 2014. SWELL1, a Plasma Membrane Protein, Is an Essential Component of Volume-Regulated Anion Channel. *Cell* **157**: 447–458.

## R

Ransom BR, Sontheimer H. 1992. The neurophysiology of glial cells. *J Clin Neurophysiol* **9**: 224–51.

Ratte S, Prescott SA. 2011. CIC-2 Channels Regulate Neuronal Excitability, Not Intracellular Chloride Levels. *J Neurosci* **31**: 15838–15843.

Reddy BVVG, Rauskolb C, Irvine KD. 2010. Influence of Fat-Hippo and Notch signaling on the proliferation and differentiation of *Drosophila* optic neuroepithelia. *Development* **137**: 2397–2408.

Reemst K, Noctor SC, Lucassen PJ, Hol EM. 2016. The Indispensable Roles of Microglia and Astrocytes during Brain Development. *Front Hum Neurosci* **10**.

Ren Q, Awasaki T, Wang Y-C, Huang Y-F, Lee T. 2018. Lineage-guided Notch-dependent gliogenesis by *Drosophila* multi-potent progenitors. *Development* **145**: dev.160127.

Rodrigues F, Schmidt I, Klämbt C. 2011. Comparing peripheral glial cell differentiation in *Drosophila* and vertebrates. *Cell Mol Life Sci* **68**: 55–69.

Rose U, Derst C, Wanischek M, Marinc C, Walther C. 2007. Properties and possible function of a hyperpolarisation-activated chloride current in *Drosophila*. *J Exp Biol* **210**: 2489–500.

Rossano AJ, Chouhan AK, Macleod GT. 2013. Genetically encoded pH-indicators reveal activity-dependent cytosolic acidification of *Drosophila* motor nerve termini in vivo. *J Physiol* **591**: 1691–1706.

Rusan ZM, Kingsford OA, Tanouye MA. 2014. Modeling glial contributions to seizures and epileptogenesis: Cation-chloride cotransporters in *Drosophila melanogaster*. *PLoS One* **9**: 1–10.

## S

Saha S, Prakash V, Halder S, Chakraborty K, Krishnan Y. 2015. A pH-independent DNA nanodevice for quantifying chloride transport in organelles of living cells. *Nat Nanotechnol* **10**: 645–651.

- Saint-Martin C, Gauvain G, Teodorescu G, Gourfinkel-An I, Fedirko E, Weber YG, Maljevic S, Ernst J-P, Garcia-Olivares J, Fahlke C, et al. 2009. Two novel CLCN2 mutations accelerating chloride channel deactivation are associated with idiopathic generalized epilepsy. *Hum Mutat* **30**: 397–405.
- Schofield R. 1978. The relationship between the spleen colony-forming cell and the haemopoietic stem cell. *Blood Cells* **4**: 7–25.
- Scholl UI, Choi M, Liu T, Ramaekers VT, Hausler MG, Grimmer J, Tobe SW, Farhi A, Nelson-Williams C, Lifton RP. 2009. Seizures, sensorineural deafness, ataxia, mental retardation, and electrolyte imbalance (SeSAME syndrome) caused by mutations in KCNJ10. *Proc Natl Acad Sci* **106**: 5842–5847.
- Seifert G, Huttmann K, Binder DK, Hartmann C, Wyczynski A, Neusch C, Steinhauser C. 2009. Analysis of Astroglial K<sup>+</sup> Channel Expression in the Developing Hippocampus Reveals a Predominant Role of the Kir4.1 Subunit. *J Neurosci* **29**: 7474–7488.
- Selleck SB, Steller H. 1991. The influence of retinal innervation on neurogenesis in the first optic ganglion of drosophila. *Neuron* **6**: 83–99.
- Sidiropoulou K, Pissadaki EK, Poirazi P. 2006. Inside the brain of a neuron. *EMBO Rep* **7**: 886–892.
- Sík A, Smith RL, Freund TF. 2000. Distribution of chloride channel-2-immunoreactive neuronal and astrocytic processes in the hippocampus. *Neuroscience* **101**: 51–65.
- Silva-Vargas V, Crouch EE, Doetsch F. 2013. Adult neural stem cells and their niche: a dynamic duo during homeostasis, regeneration, and aging. *Curr Opin Neurobiol* **23**: 935–942.
- Smith RL, Clayton GH, Wilcox CL, Escudero KW, Staley KJ. 1995. Differential expression of an inwardly rectifying chloride conductance in rat brain neurons: a potential mechanism for cell-specific modulation of postsynaptic inhibition. *J Neurosci* **15**: 4057–67.
- Sousa-Nunes R, Yee LL, Gould AP. 2011. Fat cells reactivate quiescent neuroblasts via TOR and glial insulin relays in Drosophila. *Nature* **471**: 508–513.
- Spéder P, Brand AH. 2014. Gap junction proteins in the blood-brain barrier control nutrient-dependent reactivation of Drosophila neural stem cells. *Dev Cell* **30**: 309–321.
- Spéder P, Brand AH. 2018. Systemic and local cues drive neural stem cell niche remodeling during neurogenesis in drosophila. *Elife* **7**: 1–16.
- Spindler SR, Ortiz I, Fung S, Takashima S, Hartenstein V. 2009. Drosophila cortex and neuropile glia influence secondary axon tract growth, pathfinding, and fasciculation in the developing larval brain. *Dev Biol* **334**: 355–368.

- Stapleton M, Carlson JW, Celniker SE. 2006. RNA editing in *Drosophila melanogaster* : New targets and functional consequences. 1922–1932.
- Steller H, Pirrotta V. 1985. A transposable P vector that confers selectable G418 resistance to *Drosophila* larvae. *EMBO J* **4**: 167–71.
- Stork T, Bernardos R, Freeman MR. 2012. Analysis of glial cell development and function in *Drosophila*. *Cold Spring Harb Protoc* **7**: 1–17.
- Stork T, Sheehan A, Tasdemir-Yilmaz OE, Freeman MR. 2014. Neuron-Glia interactions through the heartless fgf receptor signaling pathway mediate morphogenesis of *Drosophila* astrocytes. *Neuron* **83**: 388–403.
- Stowers R, Schwarz T. 1999. A genetic method for generating *Drosophila* eyes composed exclusively of mitotic clones of a single genotype. *Genetics* **152**: 1631–1639.
- Strauss R, Heisenberg M. 1993. A higher control center of locomotor behavior in the *Drosophila* brain. *J Neurosci* **13**: 1852–61.
- Suzuki T, Hasegawa E, Nakai Y, Kaido M, Takayama R, Sato M. 2016. Formation of Neuronal Circuits by Interactions between Neuronal Populations Derived from Different Origins in the *Drosophila* Visual Center. *Cell Rep* **15**: 499–509.
- Suzuki T, Sato M. 2014. Neurogenesis and neuronal circuit formation in the *Drosophila* visual center. *Dev Growth Differ* **56**: 491–498.

## T

- Tasdemir-Yilmaz OE, Freeman MR. 2014. Astrocytes engage unique molecular programs to engulf pruned neuronal debris from distinct subsets of neurons. *Genes Dev* **28**: 20–33.
- Taylor TD, Robichaux MB, Garrity P a. 2004. Compartmentalization of visual centers in the *Drosophila* brain requires Slit and Robo proteins. *Development* **131**: 5935–5945.
- Temple S. 2001. The development of neural stem cells. *Nature* **414**: 112–117.
- Teo A, Mantalaris A, Lim M. 2014. Influence of culture pH on proliferation and cardiac differentiation of murine embryonic stem cells. *Biochem Eng J* **90**: 8–15.
- Thiemann A, Gründer S, Pusch M, Jentsch TJ. 1992. A chloride channel widely expressed in epithelial and non-epithelial cells. *Nature* **356**: 57–60.
- Thorpe HM, Smith MCM. 1998. In vitro site-specific integration of bacteriophage DNA catalyzed by a recombinase of the resolvase/invertase family. *Proc Natl Acad Sci* **95**: 5505–5510.
- Tix S, Eule E, Fischbach KF, Benzer S. 1997. Glia in the chiasmata and medulla of the *Drosophila melanogaster* optic lobes. *Cell Tissue Res* **289**: 397–409.

Truman JW, Bate M. 1988. Spatial and temporal patterns of neurogenesis in the central nervous system of *Drosophila melanogaster*. *Dev Biol* **125**: 145–57.

Truman JW, Taylor BT, Awad TA. 1993. Formation of the adult nervous system. In *The Development of Drosophila melanogaster*. (ed. M. Bate and A. Martinez Arias), pp. 1245–1394. Cold Spring Harbor, NY: Cold Spring Harbor Laboratory Press.

Tsacopoulos M, Magistretti PJ. 1996. Metabolic coupling between glia and neurons. *J Neurosci* **16**: 877–85.

## U

Ugarte G, Delgado R, O'Day PM, Farjah F, Cid LP, Vergara C, Bacigalupo J. 2005. Putative CIC-2 chloride channel mediates inward rectification in *Drosophila* retinal photoreceptors. *J Membr Biol* **207**: 151–160.

Ulmschneider B, Grillo-Hill BK, Benitez M, Azimova DR, Barber DL, Nystul TG. 2016. Increased intracellular pH is necessary for adult epithelial and embryonic stem cell differentiation. *J Cell Biol* **215**: 345–355.

## V

Vallejo DM, Caparros E, Dominguez M. 2011. Targeting Notch signalling by the conserved miR-8/200 microRNA family in development and cancer cells. *EMBO J* **30**: 756–769.

Venken KJT, Schulze KL, Haelterman N a, Pan H, He Y, Evans-Holm M, Carlson JW, Lewis RW, Spradling AC, Hoskins R a, et al. 2011. MiMIC: a highly versatile transposon insertion resource for engineering *Drosophila melanogaster* genes. *Nat Methods* **8**: 737–743.

Viktorin G, Riebli N, Reichert H. 2013. A multipotent transit-amplifying neuroblast lineage in the central brain gives rise to optic lobe glial cells in *Drosophila*. *Dev Biol* **379**: 182–194.

Voss FK, Ullrich F, Munch J, Lazarow K, Lutter D, Mah N, Andrade-Navarro MA, von Kries JP, Stauber T, Jentsch TJ. 2014. Identification of LRRC8 Heteromers as an Essential Component of the Volume-Regulated Anion Channel VRAC. *Science (80- )* **344**: 634–638.

## W

Wang W, Li Y, Zhou L, Yue H, Luo H. 2011a. Role of JAK/STAT signaling in neuroepithelial stem cell maintenance and proliferation in the *Drosophila* optic lobe. *Biochem Biophys Res Commun* **410**: 714–720.

Wang W, Liu W, Wang Y, Zhou L, Tang X, Luo H. 2011b. Notch signaling regulates neuroepithelial stem cell maintenance and neuroblast formation in *Drosophila* optic lobe development. *Dev Biol* **350**: 414–428.

Weng M, Lee CY. 2011. Keeping neural progenitor cells on a short leash during *Drosophila* neurogenesis. *Curr Opin Neurobiol* **21**: 36–42.

Woo DH, Han K-S, Shim JW, Yoon B-E, Kim E, Bae JY, Oh S-J, Hwang EM, Marmorstein AD, Bae YC, et al. 2012. TREK-1 and Best1 Channels Mediate Fast and Slow Glutamate Release in Astrocytes upon GPCR Activation. *Cell* **151**: 25–40.

## X

Xu T, Rubin GM. 1993. Analysis of genetic mosaics in developing and adult *Drosophila* tissues. *Development* **117**: 1223–1237.

## Y

Yasugi T, Sugie A, Umetsu D, Tabata T. 2010. Coordinated sequential action of EGFR and Notch signaling pathways regulates proneural wave progression in the *Drosophila* optic lobe. *Development* **137**: 3193–3203.

Yasugi T, Umetsu D, Murakami S, Sato M, Tabata T. 2008. *Drosophila* optic lobe neuroblasts triggered by a wave of proneural gene expression that is negatively regulated by JAK/STAT. *Development* **135**: 1471–1480.

## Z

Zeydan B, Uygunoglu U, Altintas A, Saip S, Siva A, Abbink TEM, Van Der Knaap MS, Yalcinkaya C. 2017. Identification of 3 Novel Patients with CLCN2-Related Leukoencephalopathy due to CLCN2 Mutations. *Eur Neurol* **78**: 125–127.

Zhu CC, Boone JQ, Jensen PA, Hanna S, Podemski L, Locke J, Doe CQ, O'Connor MB. 2008. *Drosophila* Activin- and the Activin-like product Dawdle function redundantly to regulate proliferation in the larval brain. *Development* **135**: 513–521.



# **ANNEXES**





## Annex 1: Genotypes

### Figure 13:

A. *w; UAS-mCD8GFP/+; 05423<sup>CIC-aGAL4</sup>/UAS-H2BRFP*

B. *w; +/+; +/+*

### Figure 19:

A, D, G. *w; +/+; +/+*

B, E, H. *w; +/+; CIC-aGFP/CIC-aGFP*

C, F. *w; UAS-mCD8GFP/+; 05423<sup>CIC-aGAL4</sup>/+*

I. *w; UAS-mCD8GFP/+; 05423<sup>CIC-aGAL4</sup>/UAS-H2BRFP*

### Figure 20:

A, B, C, D, E, F, G, H, I. *w; UAS-mCD8GFP/+; 05423<sup>CIC-aGAL4</sup>/UAS-H2BRFP*

### Figure 21:

A. *w; UAS-mCD8GFP/+; 05423<sup>CIC-aGAL4</sup>/UAS-H2BRFP*

B, C. *w; mir8-Gal4/UAS-mCD8GFP; +/+*

D. *w; UAS-mCD8GFP/+; R54H02-Gal4/UAS-H2BRFP*

E, F. *w; UAS-mCD8GFP, lexO-CD2RFP/+; 05423<sup>CIC-aGAL4</sup>/wrapper932i-LexA*

### Figure 22:

A, B, C, D, E. *w; UAS-mCD8GFP/+; 05423<sup>CIC-aGAL4</sup>/wrapper932i-Gal80*

F, G, H, I, K, L, M. *w; UAS-mCD8GFP/+; 05423<sup>CIC-aGAL4</sup>/UAS-H2BRFP*

J. *w; UAS-mCD8GFP/+; 05423<sup>CIC-aGAL4</sup>/+*

### Figure 23:

B, D. *w; +/+; +/+*

C, E. *w; +/+; 14007/Df(3R)PS2*

F. *w; +/+; 05423/Df(3R)PS2*

G.

w1118: *w; +/+; +/+*

Df/+: *w; +/+; Df(3R)PS2/+*

05423/+: w; +/+; 05423/+

14007/+: w; +/+; 14007/+

05423/Df: w; +/+; 05423/Df(3R)PS2

14007/Df: w; +/+; 14007/Df(3R)PS2

14007/05423: w; +/+; 14007/05423

**Figure 24:**

**A, B.**

W1118: w; +/+; +/+

05423<sup>CIC-aGAL4</sup>/+: w; +/+; 05423<sup>CIC-aGAL4</sup>/+

14007/+: w; +/+; 14007/+

Df/+: w; +/+; Df(3R)PS2/+

05423<sup>CIC-aGAL4</sup>/14007: w; +/+; 05423<sup>CIC-aGAL4</sup>/14007

05423<sup>CIC-aGAL4</sup>/Df: w; +/+; 05423<sup>CIC-aGAL4</sup>/Df(3R)PS2

**Figure 25:**

**A.** w; +/+; 14007/+

**B.** w; +/+; 14007/Df(3R)PS2

**C.**

05423<sup>CIC-aGAL4</sup>/+: w; +/+; 05423<sup>CIC-aGAL4</sup>/+

05423/+: w; +/+; 05423/+

14007/+: w; +/+; 14007/+

Df/+: w; +/+; Df(3R)PS2/+

05423<sup>CIC-aGAL4</sup>/Df: w; +/+; 05423<sup>CIC-aGAL4</sup>/Df(3R)PS2

05423/Df: w; +/+; 05423/Df(3R)PS2

14007/Df: w; +/+; 14007/Df(3R)PS2

05423<sup>CIC-aGAL4</sup>/14007: w; +/+; 05423<sup>CIC-aGAL4</sup>/14007

05423/14007: w; +/+; 05423/14007

**D.** w; Rh1Gal4/UASmCD8GFP; 14007/+

E, F. *w; Rh1Gal4/UASmCD8GFP; 14007/Df(3R)PS2*

**Figure 26:**

A. *w; Rh4-EGFP/+; 14007/+*

B. *w; Rh4-EGFP/+; 14007/Df(3R)PS2*

C. *w; Rh6-LacZ/+; 14007/+*

D. *w; Rh6-LacZ/+; 14007/Df(3R)PS2*

E. *w; Rh6-LacZ/ Rh4-EGFP; 14007/Df(3R)PS2*

F. *w; sensGal4, UASutrGFP/+; 14007/+*

G. *w; sensGal4, UASutrGFP /+; 14007/Df(3R)PS2*

**Figure 27:**

A.

RepoGal4: *w; +/+; Repo-Gal4/+*

05423<sup>CIC-aGAL4</sup>/+: *w; +/+; 05423<sup>CIC-aGAL4</sup>/+*

CIC-aRNAi: *w; UAS-CIC-aRNAi/+; UAS-Dcr2/+*

RepoGal4>CIC-aRNAi: *w; UAS-CIC-aRNAi /+; Repo-Gal4/UAS-Dcr2*

05423<sup>CIC-aGAL4</sup>>CIC-aRNAi: *w; UAS-CIC-aRNAi /+; 05423<sup>CIC-aGAL4</sup>/UAS-Dcr2*

B.

CIC-aGFP/CIC-aGFP: *w; +/+; CIC-aGFP/CIC-aGFP*

deGRADFP: *w; UAS-deGRADFP/+; +/+*

RepoGal4: *w; Repo-Gal4/+; +/+*

RepoGal4>deGRADFP CIC-aGFP/CIC-a-GFP: *w; Repo-Gal4/UAS-deGRADFP; CIC-aGFP/CIC-a-GFP*

C.

RepoGal4: *w; Repo-Gal4/+; 14007/Df(3R)PS2*

UASCIC-a: *w; UAS-CIC-a/+; 14007/Df(3R)PS2*

UASRatCIC-2: *w; UAS-RatCIC-2/+; 14007/Df(3R)PS2*

RepoGal4>CIC-a: *w; UAS-CIC-a/Repo-Gal4; 14007/Df(3R)PS2*

RepoGal4> RatCIC-2: w; UAS-RatCIC-2/Repo-Gal4; 14007/Df(3R)PS2  
05423<sup>CIC-aGAL4</sup>/Df, UASCIC-a: w; UAS-CIC-a/+; 05423<sup>CIC-aGAL4</sup>/Df(3R)PS2  
05423<sup>CIC-aGAL4</sup>/Df, UASRatCIC-2: w; UAS-RatCIC-2/+; 05423<sup>CIC-aGAL4</sup>/Df(3R)PS2

**D.**

UASCIC-a/+: w; UAS-CIC-a/+; +/+  
UASRatCIC-2/+: w; UAS-RatCIC-2/+; +/+  
05423<sup>CIC-aGAL4</sup>/Df: w; +/+; 05423<sup>CIC-aGAL4</sup>/Df(3R)PS2  
05423<sup>CIC-aGAL4</sup>/Df, UASCIC-a: w; UAS-CIC-a/+; 05423<sup>CIC-aGAL4</sup>/Df(3R)PS2  
05423<sup>CIC-aGAL4</sup>/Df, UASRatCIC-2: w; UAS-RatCIC-2/+; 05423<sup>CIC-aGAL4</sup>/Df(3R)PS2

**Figure 28:**

GMRGal4: w; GMR-Gal4/+; +/+  
CIC-aRNAi: w; UAS-CIC-aRNAi/+; UAS-Dcr2/+  
GMRGal4>CIC-aRNAi: w; UAS-CIC-aRNAi/GMR-GAL4; UAS-Dcr2/+  
GMRGal4, 14007/Df: w; GMR-Gal4/+; 14007/Df(3R)PS2  
UASCIC-a, 14007/Df: w; UAS-CIC-a/+; 14007/Df(3R)PS2  
GMRGal4>UASCIC-a, 14007/Df: w; GMR-Gal4/UASCIC-a; 14007/Df(3R)PS2

**Figure 29:**

**A, B, C, D.** w; UAS-mCD8GFP/+; 05423<sup>CIC-aGAL4</sup>/UAS-H2BRFP  
**E, F, G, H.** w; UAS-mCD8RFP/ UAS-H2BYFP; 05423<sup>CIC-aGAL4</sup>/14007

**Figure 30:**

**A, B, C.**

14007/+: w; +/+; 14007/+  
14007/Df: w; +/+; 14007/Df(3R)PS2

**D.**

14007/+: hsFLP,FRT19A,tubGal80/ FRT19A; tubGAL4,UASmCD8GFP/+; 14007/+  
14007/Df: hsFLP,FRT19A,tubGal80/ FRT19A; tubGAL4,UASmCD8GFP/+; 14007/Df(3R)PS2

**Figure 31:**

14007/+: w; +/+; 14007/+

14007/Df: w; +/+; 14007/Df(3R)PS2

**Figure 32:**

**A.**

14007/+: *hsFLP,FRT19A,tubGal80/ FRT19A; tubGAL4,UASmCD8GFP/+*; 14007/+

14007/Df: *hsFLP,FRT19A,tubGal80/ FRT19A; tubGAL4,UASmCD8GFP/+*; 14007/Df(3R)PS2

**B.**

14007/+: w; +/+; 14007/+

14007/Df: w; +/+; 14007/Df(3R)PS2

**Figure 33:**

**A.**

14007/+: w; +/+; 14007/+

14007/Df: w; +/+; 14007/Df(3R)PS2

**Figure 34:**

**A, B, C, D, E, N, O, P, Q.** w; *UAS-mCD8GFP/+*; *05423<sup>CIC-aGAL4</sup>/UAS-H2BRFP*

**F.** w; +/+; 14007/+

**G, H, I, J, K.** w; *UAS-mCD8RFP/ UAS-H2BYFP*; *05423<sup>CIC-aGAL4</sup>/14007*

**L.** w; +/+; 14007/Df(3R)PS2

**M.**

05423<sup>CIC-aGAL4</sup>/+: w; *UAS-mCD8GFP/+*; *05423<sup>CIC-aGAL4</sup>/UAS-H2BRFP*

05423<sup>CIC-aGAL4</sup>/14007: w; *UAS-mCD8RFP/ UAS-H2BYFP*; *05423<sup>CIC-aGAL4</sup>/14007*

**Figure 35:**

**A, B.** w; *UAS-mCD8GFP, lexO-CD2RFP/R43H01-LexA*; *05423<sup>CIC-aGAL4</sup>/+*

**C.** w; *UAS-mCD8GFP/+*; *R25A01-Gal4/+*

**D, E.** w; *UAS-mCD8GFP/+*; *05423<sup>CIC-aGAL4</sup>/UAS-H2BRFP*

**F, G.** *w; UAS-G-trace/+; 05423<sup>CIC-aGAL4</sup>/+*

**Figure 36:**

**A, B.** *w; UAS-G-trace/+; R38H02-Gal4/+*

**C, D.** *w; UAS-H2BYFP /+; 05423<sup>CIC-aGAL4</sup>/14007*

**Figure 37:**

**A, B.** *w; +/+; 14007/Df(3R)PS2*

**C, D.** *w; slit<sup>dui</sup>, GMR-GFP/slit<sup>dui</sup>, GMR-GFP;+/+*

**Figure 38:**

**A, B.** *w; SlitGFP/UASmCD8RFP; 05423<sup>CIC-aGAL4</sup>/+*

**C, D.** *w; SlitlacZ/+; +/+*

**Figure 39:**

**A, B, C.** *w; SlitGFP/UASmCD8RFP; 05423<sup>CIC-aGAL4</sup>/+*

**Figure 40:**

**A.**

05423<sup>CIC-aGAL4</sup>/+ *w; +/+; 05423<sup>CIC-aGAL4</sup>/+*

SlitRNAi/+; *w; UAS-SlitRNAi/+; UAS-Dcr2/+*

05423<sup>CIC-aGAL4</sup>>SlitRNAi *w; UAS-SlitRNAi/+; UAS-Dcr2/05423<sup>CIC-aGAL4</sup>*

Slitdui/+; 05423<sup>CIC-aGal4</sup>>SlitRNAi; *w; UAS-SlitRNAi/ w; UAS-SlitRNAi/+; UAS-Dcr2/05423<sup>CIC-aGAL</sup>; UAS-Dcr2/05423<sup>CIC-aGAL</sup>*

**B.**

14007/+; *w; +/+; 14007/+*

slit<sup>dui</sup> /+; *w; slit<sup>dui</sup>, GMR-GFP/+; 14007/+*

14007/14007; *w; +/+; 14007/14007*

slit<sup>dui</sup> , 14007/14007; *w; slit<sup>dui</sup>, GMR-GFP/+; 14007/14007*

**C.**

RepoGal4; *w; RepoGal4/+; 14007/Df(3R)PS2*

GMRGal4; *w; GMRGal4/+; 14007/Df(3R)PS2*

UAS-Slit: w; UAS-Slit/+; 14007/Df(3R)PS2

RepoGal4/UAS-Slit: w; RepoGal4/UAS-Slit; 14007/Df(3R)PS2

GMRGal4/UAS-Slit: w; GMRGal4/UAS-Slit; 14007/Df(3R)PS2

**Figure 41:**

**A, B, C.** w; mir8-Gal4/UAS-mCD8GFP; +/+

**D, E, F, G.** tub>Gal80>/+; mir8-Gal4, RepoFLP6.2/+; UASmCD8GFP/+

**Figure 42:**

**B.**

14007/+: w; +/+; 14007/+

14007/Df: w; +/+; 14007/Df(3R)PS2

14007/Df, mir8Gal4/UASCIC-a (RepoFLP strategy): tub>Gal80>/+; mir8-Gal4/RepoFLP6.2, UASCIC-a; 14007/Df(3R)PS2

**C.**

tub>Gal80>/+; +/RepoFLP6.2, UASCIC-a; 14007/Df(3R)PS2

tub>Gal80>/+; mir8-Gal4/RepoFLP6.2, UASCIC-a; 14007/Df(3R)PS2

**Figure 43:**

**A, D.** w; +/+; 14007, R9D11tdtomato/+

**B, C, E.** w; +/+; 14007, R9D11tdtomato/Df(3R)PS2

**Figure 44:**

**A, B.** w; UASmCD8GFP/+; 05423<sup>CIC-aGAL4</sup>/R9D11tdtomato

**C.** w; UASmCD8GFP/+; 05423<sup>CIC-aGAL4</sup>/14007, R9D11tdtomato

**D.**

05423<sup>CIC-aGAL4</sup>/+: w; UASmCD8GFP/+; 05423<sup>CIC-aGAL4</sup>/R9D11tdtomato

05423<sup>CIC-aGAL4</sup>/14007: w; UASmCD8GFP/+; 05423<sup>CIC-aGAL4</sup>/14007, R9D11tdtomato

**Figure 45:**

**A, B, C.** w; UASmCD8GFP/+; 05423<sup>CIC-aGAL4</sup>/+

**D.** w; +/+; 14007/+

**E, F, G.** *w; UASmCD8GFP/+; 05423<sup>CIC-aGAL4</sup>/14007*

**H.** *w; +/+; 14007/Df(3R)PS2*

**I.** *hsFLP,FRT19A,tubGal80/ FRT19A; tubGAL4,UASmCD8GFP/+; 14007/+*

**J, K, L.** *hsFLP,FRT19A,tubGal80/ FRT19A; tubGAL4,UASmCD8GFP/+; 14007/Df(3R)PS2*

**Figure 46:**

**A.** *w; UASmCD8GFP/+; 05423<sup>CIC-aGAL4</sup>/R9D11tdtomato*

**B, C.** *w; UASmCD8GFP/+; 05423<sup>CIC-aGAL4</sup>/14007, R9D11tdtomato*



## Annex 2: Photoreceptor clonal analysis

At the beginning of the project, we did not have the necessary tools to assess *CIC-a* expression, so we wanted to discard any possible contribution to the photoreceptor guidance phenotypes of an hypothetical *CIC-a* expression in them. We concluded that removing *CIC-a* only from photoreceptors by clonal analysis did not phenocopy photoreceptor phenotypes.

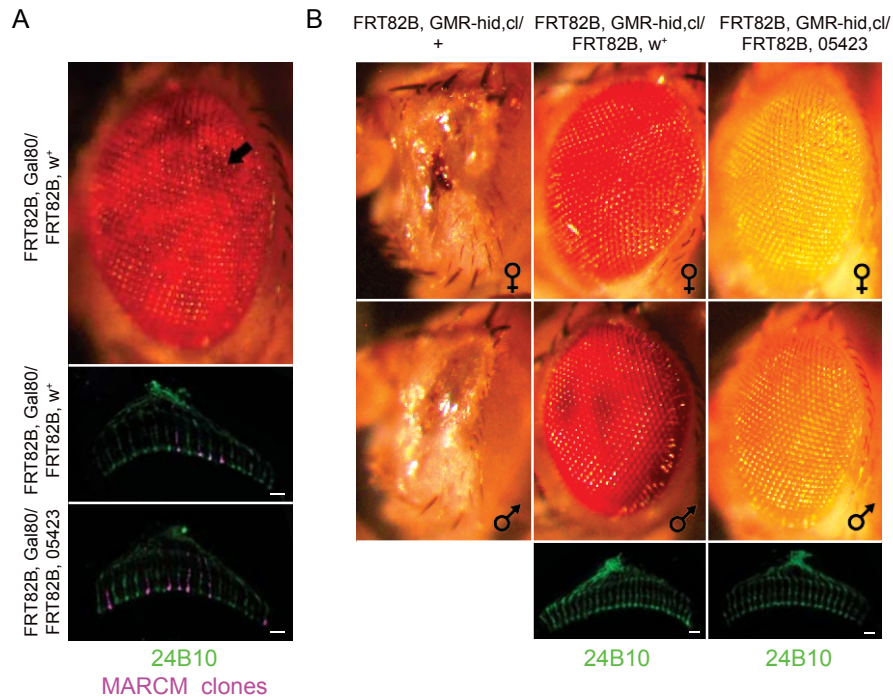


**Figure 49. *CIC-a* mutant photoreceptor clones.** (A) Homozygous photoreceptor *MARCM* clones. A control adult eye is shown, where clones can be detected by stronger pigmentation. Photoreceptor axonal guidance in controls and mutant homozygous clones is completely WT. (B) EGUF-hid photoreceptor clones, where the complete eye is homozygous mutant. When clones are induced, the eye is rescued, as only clonal photoreceptors will survive. No phenotypes were observed in photoreceptor axonal guidance in controls and mutant homozygous clones.

